Precision Propagation and Orbit Decay Prediction of Low Earth Orbit Satellites

By B D L Opperman

Thesis presented in partial fulfillment of the requirements for the degree of Master of Science in Electronic Engineering Sciences at the University of Stellenbosch

August 2003

Promotors : Prof. G.W. Milne
Prof. B.V. Bredenkamp

Declaration:

I, the undersigned, hereby declare that the work contained in this thesis is my own original work and has not previously been submitted at any university, in part or in its entirety, for a degree.

Signature Date

ABSTRACT

This study investigates the theory of precision satellite orbit propagation and satellite lifetime prediction and lead to the development of two necessary software tools for analysis in these fields. Precision propagation was achieved through the implementation of Cowell's method of special perturbations, considering perturbations due to a 70x70 asymmetrical gravity field, atmospheric drag, Luni-Solar attraction and Solar radiation pressure. The satellite's perturbed equations of motion were integrated utilizing a seven-eighth order Runge-Kutta-Fehlberg numerical integration procedure, limiting error propagation by employing adaptive step size control. The MSIS-90 atmospheric density model, providing for diurnal and semi-annual variations, was employed to determine atmospheric density. Care was taken in the precision modelling of the motion of the J2000 equator and equinox. Propagation results for this test case proved to be superior to the SGP4 propagator and a commercial package.

The long-term effects of Earth oblateness and atmospheric drag on a satellite's orbital elements were investigated and applied to the orbit decay prediction problem. Orbit decay was predicted by integrating the rates of change of the orbital elements due to Earth oblateness and atmospheric drag. A semi-analytical technique involving Runge-Kutta and Gauss-Legendre quadrature was employed in the solution process. Relevant software was developed to implement the decay theory. Optimum drag coefficients, estimated from drag analysis using precision propagation, were used in decay prediction. Two test cases of observed decayed satellites were used to evaluate the theory. Results for both test cases indicated that the theory fitted observational data well within acceptable limits.

SAMEVATTING

'n Ondersoek is gedoen oor die teorie van presiesie satelliet-wentelbaan vooruitskatting en satelliet-wentelbaanleeftyd afskatting en het gelei tot die ontwikkeling van twee analiseprogramme vir gebruik in hierdie vakgebiede. Presiesie vooruitskatting is bereik deur die gebruik van Cowell se metode van spesiale perturbasies, wat die invloed van 'n nie-simmetriese 70x070 gravitasieveld, atmosferiese sleur, Son-Maan aantrekkingskragte en druk van sonradiasie, in ag neem. Die satelliet se versteurde bewegingsvergelykings is numeries ge-ïntegreer deur gebruik te maak van die sewe-agste orde Runge-Kutta-Fehlberg metode wat fout-voortplanting inhibeer deur gebruik te maak van 'n aanpasbare integrasiestaplengte. Die MSIS-90 atmosferies model, wat voorsiening maak vir dag-nag en half-jaarlikse atmosferiese variasies, is gebruik vir die berekening van atmosferiese digtheid. Sorg is gedra by die presiesie modellering van die beweging van die J2000 ekwator en ekwinokse. Resultate vir hierdie toetsgeval toon meer voortreflik te wees as die SPG4 - en 'n kommersieël-beskikbare vooruitskatter.

Die langtermyn effekte van aard-afplatting en atmosferiese sleur op wentelbaanleeftyd is ondersoek en toegepas op die wentelbaanverval-afskattingsprobleem. Wentelbaanverval is bereken deur die integrasie van die tydsafgeleides van die wentelbaanelement onder invloed van aard-afplatting en atmosferiese sleur. Vir die doel is 'n semi-analitiese tegniek, wat gebruik maak van Gauss-Legendre kwadratuur en Runge-Kutta numeriese integrasie, gebruik gemaak. Nodige rekenaar programmatuur is ontwikkel om die vervalteorie te implimenteer. Optimale sleur-koëffisiënte is afgeskat deur van presiesie wentelbaananalise gebruik te maak. Twee gevallestudies van bekende vervalde satelliete is gebruik om die vervalteorie te evalueer. Resultate vir beide gevallestudies toon aan dat eksperimentele resultate werklike vervaltye binne aanvaarbare limiete navolg.

DEDICATION

To my parents, Ben and Tina Opperman. With deepest appreciation, thank you.

ACKNOWLEDGEMENT

To Proff. Garth Milne and Brian Bredenkamp, my thesis supervisors. Thank you for your support and encouragement, for creating the opportunity of working on the SUNSAT project and for evaluating this thesis.

To the Department of Water Affairs and Forestry for funding Project ST1/94: National Forest Inventory, which led to this thesis. I am greatly indebted to you.

To the personnel at the Forestry Faculty, thanks for the opportunity to have worked with you, the warm atmosphere and open offices. Special thanks to:

> Holger Vogt, my colleague of five years on ST1/94. It was great working with you. Prof. Theo Kleynhans for his wise mentorship and Anton Kunneke, Daleen Opperman and Basjan Van Aardt for those numerous stimulating conversations.

To my *Wifelet* transform, Karina. Thank you for your dedicated support and patience.

Vir Ben-Louis en Philip. Dankie dat Pappa sy boek kon klaarskryf.

To Jesus Christ, my firm foundation.

Table of Contents

Chapter 1

Motivation

1.1 INTRODUCTION

The aim of this study is to:

- Investigate the theories of precision satellite orbit propagation and satellite orbit decay for low Earth orbiting (LEO) satellites and
- Test these theories by developing and implementing relevant algorithms and software and applying them to case studies of observed satellite orbits.

The two topics of precision propagation and decay prediction were treated separately in this study because different propagation theories are involved. The former employs Cowell's method of special perturbations while decay is described by general perturbation techniques as employed in the semi-analytic Liu theory (SALT). Two software tools were developed to implement the respective theories. *Orblitz* employs several comprehensive perturbation models for precision short to medium term (several days or weeks) propagation and *Satdecay* only considers the effects of atmospheric drag and Earth oblateness for predicting satellite lifetime over months and years. Good synergy was achieved between these two tools by utilizing *Orblitz* to estimate accurate atmospheric drag coefficients as required by *Satdecay*.

The performance of *Orblitz* was evaluated against a section of SUNSAT orbit derived from Satellite Laser Ranging measurements. The results were also compared to results achieved by similar commercial and public domain software products for the test case. *Satdecay* was evaluated by comparing predicted decay values for two recently decayed LEO satellites, *Iridium-85* and *Starshine-2* with their observed decay dates. The results obtained by *Satdecay* for these test cases fitted the observed decay dates very well. An expected decay date for SUNSAT was predicted using *Satdecay*.

Throughout this study, special consideration was given to the use of proper time and co-ordinate reference systems, accurate perturbation models and general numerical stability of algorithms. State of the art environmental models were used where possible.

This thesis comprises a historical perspective, problem statement and findings summary (Chapter 1), introduction to two-body motion (Chapter 2), a description of orbit perturbations and their application to orbit propagation (Chapter 3), discussions of time, co-ordinate systems and transformations (Chapter 4), software and programs (Chapter 5), results for precision propagation (Chapter 6), the orbit decay problem (Chapter 7), results for drag analysis and orbit decay (Chapter 8), conclusions and future work (Chapter 9) and several appendices, including programme listings.

1.2 Historical Foundation

One of man's earliest motivations to try to understand the motions of the Sun, Moon, other stars and planets was rooted in his agricultural and religious needs. Other reasons were his need to measure time and later, the use of celestial objects for navigation [Chobotov 1996, Pp 1]. Although ancient civilizations like the Egyptians, Chaldeans and Babylonians contributed significantly to astronomy by their celestial observations and calendars, it is the Greek view of the cosmos that dominated western philosophy for two thousand years [Vallado 1997, Pp 2]. Aristotelian cosmology remained unaffected up to the Middle Ages, when it was challenged and upset by the likes of Copernicus, Galileo and Kepler. The quest for explaining the motion of celestial bodies ultimately succeeded and was epitomized in the laws of Newton.

The launch of Sputnik I ushered in the Space Age and revolutionized our perception of the use of space. Advances in rocket science and telemetry made it possible to place sensors into orbit and relay useful information back to Earth [Vallado 1997]. By mid twentieth century, man had developed the means to address some of his ancient needs through his understanding of celestial mechanics and by employing his technological prowess.

Today, thousands of artificial satellites and launch remnants fill the Earth's ex-atmospheric gravitational sphere of influence. Because of the high velocities at which space objects travel (typically greater than $7km.s^{-1}$), precise knowledge of their positions and velocities at any given time is required to successfully manage operations such as remote sensing missions, accurate antennae pointing and space debris monitoring where millisecond errors translate to large distances on the Earth's surface. This requirement for precision is the motivation for this study.

Because of the rich history behind the formulation of the laws that govern the movement of gravity-attracted objects, a short overview on the milestones in the evolution of the philosophies that shaped our view of the universe, is given before proceeding to a formal treatise of the fundamentals [Bergamini 1965, Bate *et al.* 1971, Chobotov 1996, Vallado 1997].

1.2.1 Aristotle of Stagyra (384-322 BC)

The Earth is the fixed centre of the universe and the Sun and planets move around the Earth. Circular motion is the only perfect and natural motion and heavenly bodies, therefore necessarily move in circles. Common sense dictated that Aristotle must be right as nobody was being flung off into space [due to a rotating Earth].

1.2.2 Aristarchus the Heliocentric (300 BC)

The Sun and the stars are fixed and the Earth revolves in a circular orbit around the Sun. Although this thinking was as close to the truth as our modern day understanding of planetary movement (elliptical orbits), it was set aside for the more popular Aristotelian theory that was to dominate scientific philosophy for the next 2000 years.

1.2.3 Hipparchus (130 BC)

Hipparchus introduced the epicyclical motion of the planets to explain the apparent deviation of planets' motion from a perfect circle. *Each planet is fixed to a rotating sphere of crystal, which revolves around the stationary Earth. Combinations of spheres within spheres rotating in different directions produce the complex paths of the planets across the sky.*

1.2.4 Ptolemy (150 AD)

Ptolemy further developed the epicycle theory of Hipparchus as the principal theory for *predicting* the motions of the planets. Although there were no physical principles on which to base the motions, some of the results obtained from this theory (e.g. the rise and set of planets) were very accurate. The Ptolemean model of cosmology remained unchallenged until the Middle Ages.

1.2.5 Nicholas Copernicus (1473-1543)

Copernicus postulated a model with the Sun at the centre of the universe with the planets moving in epicycles around the Sun and the Moon moving around the Earth and hypothesized that the stars lay on a sphere with very large radius. His theory could explain the retrograde movements of the planets, but relied on Ptolemy's model to match *observations.* Copernicus was the first to advance a consistent system with a *moving* Earth although his theory was erroneous and non-revolutionary. One of the very few people, who read Copernicus' book, *On the Revolutions of the Heavenly Spheres,* was a German astronomer, Johannes Kepler.

1.2.6 Johannes Kepler (1571-1630)

Kepler joined Tycho Brahe (1546-1601), Danish royal astronomer in Prague in 1598 and was set to work on the orbit of the planet Mars. After Tycho's death in 1601, Kepler succeeded him as director and spent the following years trying to fit various geometrical curves to Tycho's accurate and meticulously collected data on the position of Mars. In 1606, he found the orbit to be an *ellipse* and in 1609 published his first two laws of planetary motion with the third law following in 1619. These laws marked an epoch in the history of mathematical science.

> **First Law**: The orbit of a planet is an ellipse, with the Sun at a focus.
> **Second Law**: The line joining the planet to the Sun sweeps out equal areas in equal times.
> **Third Law**: The square of the period of a planet is proportional to the cube of its mean distance from the Sun.

Kepler alone challenged Aristotle's belief that perfect planets could only move in perfect circles. Although Kepler's laws changed our view of the universe, his laws

were still only a *description* and not an *explanation* of planetary motion and it remained for the genius of Isaac Newton to unravel the mystery of *why*.

1.2.7 Changing the Aristotelian view

While Kepler's work set the stage for the appearance of Newton, a few other individuals contributed to the change of the Aristotelian view and the development of mathematics, which were to have a profound influence on the reasoning of Newton.

1.2.7.1 Galileo Galilei (1564-1642)

Galileo patented the telescope with which he observed the non-"crystalline perfection" of the heavens, causing him to refute Aristotelian cosmology in *The System of the World in Four Dialogues.* He supported Copernicus' heliocentric system, but rejected Kepler's view of planetary motion. He also proved that heavy and light bodies fall at the same speed and that no body could be flung off the Earth's surface by its rotation.

1.2.7.2 Rene Descartes (1596-1650).

Descartes succeeded in unifying the two main branches of mathematics *viz. algebra* and *geometry* by developing *analytic geometry.* He linked the familiar figures of Euclidean geometry; lines, polygons and other conic sections, to correspond to algebraic equations by introducing *Cartesian co-ordinates.* Analytical geometry was to be the basic tool used by Newton to develop calculus and formulate his famous laws.

1.2.7.3 John Napier (1550-1617)

Napier discovered logarithms by which all multiplication and division could be reduced to adding and subtracting. This resulted in increased speed and accuracy of complex and tedious calculations.

1.2.8 Isaac Newton (1642 – 1727)

During 1666, Newton conceived the law of gravitation and the laws of motion and developed the fundamental concept of differential calculus. In 1687, he published *The Mathematical Principles of Natural Philosophy* (The *Principia*), in which he formulated the law of gravity and the three laws of motion.

First Law of Motion: Any body continues in its state of rest or of uniform motion in a straight line unless it is compelled to change its state by forces impelled on it.

Second Law of Motion: The rate of change of momentum is proportional to the force impressed and is in the same direction as that force.

Third Law of Motion: To every action there is always an opposite, but equal reaction.

Law of Gravity: Any two bodies in the universe attract one another with a force that is directly proportional to the product of their masses and inversely proportional to the square of the distance between them.

After Newton, other great men like Euler (1707-1783), Lambert (1728-1779), Lagrange (1736-1813), Laplace (1749-1827) and Gauss (1777-1855) contributed significantly to topics of celestial mechanics. Newtonian mechanics remained virtually unchanged until Einstein (1879-1953) redefined gravity, time and space in his formulation of general and special relativity in the twentieth century.

1.3 Modern Era

Whilst the basic theory for orbit determination has remained virtually unchanged over the last centuries, the means for obtaining precision measurements of celestial bodies and artificial satellites have improved significantly.

The first satellites were fitted with an Inertial Measurement Unit (IMU), consisting of a gyroscopic-stabilized platform and three accelerometers to supply a means of reference and acceleration measurement. Velocity and position were subsequently derived by numerical integration of the measured acceleration, rendering accuracy of several metres. Satellites were also tracked by terrestrial-based radar and Doppler stations to determine position and velocity, a method still in use today.

Modern satellites fitted with Global Positioning System (GPS) receivers obtain centimetre accurate position fixes from a constellation of GPS satellites. Where

millimetre accuracy of a satellite orbit is required, Satellite Laser Ranging (SLR) is employed.

Since the mid-eighties, radar-derived mean orbital elements of thousands of satellites are regularly updated and distributed by NASA/Goddard Space Flight Center as Two Line Element (TLE) sets for use with the public domain SGP4 software. Though useful for general orbit propagation, TLE's contain inherent errors, which are compounded by the SGP4-theory. SGP4-propagation results subsequently lack sufficient accuracy for conducting precision orbit analysis.

1.4 Problem Statement

The development of precision propagation models is a complex task and computer source code and techniques are generally closely guarded. High-end commercial off-the-shelf (COTS) software packages are available at a price, but are packaged as "black box" systems, which do not allow for customized application development, e.g. development of embedded software. Whilst source code is available for the widely used SGP4 propagator, it implements an application-specific theory and subsequently lacks flexibility. SGP4-inputs are furthermore restricted to TLE-specific mean orbital elements, which are compliant with the underlying theory. In either case, results from COTS and SGP4 have to be taken at face value and believed as such. These restrictions and shortcomings subsequently necessitated the development of an in-house, state of the art precision propagator with a modular design, allowing for flexibility and a wide range of applications.

The purpose of this study is to determine how accurate a low earth orbit satellite's orbit can be predicted up to ten days into the future and how well the predicted lifetime and expected decay dates of two LEO satellites compare with their observed decay dates.

1.5 Methodology

Propagation of the satellite's orbit was achieved by numerically integrating a system of second order differential equations describing the perturbed acceleration of a satellite in an inertial system. The total acceleration comprised the sum total of the

accelerations due to a non-spherical Earth, atmospheric drag, solar radiation pressure and third body attractions. The effects of nutation, precession and polar motion were accounted for in the motion of the reference frame and a switching function compensated for Earth eclipsing effects in solar radiation pressure.

For the purpose of this study, a FORTRAN computer programme, *Orblitz*, was developed, integrating existing theories with state of the art environmental models. The development of the propagator and subsequent implementation in a computer programme was a complex, time intensive process and involved the coding of numerous software modules and the integration of various state of the art environmental models and complex numerical algorithms. Extensive work has been done in sourcing and adapting state of the art numerically stable models and parameters for calculating atmospheric density, gravitational acceleration, Earth rotation, precession and nutation, various time and co-ordinate transformations, shadow conditions and third-body attractions. Extensive work has been done in sourcing, cleaning and formatting relevant environmental data. The result was source code compiled into a high-end precision propagator.

The accuracy of the propagator was evaluated by comparing it with a ten-day section of SLR-measured orbit of the SUNSAT micro satellite and to simulated results from the SGP4 propagator and results from a COTS package. In addition, *Orblitz* was successfully employed to estimate accurate drag coefficients for the satellites in the test case using TLE-derived state vectors as reference. An existing FORTRAN programme accompanying the SALT documentation [Alford and Liu May 1974] was adapted for use in the test cases.

Results indicated that data fitted the in-house developed O*rblitz* programme better than the SGP4 and COTS software for this test case. Similarly, results indicated that predicted decay data compared well with observed decay dates of the satellites in the test case.

Chapter 2

Equations of Motion

(The section following is a synthesis of the work by [Bate *et al.* 1971, Chobotov 1996, Vallado 1997])

2.1 INTRODUCTION

Satellite orbits take the form of one of three conic sections, *viz.*, the *ellipse, parabola* and *hyperbola*. Orbits taking the form of the latter two conic sections are usually associated with interplanetary probes and special classes of asteroids and meteorites and will not be further considered in this study. This section deals with the *dimension* of an elliptic orbit, which reveals information on the *energy* and *velocity* of a satellite. The elliptic orbit's *propagation* and *orientation* in space are discussed in greater detail in Chapters 3 and 4 respectively.

2.2 THE RESTRICTED TWO-BODY PROBLEM

A general expression for the relative motion of two bodies perturbed by other bodies (the *N*-body problem), is developed in Appendix A and given in **Equation 2.1.**

$$\ddot{\mathbf{r}}_i = -G\sum_{\substack{j=1 \\ j\neq i}}^{N} \frac{m_j}{r_{ji}^3}\mathbf{r}_{ji} + \mathbf{F}_{\text{Other}} \qquad \textbf{2.1}$$

Where

$\ddot{\mathbf{r}}_i$ = Acceleration vector of the ith body relative to the X, Y, Z co-ordinate system.

m_i: = Mass of the ith body.

$\mathbf{F}_{\text{Other}}$ = Other external forces due to atmospheric drag, thrust, non-spherical perturbations etc.

G = Gravitational constant, $6.672\text{x}10^{-11}\text{m}^3\text{kg}^{-1}\text{s}^{-2}$

$\mathbf{r}_{ji}$ = $\mathbf{r}_i - \mathbf{r}_j$

From **Equation 2.1** the restricted equation for two-body motion is developed under the following assumptions:

1. The bodies are spherical symmetric, allowing them to be considered point masses.
2. There are no external forces acting on the system other than the gravitational forces acting along the line joining the centres of the two bodies.
3. The two bodies move in an inertial (un-accelerated and non-rotating) reference frame, X, Y, Z.

Consider the system of two bodies of masses M and m as illustrated in **Figure 2.1**. Their position vectors with respect to the inertial frame are $\mathbf{r}_M$ and $\mathbf{r}_m$ respectively.

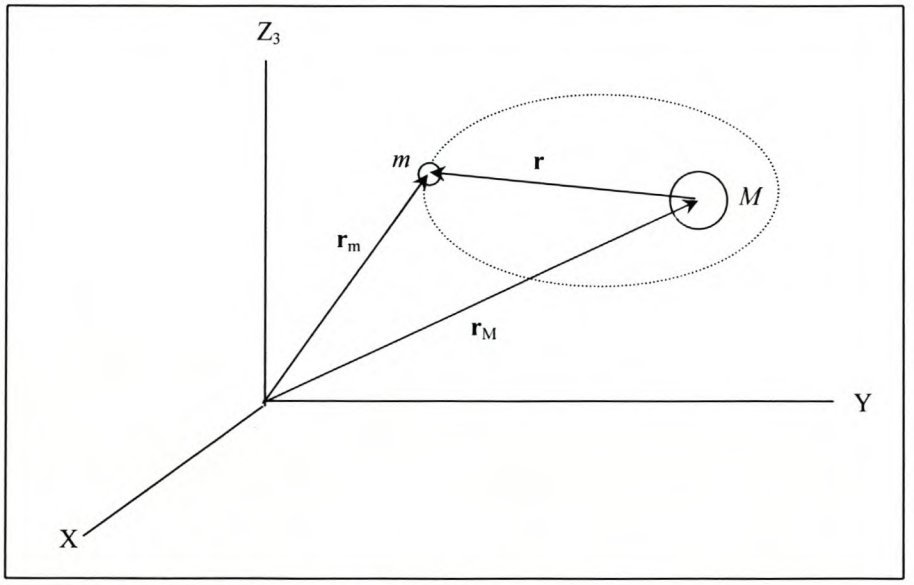

Figure.2.1. Relative Motion of Two Bodies.

By applying Newton's second law and law of gravitation (Appendix A), it can be shown that

$$\ddot{\mathbf{r}} = -\frac{G(M+m)}{r^3}\mathbf{r} \qquad \textbf{2.2}$$

Where

$\mathbf{r}$ = $\mathbf{r}_m$ - $\mathbf{r}_M$. Position of body m relative to M.

G = Gravitational constant, $6.672\text{x}10^{-11}\text{m}^3\text{kg}^{-1}\text{s}^{-2}$

M = Mass of the Earth $5.9742 \text{ x } 10^{24}$ kg

m = Mass of satellite.

In a restricted two-body problem, the principal mass, M is assumed fixed in inertial space and $M >> m$, so that m does not affect the motion of M. Subsequently $G(M + m) \cong GM$. Define the *gravitational* parameter,

$$\mu = GM \ (= 398600.4415 \ \text{km}^3.\text{s}^{-2})$$

Then **Equation 2.2** becomes

$$\ddot{\mathbf{r}} + \frac{\mu}{r^3}\mathbf{r} = \mathbf{0} \qquad \textbf{2.3}$$

Equation 2.3 is known as the *two-body equation of motion* and represents the motion of a mass m in a gravitational field of mass M.

2.3 CONSTANTS OF MOTION

The gravitational field is *conservative* [Sears *et al.* 1982, Pp 494-497], implying that an object moving under the influence of gravity alone does not lose or gain mechanical energy, but only converts one form of energy to another (i.e. *kinetic* <=> *potential* energy).

2.3.1 Conservation of Mechanical Energy

By dot multiplying **Equation 2.3** by $\dot{\mathbf{r}}$, some manipulation and simplification (As shown in Appendix A), the equation for *specific mechanical energy* is found to be

$$\frac{v^2}{2} - \frac{\mu}{r} = E = \text{constant} \qquad \textbf{2.4}$$

The first term in **Equation 2.4** is the *kinetic energy per unit mass* of the satellite and the second term the *specific potential energy per unit mass*. The specific potential energy is equal to the *gravitational potential per unit mass*. From **Equation 2.4** it is evident that when the kinetic energy increases (closer to the Earth), the potential energy decreases and when the satellite's speed is at it lowest (farthest from Earth) its potential energy is at its highest; the sum total of the two terms remaining constant.

2.3.2 Conservation of Angular Momentum.

The specific angular momentum of a satellite is obtained by cross-multiplying **Equation 2.3** by **r** and some manipulation. It is found (Appendix A) that

$$\frac{d}{dt}(\mathbf{r}\times\mathbf{v})=\mathbf{0}$$

Or

$$\mathbf{h}=\mathbf{r}\times\mathbf{v} \qquad \textbf{2.5}$$

The vector **h** is called the *specific angular momentum* of the satellite. Because $d\mathbf{h}/dt$ = **zero,** it implies that the specific angular momentum of a satellite remains constant along its orbit. Since **h** is the cross product of **r** and **v**, it must be perpendicular to the plane that contains **r** and **v**. However, as **h** is constant, **r** and **v** always remain in the same plane. The satellite's motion is therefore confined to a plane fixed in space.

2.3.3 The Trajectory Equation.

It can be shown (Appendix A) that by integrating **Equation 2.3**, the following partial solution for the position of the satellite is obtained (in polar co-ordinates).

$$r=\frac{p}{1+e\cos\nu} \qquad \textbf{2.6}$$

This solution is useful for describing the dimension and shape of the orbit.

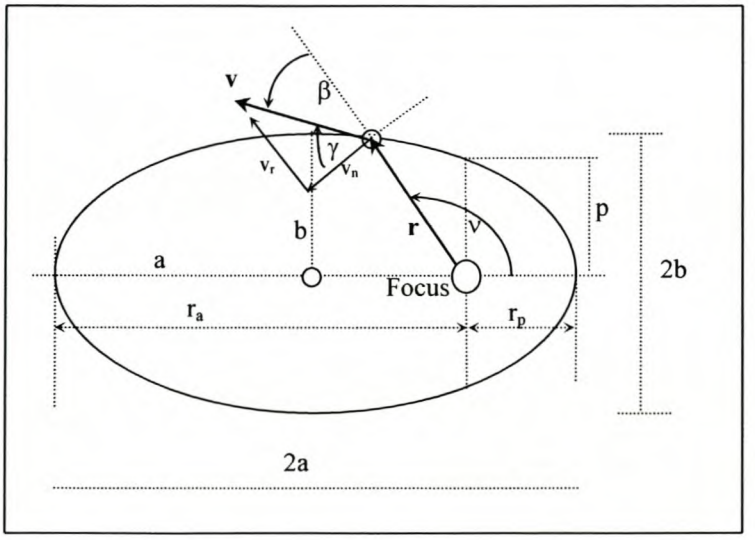

Figure. 2.2. Geometry of the ellipse

Table 2.1 Parameters defining geometry of an ellipse.

Parameter	Description	Equation	Remark
a	*Semi major axis*	$a = \frac{r_a + r_p}{2}$	
b	*Semi minor axis*	$b = \sqrt{a^2(1-e^2)}$	
e	*Eccentricity*	$e = \frac{r_a - r_p}{r_a + r_p}$	$e = 0$: *circle* $0 < e < 1$: *ellipse* $e = 1$: *parabola* $1 < e < \infty$: *hyperbola*
ν	*True anomaly*		
r_a	***Apogee radius***	$r_a = a(1+e)$	
r_p	*Perigee radius*	$r_p = a(1-e)$	
p	*Semi-latus rectum*	$p = a(1-e^2)$ $= r_p(1+e)$ $= r_a(1-e)$	
γ	*Flight path angle*	$\gamma = \pi/2 - \beta$	
h	***Angular momentum***	$h = r\nu Cos\gamma$	
v_r	***Radial velocity component***	$v_r = \sqrt{\frac{\mu}{p}} eSin\nu$	
v_n	***Normal velocity component***	$v_n = \sqrt{\frac{\mu}{p}}(1 + eCos\nu)$	
n	***Mean motion***	$n = \sqrt{\frac{\mu}{a^3}}$	
P	*Orbital period*	$P = 2\pi/n$	
M	*Mean anomaly*	$M = (t - T)$	T, t : *Time of perifocal passing, time of required position*
r	*Trajectory equation*	$r = \frac{p}{1 + \cos\nu}$	

2.4 POSITION AND VELOCITY AS FUNCTION OF TIME

At any epoch, t_0, a satellite's Cartesian co-ordinates (x_0, y_0) are obtained from its polar co-ordinates (**Equation 2.6**) by

$$\begin{bmatrix} x_0 \\ y_0 \end{bmatrix} = r_0 \begin{bmatrix} \cos \nu_0 \\ \sin \nu_0 \end{bmatrix} \qquad \textbf{2.7}$$

It is evident from **Equations 2.6** and **2.7**, that the angular displacement of true anomaly ($\Delta \nu$) is needed to determine a satellite's future (or past) position at time $t = t_0 + \Delta t$. The problem of relating angular displacement with time is addressed by employing Kepler's second law. This is accomplished by introducing two variables, E and M, which describe time-varying uniform and non-uniform circular motion respectively, from which expressions for ν are developed.

An auxiliary circle is constructed on the elliptical orbit, as indicated in **Figure 2.3** and the eccentric anomaly, E, is defined as the angle spanning perifocus and the satellite's projected position, P', on the auxiliary circle. Like ν, E traces a locus of non-uniform motion.

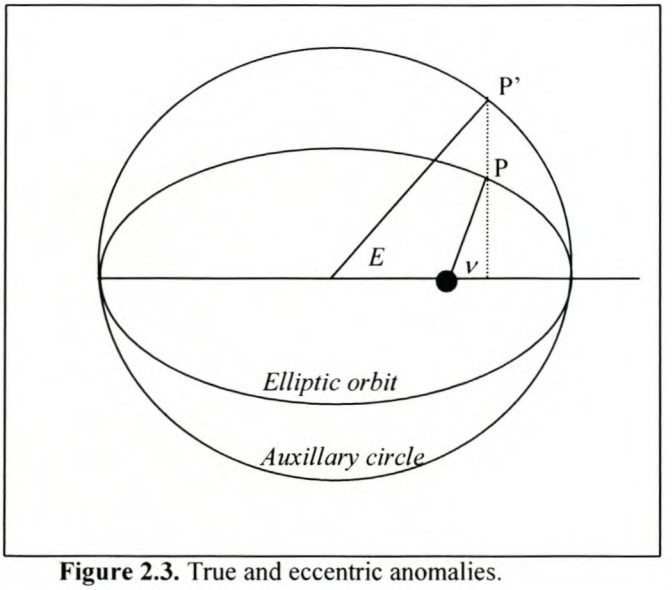

Figure 2.3. True and eccentric anomalies.

2.4.1 Time-dependent Position as Function of Anomalies

At any time t, the *eccentric anomaly*, E, is related to the true anomaly, ν,

[Bate *et al.* 1971, Pp 181-190; Escobal 1985, Pp 213-217; Vallado 1997, Pp 213-215]

by

$$E = \tan^{-1}\left(\frac{\sin E}{\cos E}\right) \qquad \textbf{2.8}$$

Where

$$\sin E = \frac{\sqrt{1-e^2}\sin\nu}{1+e\cos\nu}$$

$$\cos E = \frac{e+\cos\nu}{1+e\cos\nu} \qquad \textbf{2.9}$$

A direct relationship is obtained by employing the tangent half-angle formula

$$\tan\left(\frac{E}{2}\right) = \frac{\sqrt{1-e}}{\sqrt{1+e}}\tan\left(\frac{\nu}{2}\right) \qquad \textbf{2.10}$$

(See Appendix B for development of these equations)

By employing Kepler's second law of motion, the time-dependence of the eccentric anomaly, E, is established through *Kepler's equation*

$$n(t-T) = E - e\sin E \qquad \textbf{2.11}$$

Where

n	=	Mean motion (See **Table 2.1**)
T	=	Time of perifocal passage

(At time of perifocal passage, T, $\nu = E = M = 0°$.)

The term on the left of **Equation 2.11** defines the orbit's mean anomaly, M, which describes uniform motion along another auxiliary circle

$$M = n(t - T) \qquad \textbf{2.12}$$

Kepler's equation (**Equation 2.11**) is a transcendental function and is solved by means of iteration. By assuming some starting value for E_0 and employing the Newton-Raphson iteration technique [Vallado 1997, Pp 231-232], iteratively calculate

$$E_{n+1} = E_n - \frac{E_n - e\sin E_n - M}{1 - e\cos E_n} \qquad \textbf{2.13}$$

until $|E_{n+1} - E_n|$ vanishes. Assign $E = E_{n+1}$.

The satellite's position and velocity vectors, (**r**, **v**), are subsequently expressed in terms of the eccentric anomaly, E, by the following relations [Escobal 1985, Pp 85]:

$$\begin{aligned} x &= a(\cos E - e) \quad y = a\sqrt{1-e^2}\sin E \\ &, \qquad \textbf{2.14} \\ \dot{x} &= -a\dot{E}\sin E \qquad \dot{y} = a\dot{E}\sqrt{1-e^2}\cos E \\ \dot{E} &= \frac{1}{r}\sqrt{\frac{\mu}{a}} \\ \mathbf{r} &= [x, y] \\ \mathbf{v} &= [\dot{x}, \dot{y}] \end{aligned}$$

The position and velocity may also be expressed in terms of the true anomaly by

$$\begin{aligned} x &= r\cos\nu, \quad \dot{x} = -\frac{\sqrt{\mu}}{p}\sin\nu \\ y &= r\sin\nu, \quad \dot{y} = \frac{\sqrt{\mu}}{p}(e + \cos\nu) \end{aligned} \qquad \textbf{2.15}$$

2.4.2 Propagation

The problem of determining a satellite's future (or past) position and velocity by using values determined at some epoch, t_0, is called *Kepler's problem*. By expressing **Equation 2.12** for some epoch t_0, it can be shown [Escobal 1985 Pp 92-93]that the mean anomaly M, at time

$t = t_0 + \Delta t$, is given by

$$\begin{aligned} M - M_0 &= n(t - t_0) \\ &= \Delta E + 2S_e \sin^2\left(\frac{\Delta E}{2}\right) - C_e \sin \Delta E \end{aligned} \qquad \textbf{2.16}$$

Where

$$\begin{aligned} \Delta E &= E - E_0 \\ S_e &= e \sin E_0 \\ C_e &= e \cos E_0 \end{aligned} \qquad \textbf{2.17}$$

By solving **Equation 2.13** for ΔE, the new eccentric anomaly, E, can be obtained and (**r**, **v**) calculated from **Equation 2.14**.

Another (closed-form) solution for Kepler's problem, developed by Lagrange, is also presented because of its simplicity and robustness and its importance in Kalman filtering estimation.

2.4.3 *f* and *g* series

A solution for Kepler's problem is obtained by introducing two scalar functions, f and g and propagating the epoch solution to time t by

$$\begin{aligned} \mathbf{r} &= f\mathbf{r}_0 + g\mathbf{v}_0 \\ \mathbf{v} &= \dot{f}\mathbf{r}_0 + \dot{g}\mathbf{v}_0 \end{aligned} \qquad \textbf{2.18}$$

The functions f, g and their derivatives, are defined as functions of eccentric anomaly by

$$\begin{aligned} f &= 1 - \frac{a}{r_0}\left[1 - \cos(E - E_0)\right] \\ g &= (t - t_0) - \sqrt{\frac{a^3}{\mu}}\left[(E - E_0) - \sin(E - E_0)\right] \end{aligned} \qquad \textbf{2.19}$$

$$\dot{f} = \frac{-\sqrt{a\mu}\sin(E - E_0)}{rr_0}$$

$$\dot{g} = 1 - \frac{a}{r}(1 - \cos(E - E_0))$$

The following, numerically stable algorithm employing the *f* and *g* series, is proposed by [Escobal 1985, Pp 423-429]

Given starting values $\mathbf{r}_0$, $\mathbf{v}_0$ at time t_0, find values **r**, **v** at some future (or past) time, *t*. Calculate, in sequence

$$r_0 = |\mathbf{r}_0| \qquad \textbf{2.20}$$

$$D_0 = \frac{\mathbf{r}_0 \bullet \mathbf{v}_0}{\sqrt{\mu}} \qquad \textbf{2.21}$$

$$\left[\frac{V_0^2}{\mu}\right] = \frac{\mathbf{v}_0 \bullet \mathbf{v}_0}{\mu} \qquad \textbf{2.22}$$

$$\frac{1}{a} = \frac{2}{r_0} - \left[\frac{V_0^2}{\mu}\right] \qquad \textbf{2.23}$$

$$e^2 = \left(1 - \frac{r_0}{a}\right)^2 + \frac{1}{a}D_0^2 \qquad \textbf{2.24}$$

$$p = r_0\left(2 - \frac{r_0}{a}\right) - D_0^2 \qquad \textbf{2.25}$$

$$2q = 2r_0 - D_0^2 \qquad \textbf{2.26}$$

$$C_e \equiv [e\cos E_0] = 1 - \frac{r_0}{a} \qquad \textbf{2.27}$$

$$S_e \equiv [e\sin E_0] = \frac{D_0}{\sqrt{a}} \qquad \textbf{2.28}$$

$$M - M_0 = \sqrt{\frac{\mu}{a^3}}(t - t_0) \qquad \textbf{2.29}$$

Solve Kepler's equation for *g* using Newton-Raphson iteration in the form

$$g_{n+1} = g_n - \frac{g_n + S_e\sin^2 g_n - C_e\sin g_n\cos g_n - \frac{1}{2}(M - M_0)}{1 + 2S_e\sin g_n\cos g_n - C_e(1 - 2\sin^2 g_n)} \qquad \textbf{2.30}$$

$$E_0 - E = 2g \qquad \textbf{2.31}$$

$$C = a[1 - \cos(E - E_0)] \quad \textbf{2.32}$$

$$S = \sqrt{a}\sin(E - E_0) \quad \textbf{2.33}$$

$$f = 1 - \frac{C}{r_0} \quad \textbf{2.34}$$

$$g = \frac{1}{\sqrt{\mu}}(r_0 S + D_0 C) \quad \textbf{2.35}$$

$$r = r_0 + \left(1 - \frac{r_0}{a}\right)C + D_0 S \quad \textbf{2.36}$$

$$\dot{f} = -\frac{\sqrt{\mu}}{r r_0} S \quad \textbf{2.37}$$

$$\dot{g} = 1 - \frac{C}{r} \quad \textbf{2.38}$$

$$\mathbf{r} = f\mathbf{r}_0 + g\mathbf{v}_0 \quad \textbf{2.39}$$

$$\mathbf{v} = \dot{f}\mathbf{r}_0 + \dot{g}\mathbf{v}_0 \quad \textbf{2.40}$$

2.5 Transforming between Cartesian and Kepler Elements

To visualize the orientation of the orbit in space, the orbital (Kepler) elements, [*a, e, i, ω, Ω*], are calculated from (**r**, **v**) using the following algorithm [Bate *et al.* 1971, Pp 61-63].

Given position and velocity vectors **r** and **v**, form three vectors **h, n** and **e**:

$$\mathbf{h} = \mathbf{r} \times \mathbf{v} = h_1\mathbf{I} + h_2\mathbf{J} + h_3\mathbf{K} \quad \textbf{2.41}$$

$$\mathbf{n} = \mathbf{K} \times \mathbf{h} = h_2\mathbf{I} - h_1\mathbf{J} \quad \textbf{2.42}$$

$$\mathbf{e} = \frac{1}{\mu}\left[\left(v^2 - \frac{\mu}{r}\right)\mathbf{r} - (\mathbf{r} \bullet \mathbf{v})\mathbf{v}\right] \quad \textbf{2.43}$$

Where

h = Angular momentum, normal to the orbital plane

n = Node vector, pointing along the line of nodes in the direction of the ascending node.

e = Eccentricity vector, pointing from the centre of the Earth towards perigee with a magnitude equal to the orbit's eccentricity.

The calculation of the orbital elements are accomplished using the equations summarised in **Table 2.2**

Table 2.2. Transforming position and velocity vectors to Kepler elements

Kepler element	**Equation**	**Remark**
Semi major axis (a)		
Semi-latus rectum (p)	$p = \frac{h^2}{\mu}$	
Eccentricy (e)	$e = \lvert\mathbf{e}\rvert$	
Inclination (i)	$\cos i = \frac{h_3}{h}$	$i < 180°$
Longitude of ascending node	$\cos\Omega = \frac{n_3}{n}$	*If* $n_2 > 0$, $\Omega < 180°$
Argument of perigee (ω)	$\cos\omega = \frac{\mathbf{n} \bullet \mathbf{e}}{ne}$	*If* $e_3 > 0$, $\omega < 180°$
True anomaly (ν)	$\cos\nu = \frac{\mathbf{e} \bullet \mathbf{r}}{er}$	*If* $\mathbf{r} \bullet \mathbf{v} > 0$, $\nu < 180°$
Argument of latitude (u)	$\cos u = \frac{\mathbf{n} \bullet \mathbf{r}}{nr}$	*If* $n_2 > 0$, $u < 180°$
True longitude (l)	$l = \Omega + \omega + \nu$	$u = \omega + \nu$

The inverse transformation to the perifocal co-ordinate system is accomplished by [Bate *et al.* 1971, Pp 73]

$$\mathbf{r} = r\cos\nu\mathbf{P} + r\sin\nu\mathbf{Q} \qquad \textbf{2.44}$$

$$\mathbf{v} = \sqrt{\frac{\mu}{p}}\left[-\sin\nu\mathbf{P} + (e + \cos\nu)\mathbf{Q}\right]$$

Transformation between co-ordinate frames is accomplished through relevant co-ordinate transformations as discussed in Chapter 4.

The equations developed in this chapter serve as illustration for understanding two-body mechanics. Though useful for initial orbit determination, two-body propagation does not render results sufficiently accurate for precision applications. Chapter 3 will build on the foundations laid in this chapter to arrive at an algorithm for precision orbit propagation accounting for orbit perturbations.

Chapter 3

Orbit Perturbations

3.1 INTRODUCTION

The elliptical orbit of a near-Earth satellite would remain constant in size and shape in a plane fixed relative to the stars if the Earth were spherical, had no atmosphere and were isolated from other bodies in the solar system. Though it remains a good first-order approximation, the actual elliptic orbit of a near-Earth satellite is perturbed by the effects of the following forces [King-Hele 1987, Pp 5]:

- Departure of the Earth's gravitational attraction from spherical symmetry because of the flattening of the Earth at the poles, the bulge at the equator and the asymmetry caused by the Earth's "pear-shape"
- Atmospheric drag arising from the satellite's rapid movement through the rarefied upper atmosphere.
- Luni-solar forces constituting the gravitational attraction of the Sun and Moon and solar radiation pressure.
- Other, smaller forces such as planetary gravitational attraction and geomagnetic influences.

The equation of motion for the two-body problem with perturbations is given by

$$\ddot{\mathbf{r}} = -\frac{\mu}{r^3}\mathbf{r} + \mathbf{a}_p \qquad \textbf{3.1}$$

Where

μ = Earth gravitational parameter

$\mathbf{r}$ = Satellite position vector

$\mathbf{a}_p$ = Perturbative accelerations.

The aim of this chapter is to accurately model these perturbations and expand on the two-body equations of motions to develop an accurate orbit propagator.

3.2 PERTURBATION TECHNIQUES

When developing an accurate orbit propagator these perturbative effects have to be considered in detail. The following two techniques are commonly employed for addressing these perturbative effects [Bate *et al.* 1971, Chapter 9; Escobal 1985, Chapter 10; Vallado 1997, Chapters 7, 8].

3.2.1 General Perturbation Techniques

General perturbation techniques replace the original equations of motion with an analytical approximation. This approximation captures the essential character of the motion over some limited time interval and permits analytical integration. General perturbation techniques are used to investigate the qualitative effects of perturbations on the orbit by studying the effects of perturbations in slowly changing (Keplerian) variables, which reflect the size, shape and orientation of the orbit over time. General perturbation techniques are generally computationally economic, but to the cost of accuracy because of truncation in approximations. General perturbation techniques and their application to the orbit decay problem are discussed in more detail in Chapter 7.

3.2.2 Special Perturbation Techniques

Special perturbation techniques numerically integrate the equations of motion inclusive of all necessary perturbing accelerations. These techniques render very accurate results, but to the cost of computing time and the gradual build-up of round-off and truncation errors due to fixed computer word-length. This causes numerical solutions to degrade with increased propagation periods. Special care has been taken in this study to select a cost efficient and numerically stable integration algorithm for arriving at an accurate solution.

As special perturbation techniques form the kernel of this study, they are subsequently discussed in more detail.

3.2.2.1 Encke's Method

In Encke's method, the difference between the primary acceleration and all perturbing accelerations is integrated. A reference (conic section) orbit in an ideal Newtonian gravity field is introduced by calculating a two-body orbit from the actual position and velocity vectors at any epoch, t_0. This reference orbit is called an *osculating* (kissing) orbit because it coincides with the true orbit at t_0. This osculating orbit is the orbit that would result should all perturbing accelerations be removed at epoch t_0. Let the equation of motion for the osculating orbit be

$$\ddot{\boldsymbol{\rho}} = -\frac{\mu}{\rho^3}\boldsymbol{\rho} \qquad \textbf{3.2}$$

and define the departure from this reference orbit as

$$\delta\mathbf{r} = \mathbf{r} - \boldsymbol{\rho} \qquad \textbf{3.3}$$

where $\mathbf{r}$ satisfies the true orbit equation of motion. Differentiation renders

$$\delta\ddot{\mathbf{r}} = \mu\left(\frac{\boldsymbol{\rho}}{\rho^3} - \frac{\mathbf{r}}{r^3}\right) + \mathbf{a}_p \qquad \textbf{3.4}$$

The difference between the two orbit accelerations is integrated until the positional difference exceeds a predefined tolerance. At that point a new osculating orbit is determined, a process called rectification and the integration is continued.

3.2.2.2 Cowell's method

Cowell's method of special perturbations simply involves writing down the satellite's equations of motion, including all the perturbations and then step-wise numerically integrating them. **Equation 3.1.** constitutes a second-order non-linear differential equation, which may be written as two coupled first-order non-linear differential equations

$$\dot{\mathbf{r}} = \mathbf{v}$$

$$\dot{\mathbf{v}} = -\frac{\mu}{r^3}\mathbf{r} + \mathbf{a}_p \qquad \textbf{3.5}$$

Where

$\mathbf{r}, \mathbf{v}$ = Satellite's position and velocity vectors

Cowell's method is simpler in formulation and implementation and more accurate, but is computationally more intensive and significantly slower than Encke's method. As the selection of perturbation technique for this study is driven by accuracy requirements, Cowell's technique of handling orbit perturbations was selected above that of Encke. The remainder of this chapter is dedicated to describing and formulating perturbative accelerations and their subsequent numerical integration.

3.3 Gravity Potential

For two-body motion it can be shown that the acceleration of a satellite orbiting a central, spherical symmetrical homogeneous mass, is given by [Escobal 1985, Pp 45; Vallado 1997, Pp 471-472]

$$\ddot{\mathbf{r}}_{2-body} = \nabla \Phi_{2-body} \qquad \textbf{3.6}$$

Where

$\Phi_{2-body} = -\frac{\mu}{r^3}\mathbf{r}$, the *gravitational potential* of a spherical central body

With

∇ = Gradient vector operator (del) taking partial derivatives in each of the respective axes.

Similar to the two-body reasoning, the acceleration of a satellite due to the Earth's asphericity can be obtained by taking the gradient of a potential function, Φ, of the aspherical Earth [Escobal 1985, Pp 45-52; , NIMA 1997; Vallado 1997, Pp 492].

$$\ddot{\mathbf{r}} = \nabla \Phi \qquad \textbf{3.7}$$

Where the potential function,Φ is defined by

$$\Phi = \frac{\mu}{r}\sum_{n=0}^{\infty}\sum_{m=0}^{n}\left(\frac{R_e}{r}\right)^n P_{nm}[\sin\phi_{sat}]\{C_{nm}\cos m\lambda_{sat} + S_{nm}\sin m\lambda_{sat}\}$$
$$= \frac{\mu}{r}\left[1 + \sum_{n=2}^{\infty}\sum_{m=0}^{n}\left(\frac{R_e}{r}\right)^n P_{nm}[\sin\phi_{sat}]\{C_{nm}\cos m\lambda_{sat} + S_{nm}\sin m\lambda_{sat}\}\right] \quad \textbf{3.8}$$

The coefficients C_{nm}, S_{nm} represent the mathematical modelling of the Earth's mass distributions by using spherical harmonics and P_{nm} are their associated Legendre functions.

3.4 Acceleration Terms Using Aspheric Gravity Potential (Φ)

By applying the del operator to the gravity potential function, the acceleration of a satellite about an aspherical Earth in the IJK (ECI) frame is obtained as [Vallado 1997, Pp 497]

$$a_I = \left\{\frac{1}{r}\frac{\partial\Phi}{\partial r} - \frac{r_K}{r^2\sqrt{r_I^2 + r_J^2}}\frac{\partial\Phi}{\partial\phi_{sat}}\right\}r_I - \left\{\frac{1}{r_I^2 + r_J^2}\frac{\partial\Phi}{\partial\lambda_{sat}}\right\}r_J$$

$$a_J = \left\{\frac{1}{r}\frac{\partial\Phi}{\partial r} - \frac{r_K}{r^2\sqrt{r_I^2 + r_J^2}}\frac{\partial\Phi}{\partial\phi_{sat}}\right\}r_J + \left\{\frac{1}{r_I^2 + r_J^2}\frac{\partial\Phi}{\partial\lambda_{sat}}\right\}r_I \quad \textbf{3.9}$$

$$a_K = \frac{1}{r}\frac{\partial\Phi}{\partial r}r_K + \frac{\sqrt{r_I^2 + r_J^2}}{r^2}\frac{\partial\Phi}{\partial\phi_{sat}}$$

The partial derivatives are given by

$$\frac{\partial\Phi}{\partial r} = \frac{\mu}{r^2}\sum_{n=2}^{\infty}\sum_{m=0}^{n}\left(\frac{R_e}{r}\right)^n (n+1)\overline{P}_{nm}[\sin(\phi_{sat})]\left\{\overline{C}_{nm}\cos(m\lambda_{sat}) + \overline{S}_{nm}\sin(m\lambda_{sat})\right\}$$

$$\frac{\partial\Phi}{\partial\phi_{sat}} = \frac{\mu}{r}\sum_{n=2}^{\infty}\sum_{m=0}^{n}\left(\frac{R_e}{r}\right)^n \overline{P}_{n,m+1}[\sin(\phi_{sat})] - m\tan(\phi_{sat})\overline{P}_{nm}[\sin(\phi_{sat})]\times$$
$$\left\{\overline{C}_{nm}\cos(m\lambda_{sat}) + \overline{S}_{nm}\sin(m\lambda_{sat})\right\}$$

$$\frac{\partial \Phi}{\partial \lambda_{sat}} = \frac{\mu}{r^2} \sum_{n=2}^{\infty} \sum_{m=0}^{n} \left(\frac{R_e}{r} \right)^n m \overline{P}_{nm} [\sin(\phi_{sat})] \left\{ \overline{S}_{nm} \cos(m\lambda_{sat}) - \overline{C}_{nm} \sin(m\lambda_{sat}) \right\} \qquad \textbf{3.10}$$

Where

r = Satellite geocentric distance

ϕ_{sat} = Geocentric latitude

λ_{sat} = Geographic longitude

$\overline{C}_{nm}$, $\overline{S}_{nm}$ = Normalized gravitational constants

$\overline{P}_{nm}[\alpha]$ = Normalized associated Legendre function

n, m = Degree and order of the gravity model

Normalization is achieved by [Heiskanen1967; NIMA 1997; Vallado 1997, Pp493]

$$\overline{C}_{nm}, \overline{S}_{nm} = \prod_{nm} C_{nm}, S_{nm}$$

$$\overline{P}_{nm}[\alpha] = \frac{P_{nm}[\alpha]}{\prod_{nm}} \qquad \textbf{3.11}$$

Where C_{nm}, S_{nm} are the conventional gravitational coefficients and the normalization operator, $\prod_{nm}$, is given by

$$\prod_{nm} = \sqrt{\frac{(n+m)!}{(n-m)!(2n+1)k}} \qquad \textbf{3.12}$$

$k = 1$, m = 0;

$k = 2$, m >1,

The associated Legendre function, $P_{nm}[\alpha]$, $\alpha = \sin\phi_{sat}$, is given by

$$P_{nm}[\alpha] = \alpha^m \frac{d^m}{d(\alpha)^m} P_n[\alpha] \qquad \textbf{3.13}$$

where $P_n[\alpha]$ represents the Legendre polynomial

$$P_n[\alpha] = \frac{1}{2^n n!}\frac{d^n}{d(\alpha)^n}\left(\sin^2\alpha - 1\right)^n \qquad \textbf{3.14}$$

The associated Legendre functions are orthogonal polynomials and can be efficiently computed by recursion

$$\begin{aligned} P_{n,0}[\alpha] &= \frac{(2n-1)\alpha P_{n-1,0}[\alpha] - (n-1)P_{n-2,0}[\alpha]}{n}, n \geq 2 \\ P_{n,m}[\alpha] &= P_{n-2,m}[\alpha] + (2n-1)\cos(\phi_{gc})P_{n-1,m-1}[\alpha], m \neq 0, m < n \\ P_{n,n}[\alpha] &= (2n-1)\cos(\phi_{sat})P_{n-1,n-1}[\alpha], m \neq 0 \end{aligned} \qquad \textbf{3.15}$$

With starting values

$$P_{0,0}[\alpha] = 1$$

$$P_{1,0}[\alpha] = \alpha = \sin(\phi_{sat})$$

$$P_{1,1}[\alpha] = \cos(\phi_{sat})$$

Similarly, the trigonometric functions can be calculated recursively.

$$\begin{aligned} \sin(m\lambda_{sat}) &= 2\cos(\lambda_{sat})\sin\{(m-1)\lambda_{sat}\} - \sin\{(m-2)\lambda_{sat}\} \\ \cos(m\lambda_{sat}) &= 2\cos(\lambda_{sat})\cos\{(m-1)\lambda_{sat}\} - \cos\{(m-2)\lambda_{sat}\} \\ m\tan(\phi_{sat}) &= (m-1)\tan(\phi_{sat}) + \tan(\phi_{sat}) \end{aligned} \qquad \textbf{3.16}$$

3.4.1 Spherical Harmonics

Solid spherical harmonics are in essence a Fourier series that constitute an independent basis for the gravitational model. The indices *n* and *m* are an indication of the *degree* and *order* of the model and determine lines on the sphere along which the functions vanish. These spherical harmonics are divided into three terms: *zonal, sectorial and tesseral.* The boundaries of the harmonics represent the roots of the Legendre polynomial [Vallado 1997, pp495-497; Chobotov 1996, pp204-209].

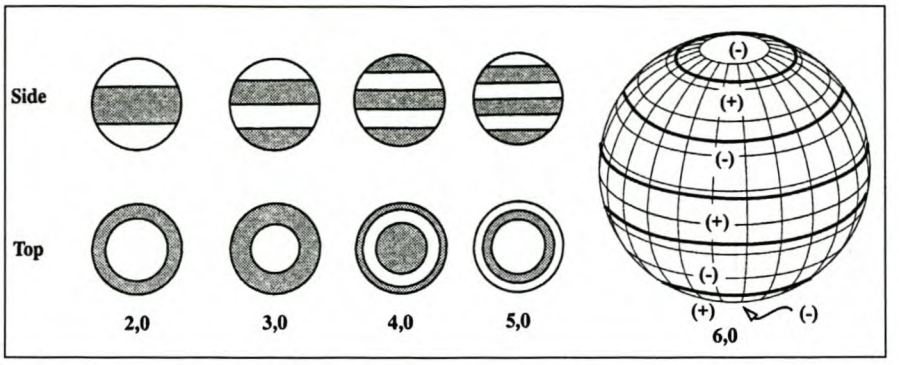

Figure 3.1. Zonal harmonics up to degree six ($J_6 = -C_{6,0}$). [Vallado 1997, Pp 495-96]

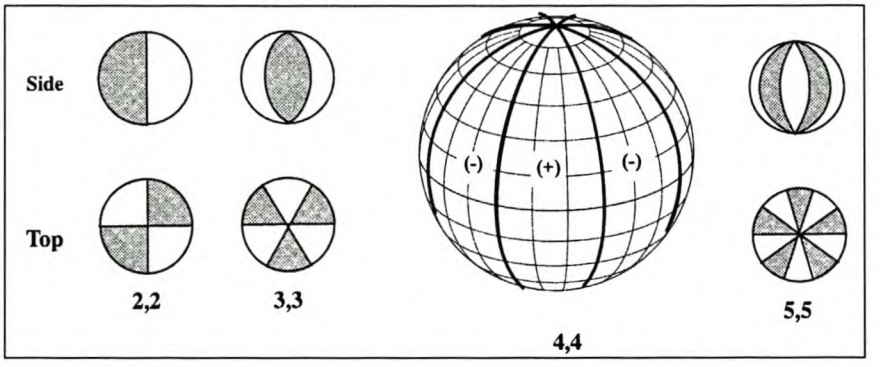

Figure 3.2. Sectorial harmonics up to degree five, order five.

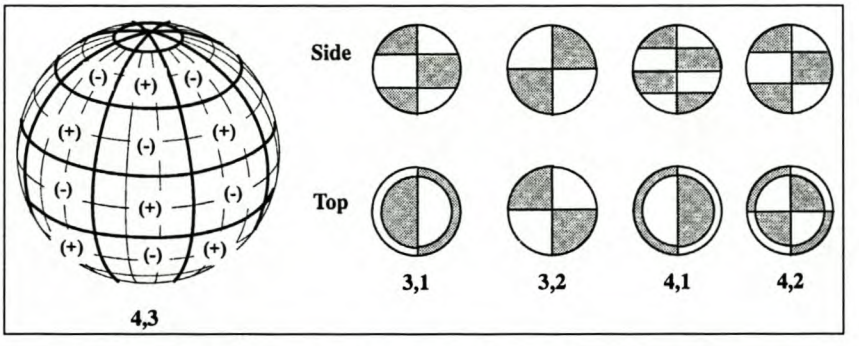

Figure 3.3. Tesseral harmonics up to degree four, order three.

3.4.2 Zonal Harmonics ($m = 0$, Figure 3.1)

Zonal harmonics are bands of latitude symmetrical about the polar axis. For any $P_n[\sin\phi_{sat}]$, there are n circles of latitude along which P_n is zero. $C_{2,0} = -J_2$ represent the bulge about the equator and is the strongest perturbation due to the Earth's shape. It is a magnitude of three larger than the next coefficient, $C_{3,0} = -J_3$.

3.4.3 Sectorial harmonics ($n = m$, Figure 3.2).

Sectorial harmonics represent bands of longitude. The lines along which the functions [cos$n\lambda$ and sin$n\lambda$]P_{nn} [sinϕ_{sat}] vanish, define meridians of longitude, which divide the sphere into $2n$ "orange slice" sectors.

3.4.4 Tesseral harmonics ($n \neq m \neq 0$, Figure 3.3)

The tesseral functions [cos$m\lambda$ and sin$m\lambda$]P_{nm}[sinϕ_{sat}] divide the sphere up into a checkerboard array of (n-m) circles of latitude along which P_{nm}[sinϕ_{sat}] is zero and $2m$ meridians of longitude along which the terms [cos$m\lambda$ and sin$m\lambda$] vanish.

3.4.5 Gravitational Parameters

The gravitational parameters, C_{nm}, S_{nm}, are derived from terrestrial gravity measurements and satellite orbit analyses based on accurate laser and Doppler observations of satellite positions [Bursa, Pec 1988]. Various gravitational models exist for which the gravitational parameters, C_{nm}, S_{nm}, have been accurately calculated using various classes of satellite orbits. For the purpose of this study, the gravitational parameters of the 1996 Earth Gravity Model (EGM96) were used. The EGM96 model comprises a complete field of normalized coefficients of degree and order (n = 360, m = 360, or 360x360), derived from data from thirty satellites and surface gravity measurements. This choice of model eliminates errors associated with (smaller) satellite-only models (JGM, GEM), which have been developed from a single class of satellite orbits [Vallado 1997, Pp 535]. For accurate propagation, a minimum field of degree and order (70x70) has been used.

3.5 Atmospheric Drag

Atmospheric drag is a non-conservative force exerted on a satellite in LEO due to the presence of gas molecules in the upper atmosphere [King-Hele 1987, Pp 12-20; Vallado 1997, Pp 607]. Drag is in the opposite direction of the velocity vector and removes energy from the orbit. It is the ultimate cause of a LEO satellite falling back to Earth and is the dominant perturbative force during the final revolutions of the satellite's life. The perturbative effect of atmospheric drag for LEO satellites is only exceeded by that due to the Earth's oblateness, making it an important force to quantify.

The basic equation for acceleration due to aerodynamic drag [Vallado 1997, Pp 498; King-Hele 1987, Pp 29] is given by

$$\ddot{\mathbf{r}}_{drag} = -\frac{1}{2}\frac{C_D A}{m}\rho r_{rel}^{\ 2}\frac{\dot{\mathbf{r}}_{rel}}{|\dot{\mathbf{r}}_{rel}|} \qquad \textbf{3.17}$$

Where

C_D = Coefficient of drag. For upper atmosphere satellites $C_D \approx 2.0$.

ρ = Atmospheric density.

A = Cross sectional area of satellite. A is normal to the satellite's velocity vector.

m = Satellite mass

$\dot{\mathbf{r}}_{rel}$ = Satellite velocity relative to the rotating Earth atmosphere given by

$$\dot{\mathbf{r}}_{rel} = \frac{d\mathbf{r}}{dt} - \boldsymbol{\omega}_e \times \mathbf{r} = \begin{bmatrix} \frac{dx}{dt} + \omega_e x \\ \frac{dy}{dt} - \omega_e y \\ \frac{dz}{dt} \end{bmatrix} \qquad \textbf{3.18}$$

Where ω_e is the Earth's rotational velocity. The vector on the right represents the velocity of the satellite relative to the rotating atmosphere, i.e., the difference between the satellite's velocity relative to the Earth's centre and the velocity of the atmosphere relative to the Earth's centre [King-Hele 1987, Pp 29].

Wind variations [Escobal 1985, Pp 60] will not be employed in this study as this information is usually not readily available and has negligible effect on LEO satellites.

3.5.1 Cross Sectional Area

For the purpose of this study, a mean cross sectional area value for a cubic-shaped micro-satellite (SUNSAT) is obtained by considering the mean of three possible maximum cross section areas A_1, A_2 and A_3 as explained in **Figure 3.4**. The mean

cross-sectional area for SUNSAT (dimensions 45cm cube) is subsequently calculated as 0.2766 m^2 using

$$A = \frac{1}{3}(A_1 + A_2 + A_3)$$

$$= \frac{1}{3}(x^2 + xy + 3 \cdot z^2 \sin 60)m^2$$

More complex structures' cross sectional area values must be obtained by attitude determination.

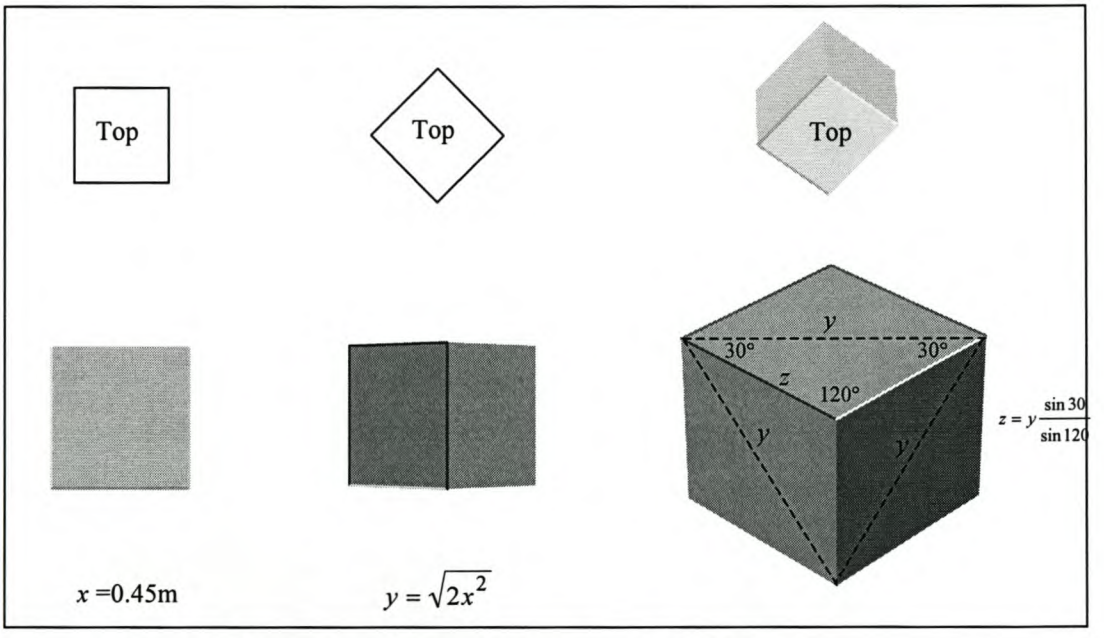

Figure 3.4. Cross-sectional views of a cubic shaped satellite

3.5.2 Calculating Atmospheric Density

Atmospheric density depends on the physical properties of the Earth's upper atmosphere and varies with time and geographic position. At intermediate altitudes (120-600km), highly variable energy sources cause large variations in atmospheric density and generate orbital perturbations [Wertz 1995]. Models for calculating atmospheric density are complex, computationally intensive and are often simplified to economise computer run time. Simplified models, such as the exponential atmosphere, assume a static atmosphere and do not account for diurnal or seasonal variations [King-Hele 1987, Pp 111]. Though useful for initial orbit determination, they fail at delivering the accuracy required for propagating precision orbits for LEO satellites.

Three classes of atmospheric models are available for calculating more accurate atmospheric density values [Vallado 1997, Pp 511; Montenbruck 2000, Pp 83].

3.5.2.1 Diffusion equations (Jacchia-models)

Models such as the Jacchia 71 and 77 atmospheric models contain analytical expressions for determining exospheric temperature as a function of time, position, solar activity and geomagnetic activity. Density values are empirically determined from temperature profiles or numerically integrated from diffusion equations. Appendix C contains the analytical Jacchia-Roberts atmosphere as described by [Vallado 1997, Appendix B].

3.5.2.2 MSISe-90 (CIRA-90)

The Committee on Space Research (COSPAR) presently recommends the CIRA-90 (COSPAR International Reference Atmosphere of 1990). CIRA-90 is in essence the *Mass Spectrometer and Incoherent Scatter model of 1990* (MSISe-90), [Hedin 1991]. The MSIS neutral atmosphere model describes the neutral temperature and densities of He, O, N_2, O_2, Ar, H and N from ground to thermospheric heights. It is based on Hedin's extensive compilation and analysis of satellite drag and ground-based data. Hedin's MSISE-90 model was used in this study because of its improved performance in calculating C_D to the Jacchia models [Chao 1996].

3.5.2.3 Soviet Cosmos (GOST)

This model derives total densities solely from satellite drag analysis of the Soviet Cosmos satellites. Total densities are calculated from a reference altitude profile, which is adjusted for factors accounting for diurnal, seasonal/latitudal, Solar and geomagnetic activity effects.

3.6 THIRD BODY PERTURBATIONS

A third-body perturbation is the result of a gravitational force exerted on a satellite by an object other than the main attracting body. Third bodies may constitute the Sun, Moon, planets, asteroids or (other) spacecrafts. From the *N*-body problem (Appendix A), it can be shown that the acceleration experienced by a satellite due to the presence of a third attracting body is given by

$$\ddot{\mathbf{r}}_{e,sat} = -\frac{Gm_e}{r_{e,sat}^3}\mathbf{r}_{e,sat} + Gm_3\left(\frac{\mathbf{r}_{sat,3}}{r_{sat,3}^3} - \frac{\mathbf{r}_{e,3}}{r_{e,3}^3}\right) \qquad \textbf{3.19}$$

This equation is prone to numerical instability should the Earth-third body distance be similar to the satellite-third body distance. As the cube of these distances in the denominators in above equation are extremely large, each value will be very small and their numerically calculated difference even smaller and might introduce errors in simulation. The following general equation for k third bodies eliminates numerical stability problems [Vallado 1997, Pp 515-516]

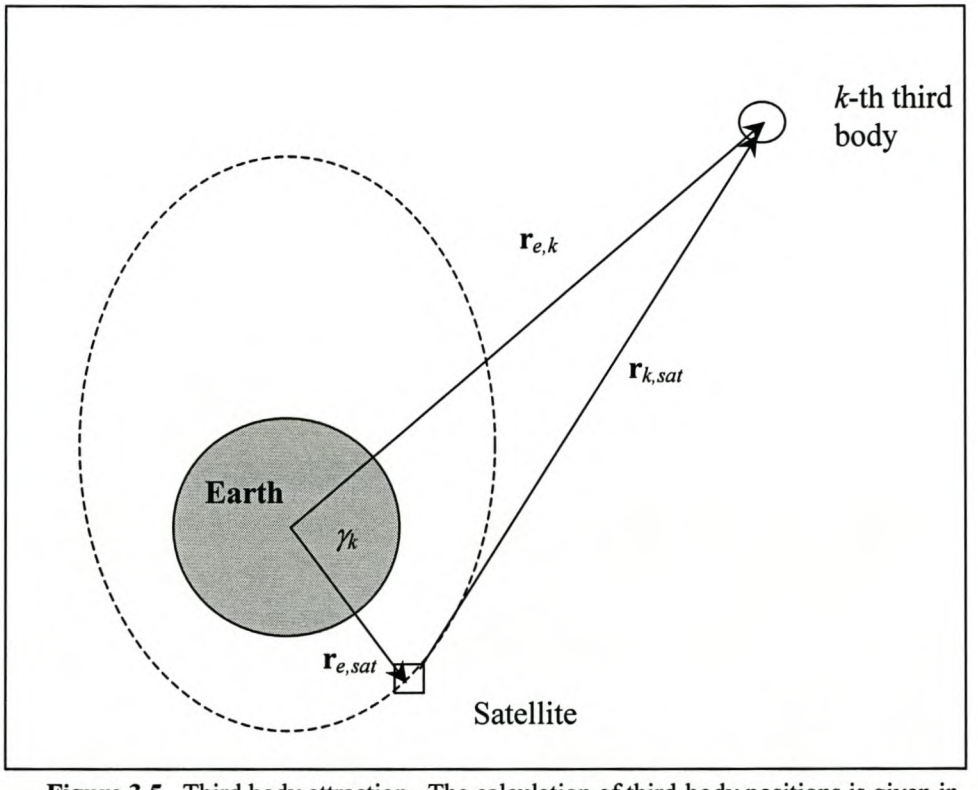

Figure 3.5. Third body attraction. The calculation of third-body positions is given in Appendix D.

$$\ddot{\mathbf{r}}_{e,sat} = -\frac{Gm_e}{r_{e,sat}^3}\mathbf{r}_{e,sat} - \sum_{k=1}^{n}\frac{Gm_k}{r_{e,k}^3}\left(\mathbf{r}_{e,sat} - \beta_k\mathbf{r}_{sat,k}\right) \qquad \textbf{3.20}$$

where

$$\beta_k = 3B_k + 3B_k^2 + B_k^3$$

$$B_k = \sum_{j=1}^{\infty} P_j[\cos\gamma_k]h_k^j \qquad \textbf{3.21}$$

$$h_k = \frac{r_{e,sat}}{r_{e,k}}$$

γ_k = Angle between third body and satellite as seen from Earth.

3.7 Solar Radiation Pressure

Solar radiation pressure is a non-conservative force exerted on the satellite by the momentum flux from the Sun. Similar to atmospheric drag, solar radiation pressure is a surface force and its effect is proportional to the area-to-mass ratio of the satellite. Above 600km, the effects of solar radiation pressure exceed those of drag, making it an important effect to quantify [King-Hele 1987, Pp 9]. A difficult aspect of analyzing solar radiation is accurately modelling and predicting solar cycles and variations. The acceleration due to solar radiation pressure is given by [Wertz 1996; Vallado 1997, Pp 520; Montenbruck 2000, Pp 77]

$$\ddot{\mathbf{r}}_{rad} = -\frac{P_{SR} c_R A_{Sun}}{m} \frac{\mathbf{r}_{Sun,sat}}{|r_{Sun,sat}|} \qquad \textbf{3.22}$$

Where

P_{SR} = Solar pressure = 4.51 x 10^{-6}N.m^{-2}

m = Satellite mass

A_{Sun} = Satellite's exposed area to the Sun.

C_R = Reflectivity value. $1.0 \leq C_R \leq 2.0$

The reflectivity, C_R indicates how the satellite reflects incoming radiation (C_R = 1.0 perfectly absorbent; C_R = 2.0 reflects all light). As with the drag coefficient, C_D, it is difficult to predict C_R, which is almost always determined as a solution parameter from the differential correction process. The same mean surface cross-sectional area value used for drag calculation will be used in **Equation 3.22.**

3.7.1 Shadow Analysis

The acceleration due to solar radiation pressure is not constant as the satellite periodically eclipses behind the Earth and subsequently experiences no solar-radiation pressure. For accurate determination of the perturbative acceleration, a "switching"

model is introduced which turns the radiation "on" and "off" as appropriate [Escobal 1985, Pp 158-159].

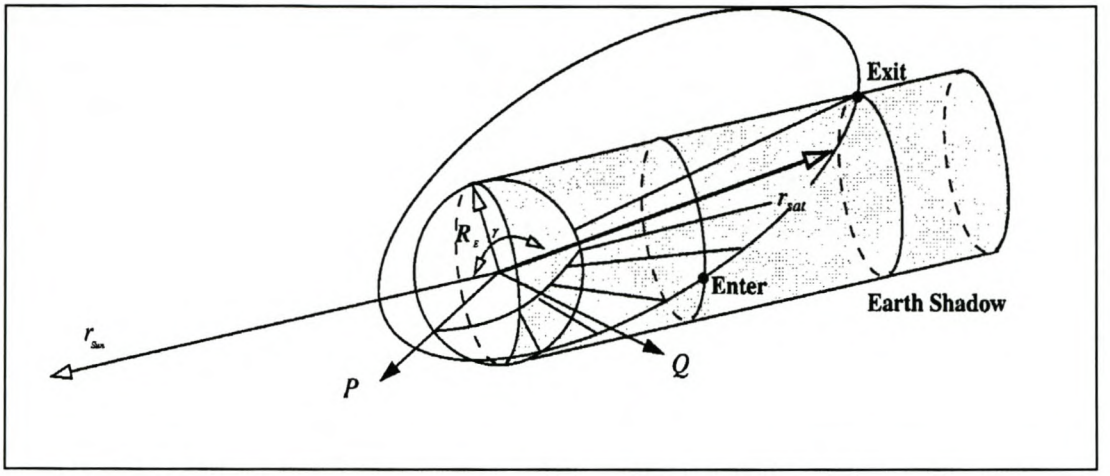

Figure 3.6. Satellite shadow entry and exit geometry [Escobal 1985, Pp 157].

$$\cos\gamma = \frac{\mathbf{r}_{Sun} \bullet \mathbf{r}_{sat}}{r_{Sun} r_{sat}}$$

$$\cos\gamma = \frac{r_{sat}\cos\nu\mathbf{r}_{Sun} \bullet \mathbf{P} + r_{sat}\sin\nu\mathbf{r}_{Sun} \bullet \mathbf{Q}}{r_{Sun} r_{sat}} \qquad \textbf{3.23}$$

$$\beta_1 = \frac{\mathbf{r}_{Sun} \bullet \mathbf{P}}{r_{Sun}}, \quad \beta_2 = \frac{\mathbf{r}_{Sun} \bullet \mathbf{Q}}{r_{Sun}}$$

$$\cos\gamma = \beta_1\cos\nu + \beta_2\sin\nu$$

The shadow function

$$S = R_e^2(1+e\cos\nu)^2 + p^2\{\beta_1\cos\nu + \beta_2\sin\nu\}^2 - p^2 \qquad \textbf{3.24}$$

Vanishes for

$$1-\left(\frac{R_e}{a(1-e)}\right)^2 < \beta_1^2 < 1-\left(\frac{R_e}{a(1+e)}\right)^2$$

Where

ν = True anomaly

γ = Sun-satellite angle

R_e = Earth equatorial radius

a = Orbit semi-major axis

e = Orbit eccentricity

p = Semi-latus rectum

P, **Q** = Unit vectors in the PQR co-ordinate system.

When cosγ = 0, the satellite will be in direct sunlight and $S < 0$. When the satellite enters the shadow ($\gamma > 90°$, cosγ < 0), S changes from negative to positive. Solve numerically by letting x = cosν and set $S = 0$.

$$Ax^2 + Bx + Cx\sqrt{1-x^2} + D = 0$$

$$x_{n+1} = x_n - \frac{f(x_n)}{f'(x_n) - \frac{f(x_n)f''(x_n)}{2f'(x_n)}} \qquad \textbf{3.25}$$

Because x = cosν, the solution must lie between –1.0 and +1.0. The initial guess could be 0.0 because it lies midway in the interval.

3.8 NUMERICAL INTEGRATION

Various integration methods exist for solving the differential equations, which govern the movement of bodies in the solar system. The major consideration factors in selecting an appropriate method of integration are accuracy, speed, stability and complexity [Bate 1971, Pp 412]. Some of the desirable qualities of a good integration scheme are:

- Allow as large a step-size as possible
- Provide for simple and fast variable step-size calculation
- Computational economic
- Stable, inhibiting exponential error growth
- Fairly insensitive to round-off errors
- Minimum and maximum control on truncation errors

The choice of method often lies between single step and multi-step methods; each having their respective advantages and disadvantages, depending on the application. Single-step methods such as Runge-Kutta, are simple, competitive and stable but slow, whilst multi-step (predictor-corrector) methods such as the Adams-Bashford-

Moulton integrator are faster, but at the expense of simplicity and stability. Most numerical integrators derive from the Taylor series expansion,

$$y(t) = y(t_0) + \dot{y}(t_0)(t-t_0) + \frac{\ddot{y}(t_0)(t-t_0)^2}{2!} + \sum_{k=3}^{\infty} \frac{y^{(k)}(t_0)(t-t_0)^k}{k!} \qquad \textbf{3.26}$$

The n-th order terminology of the method used refers to the order of Taylor series expansion around the initial value $y(t_0)$ and gives an indication of the accuracy of the approximation. E.g. $O^{(3)}$ indicates order three accuracy by employing the first three terms of the series.

For the purpose of this study, a (embedded) seventh-eighth order Runge-Kutta-Fehlberg method is employed to ensure accuracy and stability. This method ensures $O^{(8)}$ accuracy and stability respectively through the higher number of Taylor expansion terms and a variable (adaptive) integration step size (h), which keeps local truncation errors within predefined tolerances.

3.8.1 Runge-Kutta Methods

The generalized s-staged Runge-Kutta method approximates the numerical solution for the initial value problem (IVP)

$$y'(t) = f(t, y(t)), y(t_0) \text{ known}$$

by constructing an approximation y_{n+1} at $t_{n+1} = t_n + h$ from known approximation y_n at t_n. The approximation is achieved by using two formulas of order q and p (= q-1) [Fehlberg 1969, Butcher 1987, Hairer *et al* 1987]

$$y_{n+1} = y_n + h\sum_{k=1}^{10} c_k f_k + O^{(8)} \quad \textbf{(}q\textbf{-th order)} \qquad \textbf{3.27}$$

And

$$\hat{y}_{n+1} = y_n + h\sum_{k=1}^{12} \hat{c}_k f_k + O^{(9)} \quad \textbf{(}p\textbf{-th order)} \qquad \textbf{3.28}$$

Where

$$f_0 = f(t_0, y_0)$$

$$f_k = f\left(t_{k-1} + \alpha_k h, y_{k-1} + h\sum_{l=1}^{k-1} \beta_{kl} f_l\right), k = 1,2, ..12 \qquad \textbf{3.29}$$

$$c_i = \sum_{j=1}^{i-1} a_{ij}\,, i > j;\ i, j = 1, 2, \ldots s$$

The local error in the 8-th order formula is used to control the variable step size, h_{n+1}: At each step, the absolute and relative errors, ε_{abs} and ε_{rel}, are calculated as [Golub and Van Loan 1996, Pp 53]

$$\varepsilon_{abs} = \|\hat{\mathbf{y}} - \mathbf{y}\|$$

$$\varepsilon_{rel} = \frac{\|\hat{\mathbf{y}} - \mathbf{y}\|}{\|\mathbf{y}\|}$$

The number of correct significant digits in $\hat{y}$ can be determined by translating the relative error in the ∞-norm. If the given tolerances require b significant digits, the step size is adjusted to keep the expression

$$\varepsilon = \frac{\|\hat{\mathbf{y}} - \mathbf{y}\|_\infty}{\|\mathbf{y}\|_\infty} \le 10^{-b}$$

Where

$$\|y\|_\infty = \max_{1 \le i \le n} |y_i|$$

In the employed RKF 7-8 method, step size is calculated by

$$h_{n+1} = 0.7 h_n \cdot \left[\frac{1}{\varepsilon}\right]^{\frac{1}{8}} \qquad \textbf{3.30}$$

Where $\varepsilon = \max(\varepsilon, K)$ with K given by

$$K = \frac{|f_0 + f_{10} - (f_{11} + f_{12})|}{|y| \cdot \varepsilon_R + \varepsilon_A} \cdot c_{11} \cdot h_n$$

The Fehlberg coefficients α_k, β_{kl} , c_k, and $\hat{c}_k$ for the 12-stage, 7-8 order method are given in Table 3.1. The coefficients are accurate to 18 digits [Hairer 1980, Pp 196].

3.9 NORAD TWO LINE ELEMENTS

Satellite ephemeris of numerous unclassified satellites is available to the public in the form of NORAD Two Line Elements (TLE's) files, supplied by NASA/Goddard Space Flight Centre [GSFC] and published on the internet by [Celestrak]. Although these elements are supplied as classical orbital elements, they are actually Kozai *mean* elements and cannot be used in the type of propagator developed in this study. Public domain code exists for propagation using these elements, the most popular being the SGP4 propagator packaged by [Hoots, Roehrich and Kelso 1988]. The first SUNSAT TLE looks as follows:

```
1 25635U 99008B   99068.23100837  .00000196  00000-0  61890-4 0   482
2 25635  96.4768  19.8698 0151917 209.5613 149.6933 14.40791150  1989
```

By using the TLE format description (Appendix F) this data translates to [Vallado 1997, Pp 140-141]

Epoch March 9 1999, 05:32:39.12 UTC

$\overline{n}$ = 14.40791150 rev/day

$\frac{\dot{n}}{2} = 1.96x10^{-6}$ rev/day^2, $\frac{\ddot{n}}{6} = 0.0$ rev/day^3

$B^* = 6.1890\text{x}10^{-5}$

e =0.0151917

i = 96.4768°

Ω = 19.8698°

ω = 209.5613°

M = 149.6933°

The true ballistic coefficient B, is calculated from B* by [Hoots, Roehrich, Kelso TS, 1988, Pp 56]

$$B = \frac{1}{12.74621 B^*} kg.m^{-2}$$

Though very popular, TLE propagation is not useful for precision applications as the data contain inherent inaccuracies.

3.10 Propagator Evaluation Procedure

Results from the precision propagation software developed in this study (*Orblitz*), were compared with a ten-day section of precision SUNSAT orbit, derived from Satellite Laser Ranging (SLR) measurements. These results were also compared with results from the commercially available *Advanced High Precision Orbit Propagator*, (*WinHPop*), version 3.0 [Microcosm] and the public domain SGP4 propagator employing NORAD TLE's [Hoots *et. al.* 1988]./

The software outline is discussed in detail in Chapter 5. The results are respectively presented and discussed in Chapters 6 and 9. Other options for evaluation of the propagator's performance were considered.

3.10.1 Delft Precision Orbits for ERS-1 and 2.

The University of Delft post-processes precision orbits for the ERS-1 & 2 radar satellites using GPS and SLR measurements. Although these (identical) satellites orbit the Earth at approximately the same altitude as SUNSAT, the specialised attitude determination models required to model their complex geometry and rotational dynamics for cross-sectional area determination were unavailable for this study, making these orbits impractical to use.

3.10.2 Laser Geodynamic Satellite Experiment

The orbits of the spherical LAGEOS-1 & 2 satellites were designed to provide a permanent reference point in a very stable orbit for precision earth-dynamics measurements like crustal motions, regional strains, fault motions, polar motion and earth-rotation variations, solid earth tides, and other kinematic and dynamic

parameters associated with earthquake assessment and alleviation [LAGEOS]. Precision LAGEOS orbits are calculated using SLR measurements of their 6000 km-high drag-free circular orbits. As it was important to evaluate the propagator with atmospheric drag effects, these orbits were not used in the evaluation.

3.11 SUNSAT Data Sources

SUNSAT carried a laser retro-reflector for SLR measurements and, after communications with Honeywell-Technical Services Inc. [HTSI], a ten-day section of precision orbit was obtained for the period 6-15 Feb 2000. The data was supplied in mean equator and equinox of J2000 at sixty-second intervals. The following data was sourced (listed in Appendix F), cleaned and implemented in the software:

3.11.1 Solar Flux (F10.7cm) and Magnetic Index (Ap) Data

Current, historic and predicted solar activity data is available from the National Geophysical Data Centre [NGDC].

3.11.2 Earth Orientation Parameters

Current, historic and predicted Earth orientation parameters are available from the International Earth Rotation Service [IERS] through their Bulletins A and B.

Table 3.1. Fehlberg Coefficients for the Explicit 7(8) Order Runge-Kutta method

	α_k	β_{kl}												c_k	$\hat{c}_k$
l/k		0	1	2	3	4	5	6	7	8	9	10	11		
0	0	0												$\frac{41}{840}$	0
1	$\frac{2}{27}$	$\frac{2}{27}$												0	0
2	$\frac{1}{9}$	$\frac{1}{36}$	$\frac{1}{12}$											0	0
3	$\frac{1}{6}$	$\frac{1}{24}$	0	$\frac{1}{8}$										0	0
4	$\frac{5}{12}$	$\frac{5}{12}$	0	$-\frac{25}{16}$	$\frac{25}{16}$									0	0
5	$\frac{1}{2}$	$\frac{1}{20}$	0	0	$\frac{1}{4}$	$\frac{1}{5}$								$\frac{34}{105}$	$\frac{34}{105}$
6	$\frac{5}{6}$	$-\frac{25}{108}$	0	0	$\frac{125}{108}$	$-\frac{65}{27}$	$\frac{125}{54}$							$\frac{9}{35}$	$\frac{9}{35}$
7	$\frac{1}{6}$	$\frac{31}{300}$	0	0	0	$\frac{61}{225}$	$-\frac{2}{9}$	$\frac{13}{900}$						$\frac{9}{35}$	$\frac{9}{35}$
8	$\frac{2}{3}$	2	0	0	$-\frac{53}{6}$	$\frac{704}{45}$	$-\frac{107}{9}$	$\frac{67}{90}$	3					$\frac{9}{280}$	$\frac{9}{280}$
9	$\frac{1}{3}$	$-\frac{91}{108}$	0	0	$\frac{23}{108}$	$-\frac{976}{135}$	$\frac{311}{54}$	$-\frac{19}{60}$	$\frac{17}{6}$	$-\frac{1}{12}$				$\frac{9}{280}$	$\frac{9}{280}$
10	1	$\frac{2383}{4100}$	0	0	$-\frac{341}{164}$	$\frac{4496}{1025}$	$-\frac{301}{82}$	$\frac{2133}{4100}$	$\frac{45}{82}$	$\frac{45}{164}$	$\frac{18}{41}$			$\frac{41}{840}$	0
11	0	$\frac{3}{205}$	0	0	0	0	$-\frac{6}{41}$	$-\frac{3}{205}$	$-\frac{3}{41}$	$\frac{3}{41}$	$\frac{6}{41}$	0			$\frac{41}{840}$
12	1	$-\frac{1777}{4100}$	0	0	$-\frac{341}{164}$	$\frac{4496}{1025}$	$-\frac{289}{82}$	$\frac{2193}{4100}$	$\frac{51}{82}$	$\frac{33}{164}$	$\frac{12}{41}$	0	1		$\frac{41}{840}$

Chapter 4

Time, Co-ordinate Systems and Transformations

4.1 INTRODUCTION

The focus of this chapter is the description of various time and co-ordinate systems required to describe the motion of a near-Earth satellite. Given initial conditions, the state vector of a satellite is obtained at any given time by integrating the equations of motion, which, in turn, is constituted by the sum of various accelerations exerted on the satellite. Though the principal accelerations are usually expressed in rotating (body-fixed) frames, the integration of the equations of motion is done in a non-rotating (inertial) reference frame, requiring a transformation of the co-ordinate system. E.g. observing a satellite from a radar station. This transformation has to account for Earth's rotation and the motion of the equinoxes, which is the result of the combined motions of the Earth's equatorial plane and the ecliptic plane. In addition, the description of various time-dependent motions involves transformation between various time systems. To ensure precision propagation of motion, precision models for relevant time and co-ordinate systems and theories of motion are subsequently discussed.

4.2 ASTRONOMICAL FUNDAMENTALS

The following necessary astronomical terminologies are defined prior to proceeding to a formal treatise of various time, co-ordinate systems and their relations as illustrated in **Figure 4.1** [Vallado 1997, Pp 31-35].

Celestial sphere: Fictitious sphere with the observer at the centre and celestial objects fixed to, or moving on its inner surface.

Celestial equator: The plane normal to the Earth's axis of rotation and extending through the Earth's centre to the celestial sphere.

Great circles: The intersection of the celestial sphere with any plane passing through the centre of the sphere.

Hour circles: Great circles perpendicular to the celestial equator.

Celestial poles: The intersection of the Earth's rotational axis and the celestial sphere.

Ecliptic: The mean plane of the Earth's orbit about the Sun.

Equatorial plane: The plane-extension of the Earth's equator.

Obliquity of the ecliptic (ε): The angle between the Earth's mean ecliptic and equator (about 23.5°).

Line of nodes: The line of intersection of two planes. This line helps to fix a principal direction.

Equinoxes: Positions occupied by the Sun twice per year along such an intersection: at the ascending node (about March 21, *vernal equinox*) and at the descending node (about September 23, *autumnal equinox*). The seasons sited are for the Northern Hemisphere.

Vernal equinox (γ): An event occurring when the Sun's declination is 0° as it changes from negative to positive values (ascending node) as viewed from the Earth. This point differs slightly from the intersection of the equator and ecliptic because the latter is defined as the mean path of the Sun and not the true path.

Ecliptic longitude and latitude (λ, ϕ): The fundamental plane is the ecliptic. Ecliptic longitude is measured from the vernal equinox along the ecliptic and ecliptic latitude is similarly defined to geographic latitude.

Right Ascension (α): Measured positively to the east in the equatorial plane from the vernal equinox. $\alpha \in [0°, 360°]$.

Declination (δ): Measured south or northward from the equator to the object's location. $\delta \in [-90°, 90°]$.

Hour angle (HA): The angle from an observer's hour circle to the hour circle of an object. The angle is measured positively westward. $HA \in [0h, 24h]$.

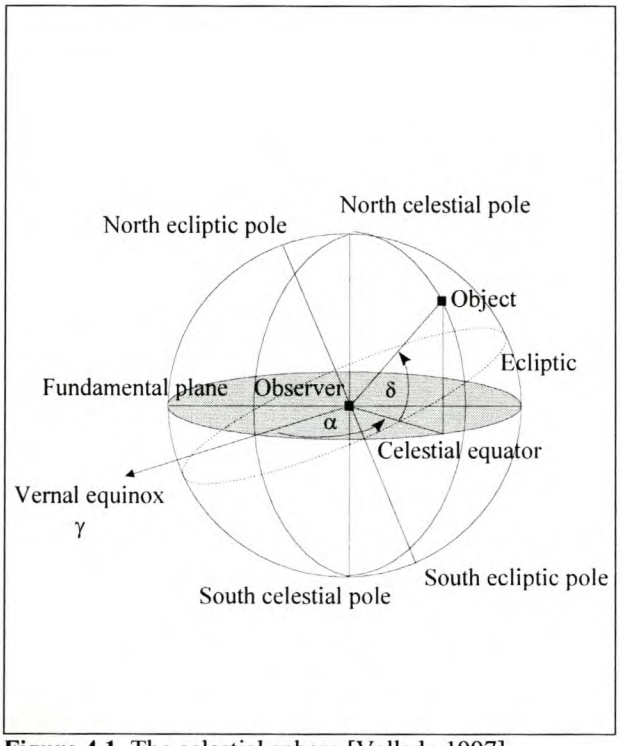

Figure 4.1. The celestial sphere [Vallado 1997].

4.3 TIME

The following time scales are of prime relevance in the precision modelling of the state of Earth orbiting satellites [Montenbruck & Gill 2000, Seidelmann 1992, Pp. 2-7]:

Terrestrial Time (TT) is a uniform time scale that would be measured by an ideal clock on the geoid's surface. TT is measured in days of 86400 SI seconds.

International Atomic Time (TAI) provides the practical realization of a uniform time scale based on atomic clocks. It agrees with TT except for a constant offset of 32.184s.
Julian date (JD) is defined as the number of days elapsed since the arbitrarily selected epoch of January 1, 4713 BC, 12:00 (Greenwich) and is measured from noon to noon. The JD for a known calendar date (with time fraction) may be obtained by the following general formula [Meeus 1991, Pp 61]

If *month* = 1 or 2, set *year* = *year* – 1 and *month* = *month* + 12

Set *day* = *day* + (*hour* + *minutes*/60 + *seconds*/3600) / 24

Let

$$B = 2 - INT\left(\frac{year}{100}\right) + INT\left(\frac{INT\left(\frac{year}{100}\right)}{4}\right)$$

Then

$$JD = \text{INT}\{365.25(year+4716)\} + \text{INT}\{30.6001(month+1)\} + day + B - 1524.5 \qquad \textbf{4.1}$$

GPS Time is similar to TAI but for the offset value of 32.184s

Greenwich Mean Sidereal Time (θ_{GMST}) defined by the Greenwich hour angle of the vernal equinox (**Figure 4.2**)

$$\theta_{GST0} = 100°.4606184 + 36000.770053T_{UT1} + 0.00038793T_{UT1}^{2} - 2.6\text{x}10^{-8}T_{UT1}^{3}$$

$$\theta_{GMST} = \theta_{GST0} + \omega_e UT1 \qquad \textbf{4.2}$$

Where

$\boldsymbol{T_{UT1}}$ = Number of Julian centuries elapsed from epoch J2000

$$= \frac{JD_0 - 2451545.0}{36525}$$

JD_0 = Julian day number for date of interest

ω_e = Earth's mean angular rotation rate ($0°.004178074622291205 0. s^{-1}$)

Local Sidereal Time (LST) is defined as the hour angle of the vernal equinox (γ) relative to the local meridian. The local sidereal time (θ_{LST}) is related to GMST through the longitude of the observer by

$$\theta_{LST} = \theta_{GMST} + \lambda$$

Universal Time (UT1) is today's realization of a mean solar time and is derived from GMST.

Co-ordinated Universal Time (UTC) is tied to the TAI by an offset of integer seconds.

Terrestrial Dynamical Time (TDT) is the theoretical time scale of apparent geocentric ephemeredes of bodies in the solar system. TDT derives directly from TAI and is given by TAI + 32.184s.

Barycentric Dynamical Time (TBD) is the independent variable of the equations of motion with respect to the barycentre of the solar system. TBD includes relativistic effects. Conversion between TBD and TDT is sufficiently obtained by

$$TDB = TDT + 0.001658 \sin M_e + 0.00001385 \sin(2M_e) \qquad \textbf{4.3}$$

$$M_e = 357^{\circ}.5277233 + 0.9856003(JD - 2451545.0)$$

(M_e = Earth mean anomaly)

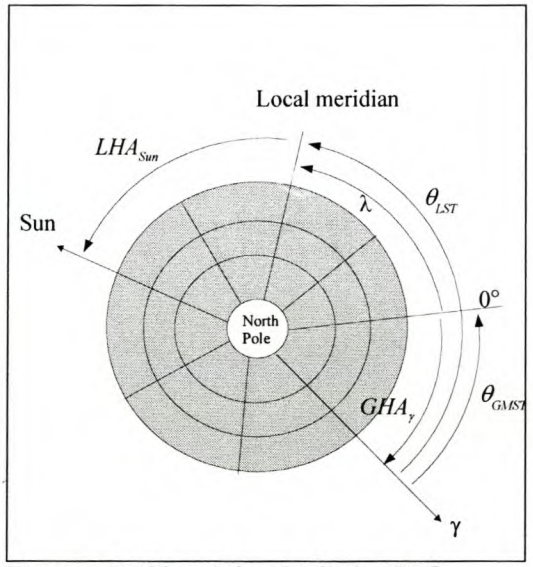

Figure 4.2. Sidereal time [Vallado 1997]

4.4 CO-ORDINATE SYSTEMS

4.4.1 Geographic Co-Ordinates

The geographical position of any point on the earth's surface may be described in terms of its *longitude* (λ) and *latitude* (ϕ). The origin of the geographic coordinate system is the intersection of the equator and the prime meridian (Greenwich). Longitude and latitude are measured in *degrees* with $\lambda \in$[-180°, 180°] and $\phi \in$[-90°, 90°]. Values for longitude are negative west of Greenwich and values for latitude negative south of the equator.

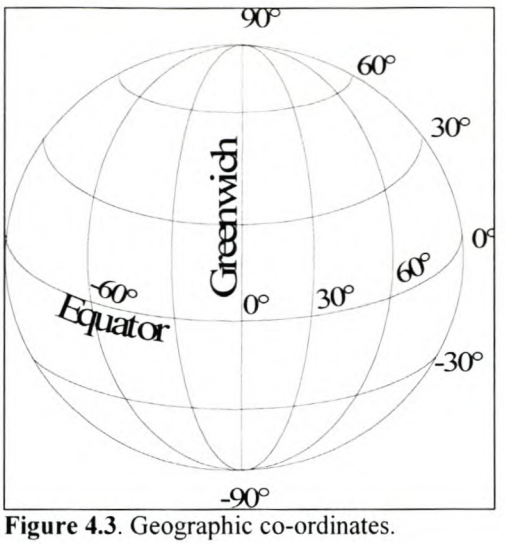

Figure 4.3. Geographic co-ordinates.

4.4.2 Heliocentric-Ecliptic system

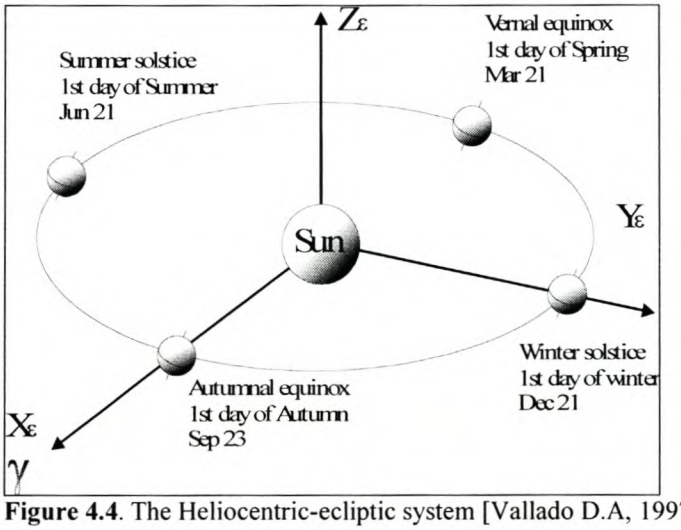

Figure 4.4. The Heliocentric-ecliptic system [Vallado D.A, 1997, Pp37].

The Heliocentric-Ecliptic coordinate system has its origin at the centre of the Sun. The Xε - Yε, or fundamental plane, coincides with the ecliptic. The line of intersection of the ecliptic plane and the Earth's equatorial plane defines the direction of the Xε - axis as indicated in **Figure 4.4**. The positive Xε - axis points to the *vernal equinox*, γ. The Zε-axis is normal to the ecliptic and the Yε-axis completes the right hand system. The heliocentric-ecliptic system is an inertial system except for precession and nutation of the Earth's axis of rotation, which causes a slow shift of the direction of γ.

4.4.3 Earth Centred Inertial System (*ECI, IJK, RAD*)

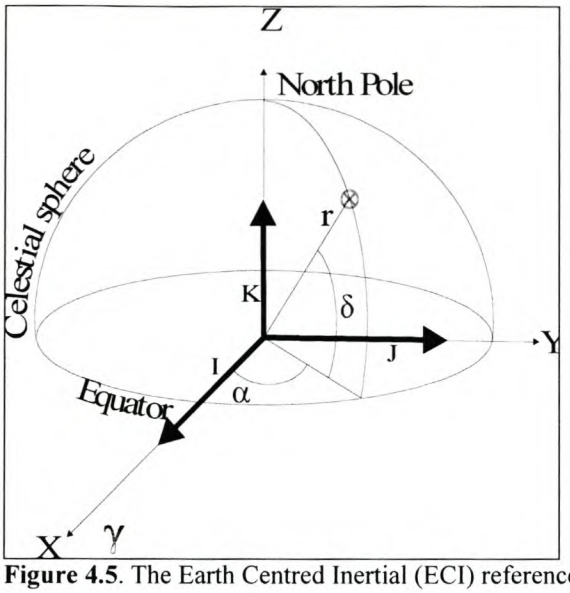

Figure 4.5. The Earth Centred Inertial (ECI) reference frame [Vallado 1997]

The *ECI* system has its origin at the Earth's centre with fundamental plane the equator, as indicated in **Figure 4.5**. The positive *X*-axis points to γ; the *Y*-axis is 90° to the east in the equatorial plane and the *Z*-axis extends through the North Pole, completing the right hand system. The *ECI* frame is fixed with respect to the stars (except for precession of the equinoxes) and the Earth turns relative to it. The vector description of an object in the ECI frame is given by

$$\mathbf{r} = x\mathbf{I} + y\mathbf{J} + z\mathbf{K}$$

where

$$x = r\cdot\sin\alpha\cdot\cos\delta,\ y = r\cdot\cos\alpha\cdot\cos\delta,\ z = r\cdot\sin\alpha \qquad \textbf{4.4}$$

and the spherical coordinates (α, δ, r):

α : **Right Ascension**. The angle measured eastward in the equatorial plane from a fixed inertial axis in space (vernal equinox) to a plane normal to the equator (meridian) which contains the object. $\alpha \in [0°, 360°]$.

δ : **Declination**. The angle between the object and the equatorial plane measured (positive above the equator) in the meridian plane. $\delta \in [-90°, 90°]$.

r : **Radial distance**. The scalar distance between the origin of the co-ordinate system and the location of the object. $r \geq 0$.

I, **J** and **K** are unit vectors along the X, Y and Z-axes respectively. The *ECI* frame is used interchangeably with the *Geocentric Equatorial* system, the *Right Ascension Declination* (*RAD*) system and the *IJK* system.

4.4.4 Earth Centred, Earth Fixed (*ECEF*) System.

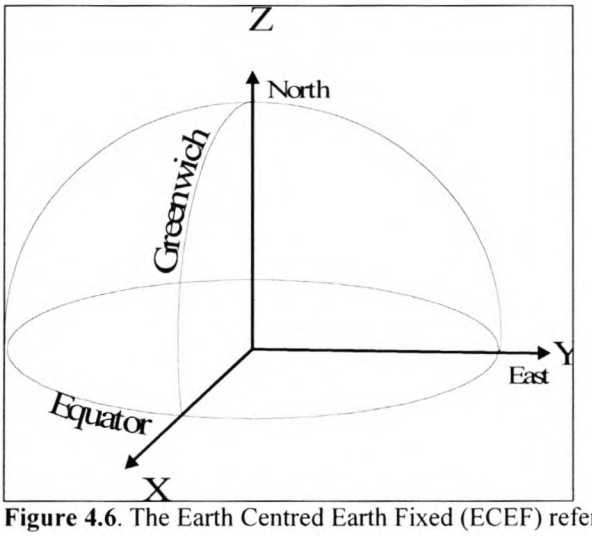

Figure 4.6. The Earth Centred Earth Fixed (ECEF) reference frame [Vallado 1997].

The ECEF system is fixed to and rotating with the Earth relative to the ECI frame. The primary axis is along the line joining the geo-centre with the intersection of the equatorial plane and the Greenwich meridian. The Y-axis is advanced 90° towards the east and the Z-axis extends through the North pole. The *ECEF* and *ECI* frames are related through Greenwich mean sidereal time (θ_{GMST}) as illustrated in **Figure 4.7**, and are discussed in more detail later in the chapter.

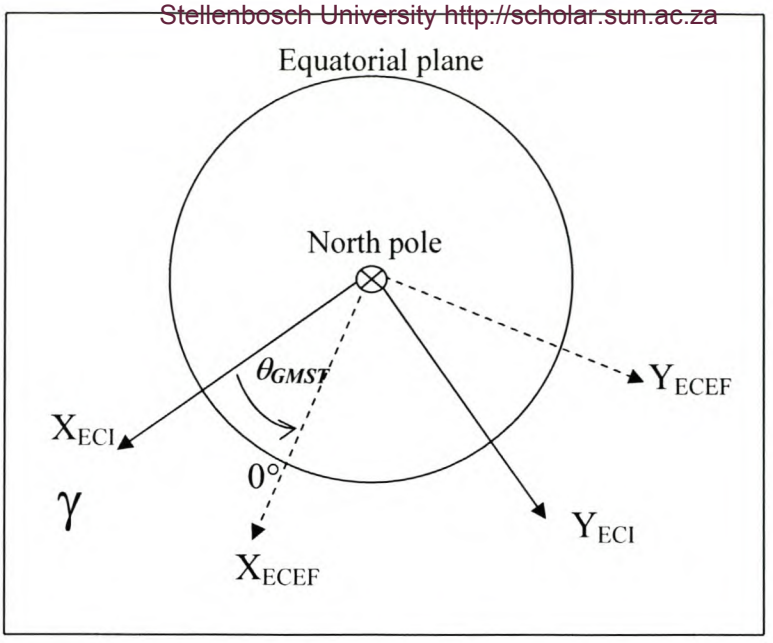

Figure 4.7. ***ECEF*** and ***ECI*** frames related by changing sidereal time, θ.

4.4.5 Azimuth Elevation (*AZEL*) System

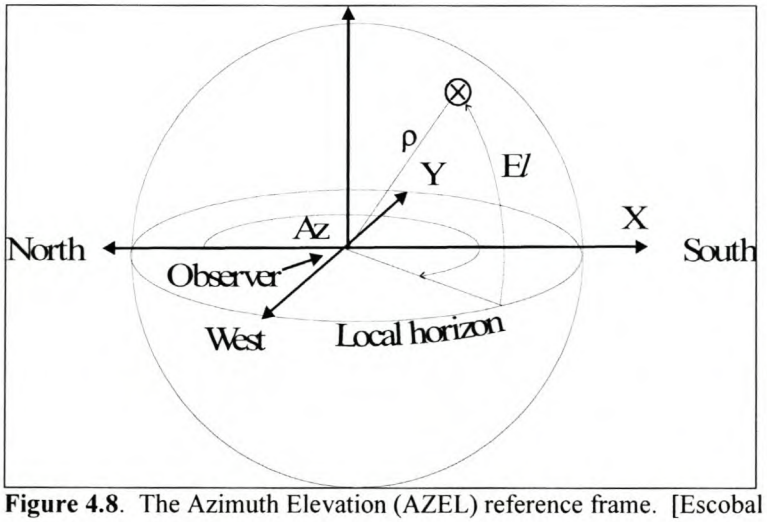

Figure 4.8. The Azimuth Elevation (AZEL) reference frame. [Escobal 1985, Pp133]

An observer standing on a particular meridian on the surface of a rotating planet sees all objects in a rotating coordinate system. In the *AZEL* system, the observer is at the origin of the coordinate system and the fundamental plane is the observer's local horizon. The principal axis points due South and the *Y*-axis points due East. The vector description of an object in the *AZEL* frame is similar to that in the *ECI* frame and is described by the spherical co-ordinates (*Az*, *El*, ρ):

Az: **Azimuth**. Angular distance measured eastward from North to the object's meridian, as measured in the local horizontal plane. $Az \in [0°, 360°]$.

E*l*: **Elevation**. Angular distance measured positively upward in the meridianal plane of an object above the local horizontal plane, which is tangent to the sphere at the observer's position. E$l \in [-90°, 90°]$.

ρ : **Slant range**. Distance from the observer to the object.

The *AZEl* system is also known as the *Topocentric Horizontal* co-ordinate system.

4.4.6 Perifocal Co-ordinate (*PQW*) System

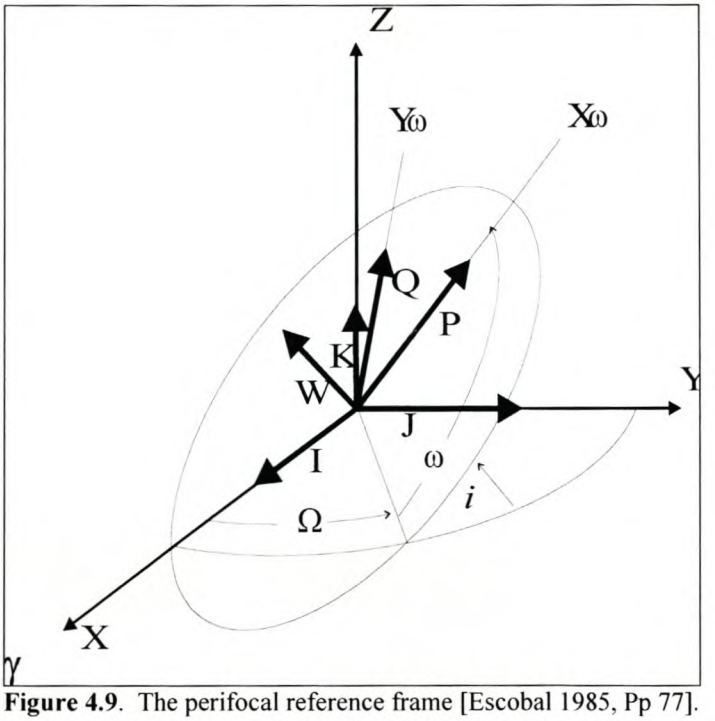

Figure 4.9. The perifocal reference frame [Escobal 1985, Pp 77].

In this system, the fundamental plane is the satellite's orbit and the origin is at the Earth's centre. The principal axis, X_ω, points in the direction of perifocus, the Y_ω-axis is 90° advanced from perifocus in the direction of satellite movement and the Z_ω-axis is normal to the orbital plane. The perifocal (or ***PQW***) system always maintains orientation towards perigee and does not rotate with the satellite. It is well suited for orbits with a well-defined eccentricity. The position of the orbit plane in space is defined by the three classical orientation angles, i, ω and Ω.

i: **Orbit Inclination.** The angle between the orbit and equatorial planes measured in a plane perpendicular to a line defining their respective intersection. $i \in [0,\pi]$.

Ω : **Right Ascension of the Ascending Node** (also Longitude of the Ascending Node). The angle measured in the equatorial plane between the principal axis (vernal equinox) and the line defining the intersection of the equatorial and orbit planes, as a point in the orbit plane passes through the equator in the sense negative to positive with respect to the Z-axis.

$\Omega \in [0,\pi]$.

ω : **Argument of Perigee.** The angle measured in the orbit plane from the line defined by the longitude of the ascending node to another line in the orbit plane, which contains the focus and passes through the perifocus. $\omega \in [0,\pi]$.

4.4.7 The Orthogonal Set (*UVW*)

This system is similar to the perifocal system with the fundamental plane the satellite's orbit, but differs in being a rotating system. The unit vector **U**, always points along the principal axis at the body under consideration. **V** is advanced to **U** in the sense of increasing true anomaly (ν) by a right angle in the plane of instantaneous motion. **W** completes the orthogonal set.

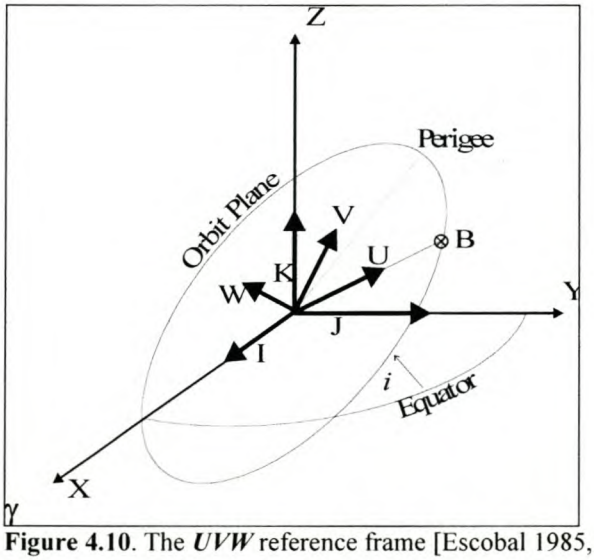

Figure 4.10. The ***UVW*** reference frame [Escobal 1985, Pp 80].

If a space vehicle or body (B) is at perifocus, the triads **U**, **V**, **W** and **P**, **Q**, **W** are coincident. At his point, the true anomaly is zero and the direction cosines are identical to those of the perifocal system. Since ν is measured in the orbital plane, the *argument of latitude* **u**, defined by

$$\mathbf{u} = \nu + \omega,$$

could be substituted for ω in order to obtain the direction cosines of the ***UVW*** set, that is $\mathbf{U} = \mathbf{P}(i, \Omega, u)$ and $\mathbf{V} = \mathbf{Q}(i, \Omega, u)$. **W** is the same in both frames.

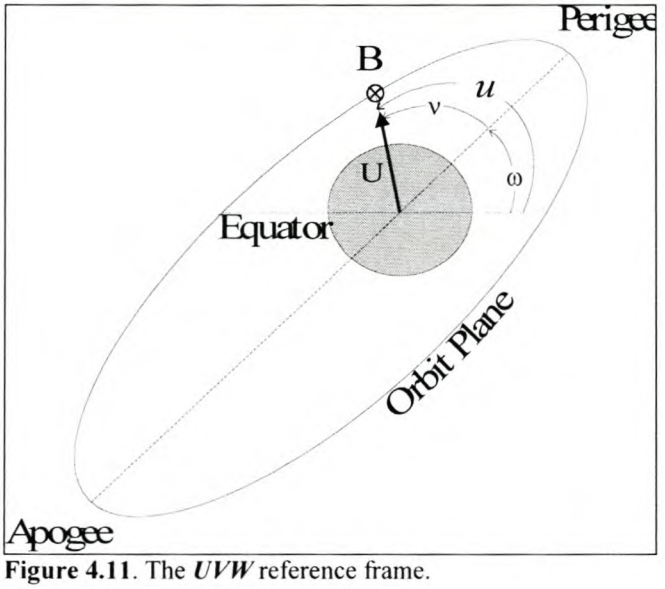

Figure 4.11. The ***UVW*** reference frame.

4.4.8 Orthogonal Transformations

Transformations to and from the orbital plane are frequently used in the orbit propagation process. In practise, for example, a body located in the *ECI* co-ordinate system is mapped from this system to the orbital plane. Analysis is then performed in the orbital plane and later the body is mapped back to the *ECI* system. The mapping of a vector **r,** located in the *PQW* system, to a vector **r** located in the *ECI* system, is accomplished by a vector transformation from one frame to the other [Escobal 1985, Pp 80]. This mapping function constitutes a *transformation matrix*, or *direction cosine matrix* constructed from the direction cosines of the *PQW* system. The theory of a direction cosine matrix construction from unit vector dot products and its relation to composite rotation matrices are presented in Appendix A.

The elements of a direction cosine matrix are essentially scalar components expressing each of the unit vectors **P**, **Q**, **W** as a linear combination of unit vectors **I**, **J**, **K** in the ECI frame.

$$\begin{bmatrix} \mathbf{P} \\ \mathbf{Q} \\ \mathbf{W} \end{bmatrix} = \begin{bmatrix} P_x & P_y & P_z \\ Q_x & Q_y & Q_z \\ W_x & W_y & W_z \end{bmatrix} \begin{bmatrix} \mathbf{I} \\ \mathbf{J} \\ \mathbf{K} \end{bmatrix}$$

For known angles Ω, ω, i (Figure 4.9), the transformation matrix constituting the direction cosines of **P**, **Q**, **W** is given by

$$\mathbf{M} = \begin{bmatrix} P_x & P_y & P_z \\ Q_x & Q_y & Q_z \\ W_x & W_y & W_z \end{bmatrix} = \mathbf{R}_z(\omega)\mathbf{R}_x(i)\mathbf{R}_z(\Omega)$$

or

$$\mathbf{M} = \begin{bmatrix} (\cos\omega\cos\Omega - \sin\omega\cos i\sin\Omega) & (\cos\omega\sin\Omega + \sin\omega\cos i\cos\Omega) & \sin\omega\sin i \\ (-\sin\omega\cos\Omega - \cos\omega\cos i\sin\Omega) & (-\sin\omega\sin\Omega + \cos\Omega\cos\omega\cos i) & \cos\omega\sin i \\ \sin\Omega\sin i & -\sin i\cos\Omega & \cos i \end{bmatrix} \quad \textbf{4.5}$$

where $\mathbf{R_x}$, $\mathbf{R_y}$, $\mathbf{R_z}$ represent X, Y and Z-axis rotation matrices (See Appendix A)

In matrix form,

$$\mathbf{r}_{PQW} = \mathbf{M} \cdot \mathbf{r}_{ECI}$$

By noting that $\mathbf{M}^{-1} = \mathbf{M}^{\mathrm{T}}$ because of matrix orthogonality, a vector $\mathbf{r}_{PQW}$ in the *PQW* frame will thus be presented in the *ECI* frame by

$$\mathbf{r}_{ECI} = \mathbf{M}^{\mathrm{T}} \cdot \mathbf{r}_{PQW}$$

4.5 MOTION OF THE CO-ORDINATE SYSTEM

The position of a near-Earth satellite is usually referenced to an Earth-tied reference frame such as the Perifocal (*PQW*) or *AZEL* frames. Certain calculations require this position to be transformed to the Earth Centred Earth Fixed (*ECEF*) and then to the Earth Central Inertial (*ECI*) frames. Both these frames are tied to the Earth's equator

and, in turn, the *ECI* frame also depends on the vernal equinox, which is tied to the ecliptic plane. The equatorial and ecliptic planes, however, are not fixed relative to the stars, but are time-dependent because of planetary and luni-solar gravitational actions (*precession* and *nutation*) on the Earth. When transforming a satellite's position between these frames, the time-dependent motion of the ecliptic and equatorial planes have to be taken into account [Vallado 1997, Pp 74].

To describe the time-dependent orientation of the equator and ecliptic, the standard reference frame based on the mean equator, ecliptic and equinox of the fixed epoch, 2000 January 1.5 (J2000, FK5 star catalogue), is used [Seidelmann 1992, Pp 99-121]. The following section describes these motions in more detail.

4.5.1 Precession and Nutation

General precession is a combined effect of *planetary* and *luni-solar* precession and amounts to a change in longitude of about 50" per year [Seidelmann 1992, Pp 99]. Planetary precession is the result of the gravitational action of the planets on the Earth's orbit, which results in a very slow, secular change in the ecliptic's orientation. This causes a westward precession of the equinox of about 12" per century and a decrease in the obliquity of the ecliptic (ε) of about 47" per century [Vallado 1997, Pp 75]. A torque exerted on the Earth's equatorial bulge by the Sun and Moon causes luni-solar precession. This torque attempts to align the equator with the ecliptic and results in a gyroscopic motion of the Earth's rotation axis around the pole of the ecliptic with a period of about 26 000 years, causing the vernal equinox to recede along the ecliptic at a rate of about 49.846" per year [Vallado 1997, Pp 75].

Nutation consists of small oscillations in the Earth's rotation axis and is caused by an additional torque on the equatorial bulge by the Moon. Because the Moon's orbital plane precesses around the Earth with a period of 18.6 years, nutation is a short-term, periodic motion of about 18.6 years with amplitude of about 9".

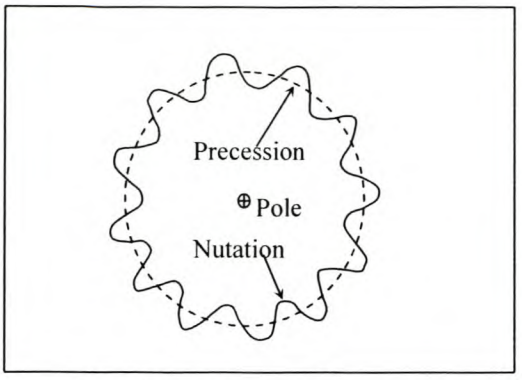

Figure 4.12. Polar motion due to precession and nutation.

Before formulating the effects of precession and nutation, the following set of terms is introduced to completely specify the frame of reference [Seidelmann 1992, Pp 99; Vallado 1997, Pp 76-77]:

Ecliptic of epoch: The orientation of the ecliptic at a fixed epoch, $\varepsilon_F = t_0$ (J2000)

Ecliptic of date: The orientation of the ecliptic at a specific date, $\varepsilon_D = t$.

Mean equator of date: The Earth's equator modelled at a specific date, taking into account planetary precession only.

Mean equinox of date: The intersection, at a given date, of the planes of the ecliptic of date and the mean equator of date.

True equator of date: The Earth's equator modelled by taking into account planetary precession and nutation.

To transform completely from the inertial, *J2000* frame to *ECEF* co-ordinates of an arbitrary date, four separate groups of rotations and conversions are necessary *viz.*, precession, nutation, sidereal time and polar motion. Given *ECI* position and velocity vectors $\mathbf{r}_{J2000}$, $\mathbf{v}_{J2000}$, in the J2000 system, their co-ordinates in *ECEF* are obtained by

$$\mathbf{r}_{ECEF} = \mathbf{MSNP} \cdot \mathbf{r}_{J2000} \;,\; \mathbf{v}_{ECEF} = \mathbf{M}\{\mathbf{SNPv}_{J2000} - \boldsymbol{\omega}_e \times \mathbf{r}_{ECEF}\} \qquad \mathbf{4.6}$$

Where the respective matrices indicate rotations due to precession (**P**), nutation (**N**), Sidereal time (**S** = $\mathbf{R}_z(\theta_{AST})$) and Polar motion (**M**).

By using the J2000 position vector and the time rate of change of the rotation matrix for sidereal time, the equation for velocity reduces to

$$\mathbf{v}_{ECEF} = \mathbf{M}\dot{\mathbf{S}}\mathbf{N}\mathbf{P}\mathbf{r}_{J2000} + \mathbf{M}\mathbf{S}\mathbf{N}\mathbf{P}\mathbf{v}_{J2000} \qquad \textbf{4.7}$$

Where

$$\dot{\mathbf{S}} = \begin{bmatrix} -\omega_e \sin\theta_{AST} & \omega_e \cos\theta_{AST} & 0 \\ -\omega_e \cos\theta_{AST} & -\omega_e \sin\theta_{AST} & 0 \\ 0 & 0 & 0 \end{bmatrix}, \ \theta_{AST} = \text{sidereal time}$$

The development of the individual rotation matrices is subsequently presented [Kaplan 1989, Seidelmann 1992 Pp 100-120, Vallado 1997, Pp 75-89; Montenbruck 2000, Pp 174-185].

4.5.2 Reduction of Precession (*J2000*)

This process converts an *ECI* vector, r_{J2000}, in the *J2000* system (having a mean equinox of *J2000*), to an *ECI* vector, r_{ECImod}, having the mean equinox of date.

$$\mathbf{r}_{ECImod} = \mathbf{P} \cdot \mathbf{r}_{J2000} \qquad \textbf{4.8a}$$

Where

$$\mathbf{P} = \mathbf{R}_z(-z) \cdot \mathbf{R}_y(\Theta) \cdot \mathbf{R}_z(-\xi) \qquad \textbf{4.8b}$$

The rotation angles, (z, Θ, ξ) are calculated from

$$\begin{aligned} \xi &= 0^\circ.640616 \cdot T_{TDB} + 0.0000839 \cdot T_{TDB}^2 + 5.0 \times 10^{-6} T_{TDB}^3 \\ z &= 0^\circ.640616 \cdot T_{TDB} + 0.0003041 \cdot T_{TDB}^2 + 5.1 \times 10^{-6} T_{TDB}^3 \\ \Theta &= 0^\circ.556753 \cdot T_{TDB} + 0.0001185 \cdot T_{TDB}^2 - 1.16 \times 10^{-6} T_{TDB}^3 \end{aligned} \qquad \textbf{4.8c}$$

where T_{TDB} represents the number of Julian centuries from epoch, *J2000*,

$$T_{TDB} = \frac{JD_{TDB} - 2451545.0}{36525} \qquad \textbf{4.8d}$$

and JD_{TDB} is the Julian date expressed in Dynamic Barycentric Time.

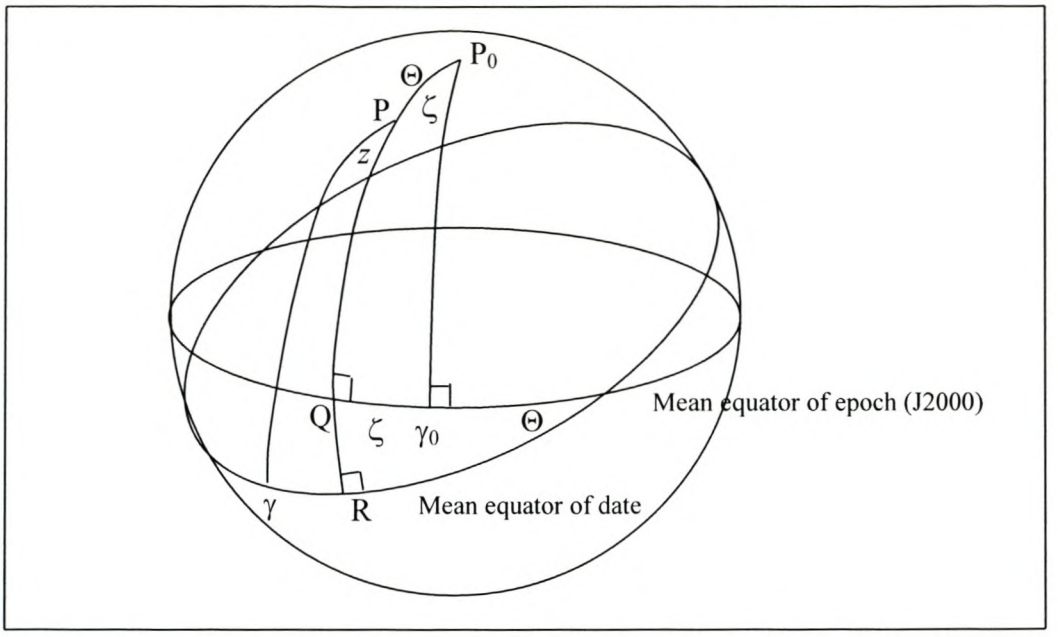

Figure 4.13. Transformation geometry due to precession [Seidelmann 1992, Pp 102]

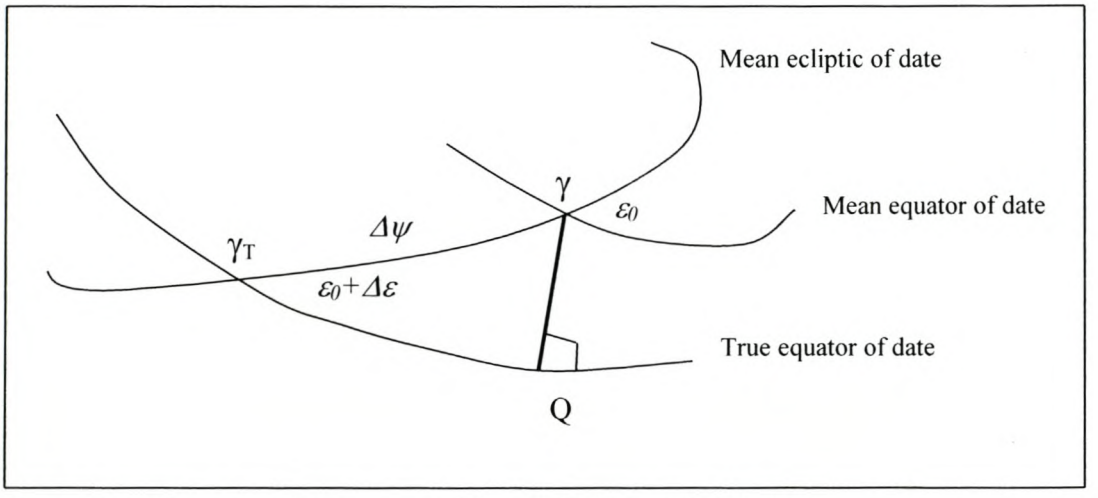

Figure 4.14. The mean and true equators of date [Seidelmann 1992, Pp 115]

4.5.3 Reduction of Nutation (*J2000*)

By adding the effects of nutation, co-ordinates are transformed from the mean equator of date to the true equator of date. This is accomplished by

$$\mathbf{r}_{ECltod} = \mathbf{N} \cdot \mathbf{r}_{EC\,\mathrm{Im}\,od} \qquad \textbf{4.9a}$$

Where the nutation matrix, **N**, is given by

$$\mathbf{N} = \mathbf{R}_x(-\varepsilon) \cdot \mathbf{R}_z(-\Delta\psi) \cdot \mathbf{R}_x(+\varepsilon_0) \qquad \textbf{4.9b}$$

The rotation angles, (ε, $\Delta\psi$, ε_0), are obtained from the following definitions:

ε_0: The mean obliquity of the ecliptic expressed as a function of time (from J2000), given by

$$\varepsilon_0 = 23^\circ.439291 - 0.0130042 \cdot T_{TDB} - 1.64 \times 10^{-7} \cdot T_{TDB}^2 + 5.04 \times 10^{-7} T_{TDB}^3 \qquad \textbf{4.9c}$$

ε The true obliquity of date given by

$$\varepsilon = \varepsilon_0 + \Delta\varepsilon \qquad \textbf{4.9d}$$

The nutation angles $\Delta\psi$ and $\Delta\varepsilon_{\text{are}}$ evaluated from

$$\Delta\psi = \sum_{i=1}^{n} S_i \sin A_i \,, \quad \Delta\varepsilon = \sum_{i=1}^{n} C_i \cos A_i \qquad \textbf{4.9e}$$

Where

$$A_i = a_i M_{Moon} + b_i M_{Sun} + c_i u_M + d_i D + e_i \Omega \qquad \textbf{4.9f}$$

A table of the multipliers a_i, b_i, c_i, d_i, e_i and the coefficients S_i and C_i are given in [Vallado 1997, Pp 880; Seidelmann 1992, Pp 112-113]. These coefficients define the 106 terms of the IAU 1980 nutation series. The fundamental arguments M_{Moon}, M_{Sun}, u_M, D and Ω in the FK5 reference system are, in turn, defined by [Vallado 1997, Pp 79]

Moon mean anomaly:

$$M_{Moon} = 134^0.9629814 + (1325r + 198.8673981) \cdot T_{TDB} + 0.0086972 \cdot T_{TDB}^2 + 1.778 \times 10^{-5} T_{TDB}^3 \qquad \textbf{4.10}$$

Sun mean anomaly:

$$M_{Sun} = 357^0.5277233 + (99r + 359.05034) \cdot T_{TDB} - 0.00016028 \cdot T_{TDB}^2 - 3.33 \times 10^{-6} T_{TDB}^3 \qquad \textbf{4.11}$$

Moon mean argument of latitude:

$$u_M = 93.^0.2719103 + (1342r + 82.0175381) \cdot T_{TDB} - 0.0036825 \cdot T_{TDB}^2 + 3.06 \times 10^{-6} T_{TDB}^3 \qquad \textbf{4.12}$$

Mean elongation of the Sun:

$$D = 297^0.8503631 + (1236r + 307.111480) \cdot T_{TDB} - 0.00191417 \cdot T_{TDB}^2 + 5.28 \times 10^{-6} T_{TDB}^3 \qquad \textbf{4.13}$$

Moon's mean orbit longitude of the ascending node:

$$\Omega = 125^0.0445222 - (5r + 134.1362608) \cdot T_{TDB} + 0.0020708 \cdot T_{TDB}^2 + 2.22 \times 10^{-6} T_{TDB}^3$$

(r = 360°) **4.14**

4.5.4 Sidereal Time (*J2000*)

Greenwich apparent sidereal time is measured on the true equator relative to the true equinox and *Greenwich mean sidereal time* is measured along the mean equator relative to the mean equinox. The difference between these two times is called the *equation of the equinoxes*. The equation of the equinoxes is used to convert between the apparent (θ_{AST}) and mean (θ_{GST}) sidereal times and is given by

$$\theta_{AST} = \theta_{GST} + \Delta\psi \cos\varepsilon + 0.00264'' \sin(\Omega) + 0.000063 \sin(2\Omega) \qquad \textbf{4.15}$$

The rotation (without polar motion) is then given by

$$\mathbf{r}_{ECEFnopm} = \mathbf{R}_z(\theta_{AST}) \cdot \mathbf{r}_{ECItod} \qquad \textbf{4.16}$$

4.5.5 Polar Motion

Polar motion accounts for the North pole's changing position due to internal, non-rigid Earth motions. The *Celestial Ephemeris Pole* (CEP) is the axis of Earth rotation, which is normal to the true equator, while the *Conventional International Origin* (CIO) is the mean (terrestrial) location of the pole. The x and y displacements are measured positive south along the 0° and 270° meridians respectively and reach a maximum amplitude of 9m in any direction. The transformation is accomplished by

$$\mathbf{r}_{ECEF} = \mathbf{M}\mathbf{r}_{ECEFnopm} \qquad \textbf{4.17}$$

Where the polar motion matrix, M, is given by [Montenbruck 2000, Pp 181-185]

$$\mathbf{M} = \mathbf{R}_y(-x_p) \cdot \mathbf{R}_x(-y_p) \approx \begin{bmatrix} 1 & 0 & +x_p \\ 0 & 1 & -y_p \\ -x_p & +y_p & 1 \end{bmatrix} \qquad \textbf{4.18}$$

In view of the small angles involved, the angles are approximated by their first terms in the linear expansion of their respective trigonometric functions and are subsequently taken to be x_p and y_p, measured in radians.

Chapter 5

Methodology, Software and Data

5.1 INTRODUCTION

This chapter describes the methodology implemented, software developed, data employed and result verification in calculating the position and velocity of a near-Earth satellite, subject to perturbative forces.

5.2 METHODOLOGY

The perturbed equations of motion developed in Chapter 3 were coded in a FORTRAN programme and numerically integrated using the Runge-Kutta-Fehlberg $7(8)^{th}$ order integrator with adaptive step-size through error control. An initial integration step-size of sixty seconds and relative and absolute errors of 1.0×10^{-8} were used. The epoch of propagation (t_0) was selected as 06 April 2000 at 00h00.00 UTC, corresponding to the epoch of the reference orbit obtained from [HTSI]. The initial conditions in ECI, mean equinox and equator of J2000 co-ordinates were

$$\mathbf{r_0} = [-611359.6934,\ 6818312.96,\ 1885999.168]^T \text{ (m)}$$
$$\mathbf{v_0} = [705.8965616,\ 1956.498735,\ -7218.130064]^T \text{ (m.s}^{-1}\text{)}$$

At each integration step t_i, the accelerations due to the various perturbative forces were calculated and, using the integrated position and velocity values from the previous integration step, t_{i-1} as new initial conditions, an updated state vector was calculated for time t_{i+1}. Integration results were written to an ASCII file at sixty-second intervals. Propagation was done from time t_0 to t_0 + 864000 s and was terminated on 16 Feb 2000, 00:00:00.0 UTC.

Propagation results were evaluated by calculating absolute errors at 24h-intervals using the ten-day section of SLR-derived precision orbit, obtained from [HTSI] as reference. The results were also compared to results obtained by the commercial *WinHpop* [Microcosm] propagator and the public domain SGP4 propagator.

For comparative purposes, propagation with *WinHpop* was done using the same initial conditions and the same perturbative forces used by *Orblitz* (i.e. Atmospheric drag, Solar radiation pressure, Luni-Solar and Earth non-symmetry perturbations (EGM96 70x70 gravity). The Harris-Priester atmospheric model employed by *WinHpop* used the same daily and 81-day mean Solar Flux (F10.7cm) values, but only required a single Magnetic Index (Ap) value, compared to the 8x3-hourly values required by the MSIS90 model employed by *Orblitz*.

Propagation with the SGP4 propagator was done with Satellite Toolkit (STK) [Analytical Graphics] using the following TLE file, captured on 4 Feb 2000 05:33:53.31 UTC

```
1 25636U 99008C   00035.23186697  .00000318  00000-0  94780-4 0  1501
2 25636  96.4675 271.9863 0151557 243.2466 115.3161 14.41106294 49797
```

Absolute-errors for SGP4 and *WinHpop* propagation were calculated using the same section of SLR-derived reference orbit. These results are respectively presented and discussed in Chapters 6 and 9 .

5.3 Software Design Considerations

5.3.1 Programming Language

Three major factors were considered in selecting an appropriate programming language for the software development, *viz.*, ease of implementation, execution speed and availability of source code for complex libraries such as calculating atmospheric density. The programming environment also had to be flexible, allowing for quick modifications to the algorithms [Du Toit 1997, Pp 3-1]. An optimal solution was obtained by the use of a (MS) FORTRAN compiler for ease of implementation and execution speed. The Pascal and C/C++ programming languages were ruled out for use in this study for their lack of certain basic intrinsic mathematical functions, programming complexity and lack of availability of software libraries. Matlab was excluded for its relative slow execution speed.

5.3.2 Precision

As stated previously, a major drawback of Cowell's method is the potential for error propagation in long-term numerical integration. The following precautions were taken to minimize the effects of round-off and truncation errors in this study:

5.3.2.1 Floating point arithmetic

Round-off and truncation error propagation was minimized by defining all floating-point numbers as double precision (64 bits, 16 significant digits) and by using proper techniques to avoid numerical phenomena like absorption, cancellation and smearing. Under/overflow errors were avoided by appropriate choice of units and by taking cognizance of the IBM PC's limitations in presenting very large/small numbers.
(The largest and smallest numbers presented by the IBM PC are respectively 1.79e+308 and 2.23e-308. The largest number, δ, permitted so that $1.0 + \delta = 1.0$ is 1.11e-16. See the Netlib library Routine **D1MACH** from the **SLATEC** library attached in Appendix E)

5.3.2.2 High order integration with step size control

The seventh order RKF integrator with eighth-order error estimate keeps the local and global errors within predefined boundaries of 1.0e-8 by automatically adapting the integration step size.

5.4 PROGRAMME STRUCTURE OF ORBLITZ

5.4.1 Programme Outline

The developed programme structure is outlined in **Figure 5.1** with a description of the routines and functions given in **Table 5.1**. Relevant routines are attached in the programme listing in Appendix E. A few well-documented routines, such as the **NWGTD6** atmospheric density routine, the **RK78** numerical integrator and Kaplan's routines on precession and nutation (**NOVAS**), were sourced from existing libraries. These routines are well-tried industry-standard and no other purpose would have been served in developing them anew.

Figure 5.1. Orblitz Programme Structure

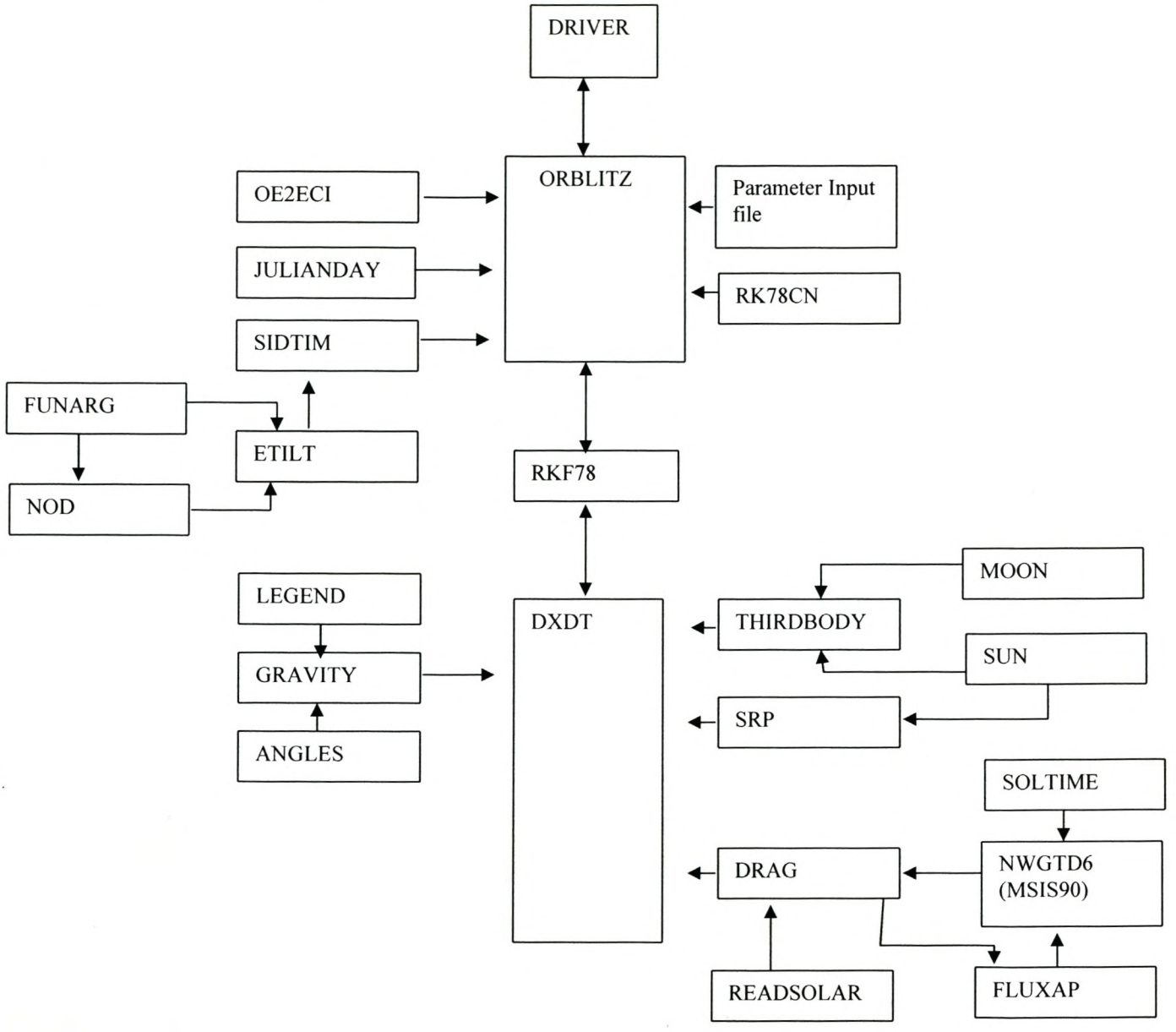

JulianDay	*Computes Julian date for given (Gregorian) calendar date and time.*
Sidtim	*Calculates the sidereal time (Greenwich hour angle). Uses the NOVAS library (Kaplan, Seidelmann)*
Funarg	*Calculates fundamental arguments (mean elements) of the Sun and Moon. Uses NOVAS library (Kaplan, Seidelmann)*
NOD	*Calculates the nutation series. Uses NOVAS library (Kaplan, Seidelmann)*
Etilt	*Calculates quantities required for nutation and precession. Uses NOVAS library (Kaplan Seidelmann)*
Kepler	*Solves Kepler equation*
Oe2eci	*Transform orbital element a, e, i, Ω, ω and ν to Cartesian coordinates x, y, z, vx, vy, vz*
ReadSolar	*Reads F10.7 solar flux and Ap magnetic index values from file.*
FluxAp	*Assigns correct solar flux and magnetic index values to relevant time intervals for atmospheric density calculations.*
Rk78cn	*Computes the Fehlberg coefficients for a Runge-Kutta 7(8) integrator*
Rk78	*Runge-Kutta 7(8) method as given by the Fehlberg coefficients*
SRP	*Calculates solar radiation pressure*
DXDT	*Compute derivatives of the equations of motion*
Gravity	*Computes the perturbation due to an aspherical Earth using spherical harmonics (Calls Legend and Angles)*
Legend	*Computes Legendre and associated Legendre functions up to degree n and order m, $n \geq .m$*
Angles	*Computes cos(ma), sin(ma), m.tan(b) and store values in arrays Cn, Sn, Tn*
Sun/Moon	*Computes the Cartesian ECI positions for the Sun/ Moon*
Thirdbody	*Computes Cartesian ECI position of a perturbing third body*
Drag	*Computes drag perturbation on the satellite due to motion through an atmosphere*
NWGTD6	*Computes density for altitudes between 90km to 1000 km using the MSIS90 model of AE Hedin*

Table 5.1.Subroutine and Functions employed in *Orblitz*

5.4.2 Data Files

The ASCII data files utilized by the software are listed in **Table 5.2** and their respective formats, with examples, are described in Appendix F.

Table 5.2. Data files used in Orblitz

File name	Description	Source
parameters.dat	Epoch values, constants and switches	
egm96.dat	EGM96 gravity file	NIMA 1997
solar.dat	Solar flux and Ap index data	Compiled from www.spaceweather.com

The file containing the EGM96 spherical harmonic coefficients (C_{nm}, S_{nm}) for aspherical Earth gravity acceleration calculation, is too large to reproduce in this document, but is available in the public domain [NIMA 1997]. The Solar flux (F10.7 and F10.7A) and magnetic index (Ap) values used to calculate atmospheric density are presented in **Figures 5.2** and **5.3** respectively. Their numeric values are listed in Appendix F.

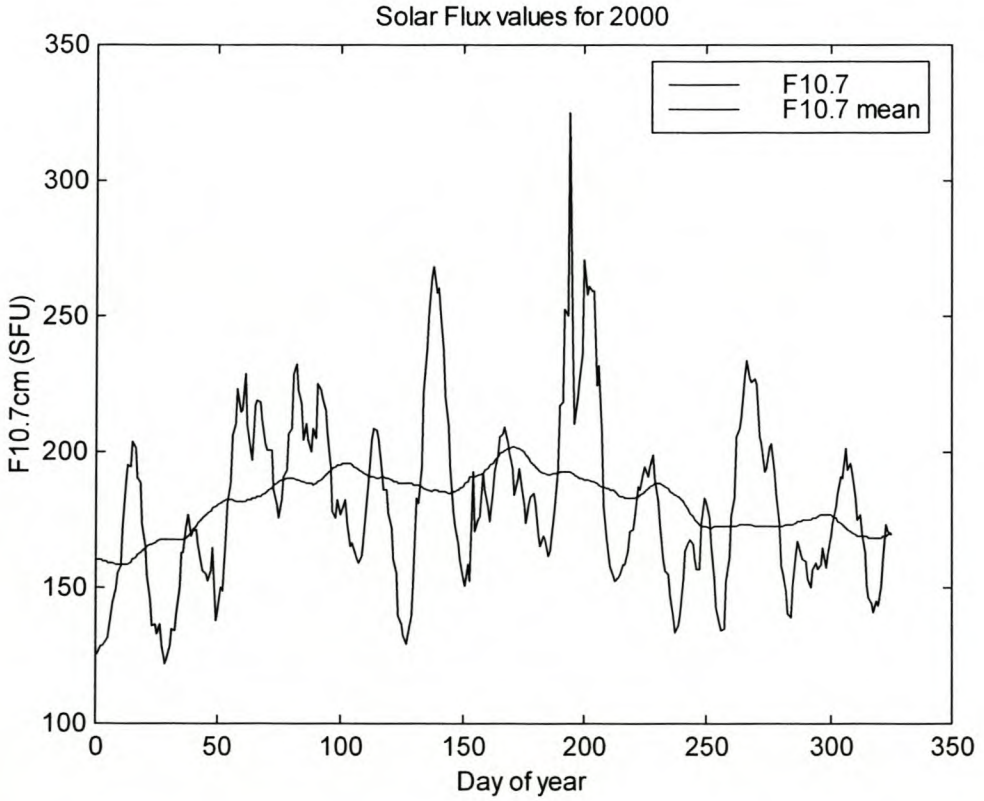

Figure 5.2. Daily Solar Flux data for 2000. The 81-day mean value is centred on the day of interest.

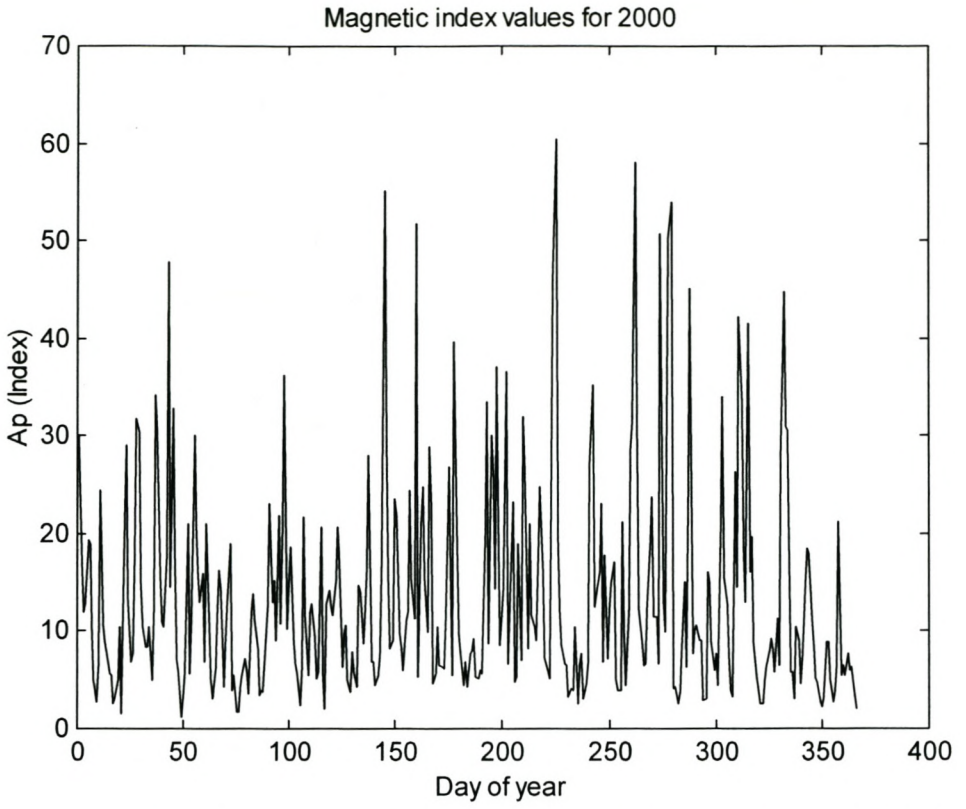

Figure 5.3. Mean daily magnetic index data for 2000. Mean Ap is calculated from daily 8 x 3hour measurements.

Chapter 6

Results: Precision propagation

6.1 RESULTS

The complete ten-day state vectors computed by respectively *Orblitz*, *WinHpop* and SGP4, along with the SLR-derived reference orbit, is supplied on CD-Rom due to their relative large file sizes. For illustration purposes, the first twenty-four hour section of the *Orblitz* state vector and the reference orbit is listed in Appendix G.

The following results are presented.

Table 6.1. The state vectors, as computed by the different programmes, at twenty-four hour intervals. Absolute errors are calculated using the SLR-derived orbit as reference.

Figures 6.1 and **6.2**. Graphical representation of the absolute errors in position and velocity error at twenty-four hour intervals.

6.2 DISCUSSION

A short discussion on the results is presented and final conclusions are presented in Chapter 9. As illustrated in **Figures 6.1** and **6.2** and **Table 6.1**, the smallest propagation errors in position and velocity were obtained with *Orblitz*, followed by *WinHpop* and SGP4. *Orblitz* propagation, *sans* atmospheric drag, gave the largest deviation from the reference orbit, underlining the importance of quantifying atmospheric drag as perturbative force. At the end of the ten-day propagation period, a relative small difference in absolute error (max 3686m in position) exists between *WinHpop* and SGP4, placing these two propagators in the same accuracy class for the test case. These comparative errors give a good indication of the efficient use of the SGP4 model's B-star drag coefficient as free parameter to account for unmodelled perturbation errors.

Orblitz' improved performance to *WinHpop* in this test case may probably be attributed to the use of an improved atmospheric model, rather than to a superior propagation theory. *WinHpop* employs the Harris-Priester density model and *Orblitz* the MSIS-90 model. These models differ in mathematical and computational complexity with more stringent data requirements exacted by MSIS-90. Results of this test case confirm the findings of [Chao *et. al.*, 1996] on the superior performance of the MSIS-90 model at calculating atmospheric density.

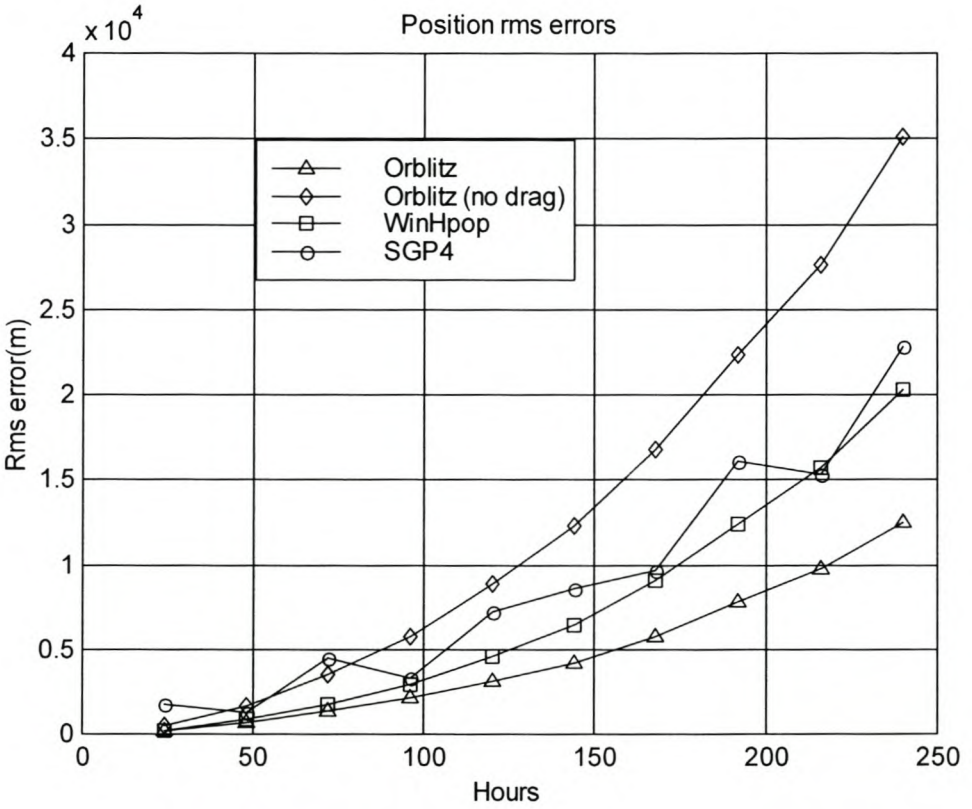

Figure 6.1. Absolute errors in position at twenty-four hour intervals. Errors were calculated using the SLR-derived orbit as reference.

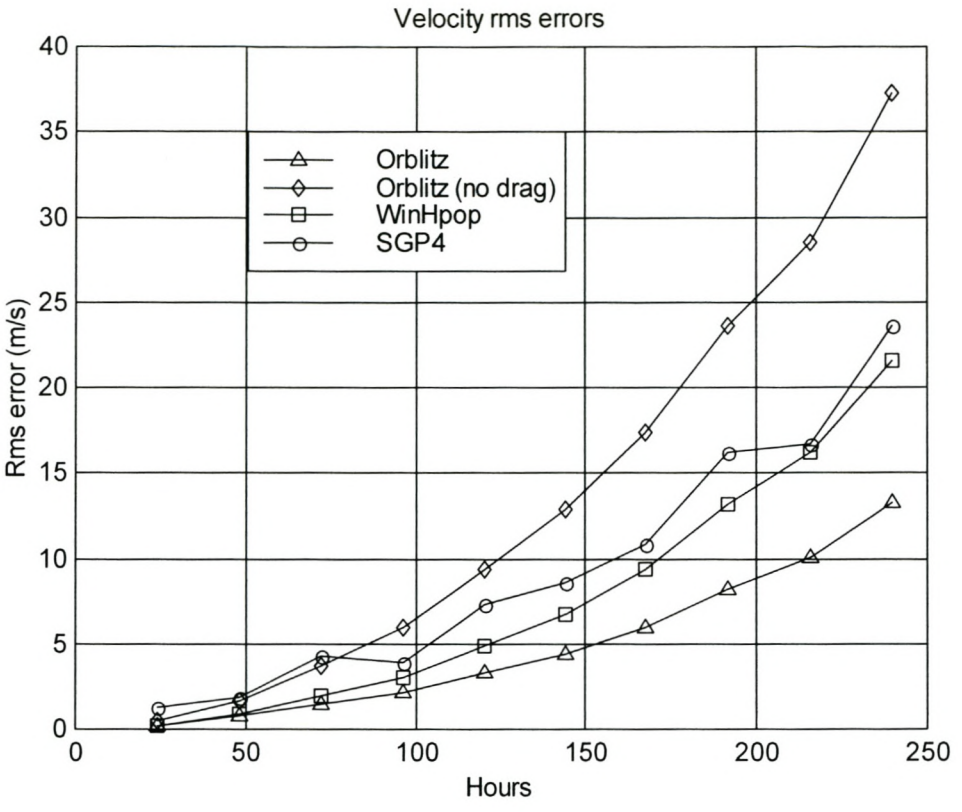

Figure 6.2. Absolute errors in velocity at twenty-four hour intervals. Errors were calculated using the SLR-derived orbit as reference.

Table 6.1. Ephemeris propagation results using various methods, compared to the NASA-generated SLR-ephemeris for SUNSAT.

Date	Program	X (m)	Y (m)	Z (m)	V_x (m.s^{-1})	V_y (m.s^{-1})	V_z (m.s^{-1})	Err **r** (m)	Err **v** (m.s^{-1})
6 Feb 2000	SLR	941064.0962	-4405141.5020	-5500736.4241	-98.0065	-5926.7153	4590.3241		
00:00:00	ORBLITZ	941085.4530	-4404949.2540	-5500879.5910	-97.9900	-5926.8650	4590.1420	240.6495	0.2363
UTC	ORB/DRAG	941088.6990	-4404773.5910	-5501018.5150	-97.9590	-5927.0110	4589.9580	464.2619	0.4730
	WinHPop	941070.4822	-4404975.4996	-5500866.9438	-97.9848	-5926.8539	4590.1497	211.2652	0.2239
	SGP4	940036.7515	-4403897.5911	-5501363.9659	-98.2798	-5927.8308	4589.7629	1731.0575	1.2783
7 Feb 2000	SLR	-855040.3813	497331.9959	7135069.7167	-548.5282	7346.3337	-655.4201		
	ORBLITZ	-855027.5530	496604.6790	7135132.7810	-548.6170	7346.3840	-654.6780	730.1585	0.7491
	ORB/DRAG	-854960.9490	495696.0610	7135224.0130	-548.7280	7346.4420	-653.7400	1645.1139	1.6954
	WinHPop	-854992.8634	496500.6030	7135152.0351	-548.6218	7346.3871	-654.5620	836.8084	0.8648
	SGP4	-854478.8635	496353.7136	7135569.1148	-547.7736	7346.0214	-653.7046	1233.5870	1.9000
8 Feb 2000	SLR	357697.4419	3459930.2996	-6114373.7263	1060.3259	-6541.1546	-3670.2167		
	ORBLITZ	357533.7600	3461151.4740	-6113686.6870	1060.4350	-6540.4250	-3671.5030	1410.7025	1.4828
	ORB/DRAG	357237.6650	3462982.5680	-6112663.2320	1060.5480	-6539.3220	-3673.4590	3528.9556	3.7309
	WinHPop	357465.6964	3461487.2806	-6113501.2606	1060.4244	-6540.2179	-3671.8787	1799.7478	1.9102
	SGP4	357228.9991	3463846.8476	-6112263.1407	1059.2939	-6539.2738	-3673.9703	4473.6292	4.3233
9 Feb 2000	SLR	367746.2426	-6508346.3917	3137637.3411	-1097.7664	3090.2188	6601.3751		
	ORBLITZ	368068.8330	-6509242.5160	3135746.0170	-1097.6940	3088.2440	6602.3140	2117.5954	2.1878
	ORB/DRAG	368610.1310	-6510781.5820	3132500.3760	-1097.5010	3084.8570	6603.9340	5750.2057	5.9470
	WinHPop	368165.7709	-6509590.0450	3135020.1171	-1097.6245	3087.4863	6602.6801	2927.8898	3.0314
	SGP4	367320.6446	-6509437.9355	3134511.5759	-1096.7296	3087.0506	6603.4735	3338.1146	3.9390
10 Feb 2000	SLR	-1011120.1279	6865805.3613	1337515.1956	661.4067	1450.7946	-7376.8058		
	ORBLITZ	-1011434.5820	6865203.7450	1340573.5960	660.9320	1453.9930	-7376.1770	3132.8321	3.2940
	ORB/DRAG	-1011940.7900	6864101.1610	1346218.9570	660.0580	1459.9200	-7375.0100	8906.9214	9.3977
	WinHPop	-1011518.6686	6864929.2689	1342013.5163	660.7328	1455.5172	-7375.8767	4600.1372	4.8602
	SGP4	-1010612.2057	6865344.6002	1344740.1959	660.1392	1457.6742	-7374.6340	7257.4730	7.3248

Table 6.1 (Continued)

Date	Program	X (m)	Y (m)	Z (m)	V_x (m.s^{-1})	V_y (m.s^{-1})	V_z (m.s^{-1})	Err **r** (m)	Err **v** (m.s^{-1})
11 Feb 2000	SLR	1262347.6358	-5087331.9173	-4868842.7147	113.5667	-5217.5549	5319.5390		
	ORBLITZ	1262300.8740	-5084396.5520	-4871838.3110	114.4110	-5220.6570	5316.5570	4194.3001	4.3849
	ORB/DRAG	1262178.2950	-5078742.7730	-4877614.8550	115.9000	-5226.6510	5310.7800	12278.1319	12.8414
	WinHPop	1262256.0092	-5082821.3745	-4873455.8103	114.7376	-5222.3471	5314.9281	6452.4447	6.7525
	SGP4	1260827.6971	-5081088.1505	-4874467.6742	114.4872	-5224.2794	5314.2803	8540.1995	8.5860
12 Feb 2000	SLR	-949740.6355	923233.4683	7049685.7144	-968.7113	7268.2746	-1183.5710		
	ORBLITZ	-948914.7860	917612.8420	7050638.9480	-969.5910	7269.0010	-1177.7100	5760.3925	5.9710
	ORB/DRAG	-947483.6890	906863.4440	7052404.2280	-971.0920	7270.4290	-1166.4780	16746.9943	17.3919
	WinHPop	-948575.8698	914380.3835	7051152.9167	-969.9385	7269.4553	-1174.3236	9049.1145	9.4028
	SGP4	-947945.3275	914014.2091	7051915.9158	-968.8196	7269.0777	-1172.8179	9653.5833	10.7836
13 Feb 2000	SLR	246022.5601	2958328.8186	-6394024.8932	1472.0548	-6723.0775	-3124.7108		
	ORBLITZ	244342.0770	2965212.8770	-6390827.0340	1472.3700	-6719.6320	-3132.1740	7774.3545	8.2262
	ORB/DRAG	241509.7100	2978143.4950	-6384796.2910	1472.8980	-6713.1510	-3146.1460	22319.3709	23.6372
	WinHPop	243616.0007	2969372.3558	-6388887.5313	1472.5089	-6717.5641	-3136.6466	12415.4633	13.1555
	SGP4	243021.6687	2972638.2316	-6387284.6103	1471.0625	-6716.7414	-3139.5807	16099.5672	16.1940
14 Feb 2000	SLR	712214.4620	-6265331.6150	3557648.8656	-1353.2431	3467.5040	6355.0032		
	ORBLITZ	714192.8110	-6269911.9460	3549285.4220	-1352.1350	3458.8100	6359.9330	9738.6080	10.0557
	ORB/DRAG	717475.3790	-6278331.1300	3533853.8950	-1350.3030	3442.7950	6368.9600	27620.0157	28.5302
	WinHPop	715086.7755	-6272735.0213	3544144.5503	-1351.6458	3453.4814	6362.9276	15666.1145	16.1858
	SGP4	713959.8867	-6272331.1082	3544166.1166	-1350.5070	3453.5374	6363.6605	15291.3026	16.6583
15 Feb 2000	SLR	-1409404.6620	6859194.2126	748490.5303	689.8481	905.9237	-7488.0113		
	ORBLITZ	-1410625.1010	6857686.4890	760830.9040	686.9620	918.7770	-7486.6110	12491.8983	13.2475
	ORB/DRAG	-1412673.1980	6854922.5950	783225.7530	682.1410	942.1980	-7483.9620	35149.1926	37.3044
	WinHPop	-1411243.5035	6856757.6616	768537.3995	685.5451	926.8892	-7485.6840	20277.9457	21.5287
	SGP4	-1410147.4610	6857704.8412	771248.7928	684.7133	928.7252	-7484.4399	22819.0379	23.6438

Chapter 7

The Orbit Decay Problem

7.1 INTRODUCTION

The purpose of this chapter is the description of the orbit decay problem and its application to satellite lifetime and re-entry prediction. A short introduction to general perturbations, as applicable to the problem, is given and a semi-analytic solution to the problem of predicting the decay of a low Earth orbit (LEO) satellite is presented. The theory is finally evaluated by comparing predicted decay dates of two LEO satellites, *Iridium-85* and *Starshine-2* with their observed decay dates. A decay date for SUNSAT was then predicted at two possible solar activity levels.

For the purpose of this study, the semi-analytic Liu theory (SALT) is employed. This general method of averaging described by JJF Liu is employed to obtain the *mean* elements and expressions for their time rates of change. The derivation of these equations is explained in full in [Liu, 1974] and is presented here without derivation. The presented theory determines the time histories of semi-major axis (a), eccentricity (e), argument of perigee (ω) and longitude of ascending node (Ω) due to the influence of *Earth oblateness* and *atmospheric drag* as principal perturbative forces.

The rate of change of the orbital elements due to Earth oblateness is solved by analytic expressions and that due to drag is determined by direct numerical integration (quadrature) over true anomaly using fourth-order Runge-Kutta procedure. Inclination is assumed to be constant throughout the orbital lifetime. Satellite position and velocity are not calculated during the process but rather the evolution of the elements is propagated until sufficient altitude decrease (<90 km) indicates re-entry.

7.2 GENERAL PERTURBATIONS

The total variance experienced by any orbital element (q) due to perturbations can be presented by the following hypothetical equation

$$q = q_0 + \dot{q}_0(t - t_0) + K_1 \cos(2\omega) + K_2 \sin(2\nu + 2\omega) \qquad \textbf{7.1}$$

The first term on the right is the adopted epoch *mean element*; the second term is the *secular variation*; the third term the *long period variation* and the last term the *short period variation* [Escobal 1985, Pp 360; Vallado 1997, Pp 545].

Secular variations result in the steady, non-oscillating, continuous drift of an element from an adopted epoch value and increases or decreases as a linear, or at most, a quadratic function with time.

Short periodic variations are trigonometric functions of fast varying elements such as true anomaly (ν), eccentric anomaly (E), mean anomaly (M) or linear combinations of ν and ω (argument of perigee). These variations typically repeat on the order of the satellite's period or less, around some mean value of the element.

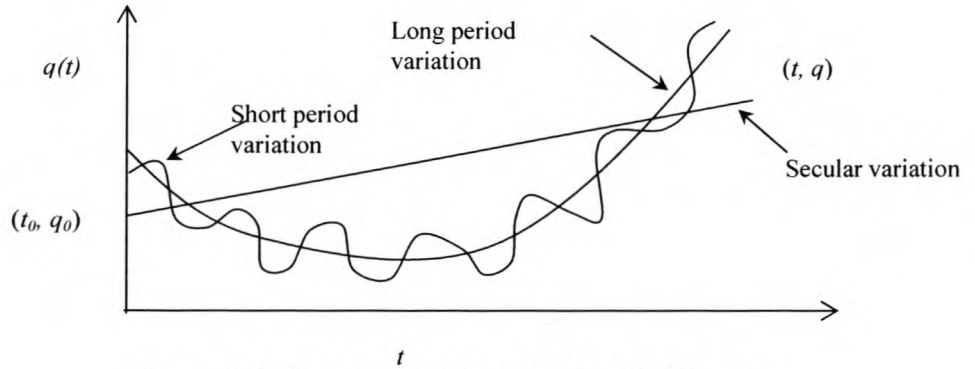

Figure 7.1 Effects of perturbation forces on orbital elements [Escobal 1985, Pp 362]

Long period variations are trigonometric functions of the slow varying argument of perigee,ω or multiples thereof. The typical period of this variation is the time to

complete a revolution of the argument of perigee or line of nodes and may be as long as several weeks. The difference between these variations is illustrated in **Figure 7.1** [Escobal 1985, Pp 362].

7.3 Influence of Earth Oblateness and Drag on Orbital Elements

7.3.1 Earth Oblateness

The asymmetry of the Earth, especially the bulge at the equator due to the J_2 ($-C_{20}$) zonal harmonic, exercises a torque on the satellite in orbit, resulting in a departure from two-body motion [Chobotov 1996, Pp 215]. Analytical investigation into the *oblateness* effects of a central body on a satellite has shown that certain elements such as ω, Ω and M experience *secular variations* from the adopted epoch values and *periodic variations* about these epoch values [Escobal 1985, Pp 361]. Other elements such as a, e, i only experience periodic variations about their mean values. In this study, the effects of perturbations due to Earth oblateness are addressed by the development of analytic expressions for the slow drift of the elements ω, Ω and M from their adopted epoch values at t_0.

7.3.2 Atmospheric Drag

Atmospheric drag is a non-conservative force, which removes energy directly from the orbit by reducing the satellite's inertial velocity [Liu, Alford, 1974]. The atmospheric drag effects on a LEO satellite are secular changes in semi-major axis (a), eccentricity (e) and to a small degree inclination (i). Periodic variations are experienced in all elements, especially i, Ω and ω. No analytic theory exists for drag due to the intrinsic difficult nature of calculating the variation of atmospheric density and accurately predicting drag coefficients. For the purpose of this study, the effects of drag perturbations are addressed with a hybrid of general and special perturbation procedures (semi-analytic) [Escobal 1985, Pp 382].

7.4 MEAN ELEMENTS

The long-term behaviour of satellite orbits is best determined by employing *mean* orbit elements rather than *osculating* orbit elements, which are better suited for short-term precision calculations. Mean elements are "averaged" over some selected time period (or angle such as v, M or E) and are free of short period variations [Escobal 1985, Pp 365]. Several theories exist for calculating mean elements such as the methods of Kozai and Brouwer. These theories differ from one another in the manner of separating secular, short-periodic and long-periodic variations. The mixing of elements or formulas from different theories will subsequently render erroneous results [Vallado 1997, Pp 626].

7.5 EQUATIONS OF MOTION

The variational equations of motion for a LEO satellite under the influence of Earth oblateness and atmospheric drag can be written in terms of the osculating elements a, e, i, Ω, ω and M as [Liu and Alford, 1974]

$$\dot{a} = \dot{a}_U + \dot{a}_{OB} + \dot{a}_D$$

$$\dot{e} = \dot{e}_U + \dot{e}_{OB} + \dot{e}_D$$

$$\dot{i} = \dot{i}_U + \dot{i}_{OB} + \dot{i}_D$$

$$\dot{\Omega} = \dot{\Omega}_U + \dot{\Omega}_{OB} + \dot{\Omega}_D$$

$$\dot{\omega} = \dot{\omega}_U + \dot{\omega}_{OB} + \dot{\omega}_D$$

$$\dot{M} = \dot{M}_U + \dot{M}_{OB} + \dot{M}_D \qquad \textbf{7.2 (a-f)}$$

The subscripts U, OB and D respectively represent the unperturbed variations, variations due to Earth oblateness and drag-induced variations. Initial conditions are given as a_0, e_0, i_0, Ω_0, ω_0 and M_0.

The given osculating elements are transformed to mean elements to obtain the following transformed variational equations:

$$\dot{a}_m = (\dot{a}_m)_U + (\dot{a}_m)_{OB} + (\dot{a}_m)_D$$

$$\dot{e}_m = (\dot{e}_m)_U + (\dot{e}_m)_{OB} + (\dot{e}_m)_D$$

$$\dot{i}_m = (\dot{i}_m)_U + (\dot{i}_m)_{OB} + (\dot{i}_m)_D$$

$$\dot{\Omega}_m = (\dot{\Omega}_m)_U + (\dot{\Omega}_m)_{OB} + (\dot{\Omega}_m)_D$$

$$\dot{\omega}_m = (\dot{\omega}_m)_U + (\dot{\omega}_m)_{OB} + (\dot{\omega}_m)_D$$

$$\dot{M}_m = (\dot{M}_m)_U + (\dot{M}_m)_{OB} + (\dot{M}_m)_D \qquad \textbf{7.3 (a-f)}$$

The drag effects on i,Ω,ω and M are ignored since the principal effect of atmospheric drag is the secular decrease in a and e. It subsequently follows that

$$(\dot{a}_m)_U = (\dot{e}_m)_U = (\dot{i}_m)_U = (\dot{\Omega}_m)_U = (\dot{\omega}_m)_U = 0$$

$$(\dot{a}_m)_{OB} = (\dot{i}_m)_D = (\dot{\Omega}_m)_D = (\dot{\omega}_m)_D = (\dot{M}_m)_D = 0 \qquad \textbf{7.4a}$$

Substitution of Equations **7.4a** into Equations **7.3 (a-f)** renders [Liu, 1974]

$$(\dot{e}_m)_{OB} = -\frac{3}{2} n J_2^2 \left(\frac{R}{p}\right)^4 \sin^2 i \cdot (14 - 15\sin^2 i) \cdot e \cdot (1 - e^2) \cdot \sin 2\omega$$
$$-\frac{3}{8} n J_3 \left(\frac{R}{p}\right)^3 \sin i \cdot (4 - 5\sin^2 i) \cdot (1 - e^2) \cdot \cos\omega \qquad \textbf{7.4b}$$
$$-\frac{15}{32} n J_4 \left(\frac{R}{p}\right)^4 \sin^2 i \cdot (6 - 7\sin^2 i) \cdot e \cdot (1 - e^2) \cdot \sin 2\omega$$

$$\left(\dot{i}_m\right)_{OB} = \frac{3}{64} nJ_2^2 \left(\frac{R}{p}\right)^4 \sin 2i\left(14 - 15\sin^2 i\right) e \sin 2\omega$$

$$+ \frac{3}{8} nJ_3 \left(\frac{R}{p}\right)^3 \cos i\left(4 - 5\sin^2 i\right) e \cos\omega \qquad \textbf{7.4c}$$

$$+ \frac{15}{64} nJ_4 \left(\frac{R}{p}\right)^4 \sin 2i\left(6 - 7\sin^2 i\right) e^2 \sin 2\omega$$

$$\dot{\Omega} = \left(\dot{\Omega}_m\right)_{OB} = -\frac{3}{2} nJ_2 \left(\frac{R}{p}\right)^2 \cos i$$

$$-\frac{3}{2} nJ_2^2 \left(\frac{R}{p}\right)^4 \cos i\left[\left(\frac{9}{4} + \frac{3}{2}\sqrt{1-e^2}\right) - \sin^2 i\left(\frac{5}{2} + \frac{9}{4}\sqrt{1-e^2}\right) + \frac{1}{4}\left(1 + \frac{5}{4}\sin^2 i\right) e^2\right]$$

$$+ \frac{15}{16} nJ_4 \left(\frac{R}{p}\right)^4 \left(4 - 7\sin^2 i\right) \cdot \cos i\left(1 + \frac{3}{2} e^2\right)$$

$$-\frac{3}{16} nJ_2^2 \left(\frac{R}{p}\right)^4 \cos i \cdot \left(7 - 15\sin^2 i\right) e^2 \cos 2\omega$$

$$-\frac{3}{2} nJ_3 \left(\frac{R}{p}\right)^3 \left(\frac{15}{4}\sin^2 i - 1\right) e \cot i \sin\omega$$

$$-\frac{15}{16} nJ_4 \left(\frac{R}{p}\right)^4 \cos i\left(3 - 7\sin^2 i\right) e^2 \cos 2\omega$$

7.4d

$$\left(\dot{a}_m\right)_D = -\frac{1}{2\pi} \int_0^{2\pi} B\rho V \frac{a}{1-e^2}\left[1 + e^2 + 2e\cos\nu - \omega_a \cos i \sqrt{\frac{a^3\left(1-e^2\right)^3}{\mu}}\right] dM$$

7.4e

$$\left(\dot{e}_m\right)_D = -\frac{1}{2\mu} \int_0^{2\pi} B\rho V \left\{e + \cos\nu - \frac{\omega_a}{2} \frac{r^2 \cos i}{\sqrt{\mu a\left(1-e^2\right)}}\left[2\left(e + \cos\nu\right) - e\sin^2\nu\right]\right\} dM$$

7.4f

where

B: Inverse ballistic coefficient $= \dfrac{C_D A}{M_{sat}}$ with C_D, A and M_{sat} respectively the drag coefficient, cross-sectional area and satellite mass.

ρ: Atmospheric density

V: Magnitude of satellite velocity given by

$$V = \sqrt{\mu p}\sqrt{\left(1 + e^2 + 2e\cos\nu\right)}\left[1 - \frac{\left(1-e^2\right)^{3/2}}{1 + e^2 + 2e\cos\nu}\frac{\omega_a}{n}\cos i\right]$$

ω_a: Atmospheric rotational speed with respect to Earth centre.

The integrals employed in **Equations 7.4 (e-f)** to compute the average drag effects with respect to mean anomaly, are calculated by means of Runge-Kutta numerical integration. The integration is done over *true anomaly* (ν) in the range [0, 2π] instead of *mean anomaly* (M) and is obtained by the transformation

$$dM = \left(\frac{r}{a}\right)^2 \frac{1}{\sqrt{1-e^2}}\, d\nu$$

$$\left(\dot{M}_m\right)_U = n \qquad \textbf{7.4g}$$

$$
\begin{aligned}
\left(\dot{M}_m\right)_{OB} &= n+\frac{3}{2}J_2\left(\frac{R}{p}\right)^2\left(1-\frac{3}{2}\sin^2 i\right)\sqrt{1-e^2} \\
&-\frac{15}{8}nJ_2^2\left(\frac{R}{p}\right)^4\sqrt{1-e^2}\left[\left(-1+\frac{5}{2}\sin^2 i-\frac{13}{8}\sin^4 i\right)+\frac{1}{2}e^2\left(-1+\sin^2 i+\frac{5}{8}\sin^4 i\right)\right] \\
&+\frac{3}{2}nJ_2^2\left(\frac{R}{p}\right)^4\left(1-\frac{3}{2}\sin^2 i\right)^2\left(1-e^2\right) \\
&-\frac{45}{128}nJ_4\left(\frac{R}{p}\right)^4\left(8-40\sin^2 i+35\sin^4 i\right)e^2\sqrt{1-e^2} \\
&-\frac{9}{64}nJ_2^2\left(\frac{R}{p}\right)^4\sin^2 i\left(14-15\sin^2 i\right)e^2\sqrt{1-e^2}\cos 2\omega \\
&+\frac{3}{32}nJ_2^2\left(\frac{R}{p}\right)^4\sin^2 i\left(14-15\sin^2 i\right)\left(1-e^2\right)^{3/2}\cos 2\omega \\
&-\frac{3}{8}nJ_3\left(\frac{R}{p}\right)^3\sin i\left(4-5\sin^2\right)\frac{1-4e^2}{e}\sqrt{1-e^2}\sin\omega \\
&+\frac{5}{64}nJ_4\left(\frac{R}{p}\right)^4\sin^2 i\left(6-7\sin^2\right)\left(2-5e^2\right)\sqrt{1-e^2}\cos 2\omega \\
&+\frac{9}{8}nJ_2^2\left(\frac{R}{p}\right)^4\frac{1}{\sqrt{1-e^2}}\left\{\begin{array}{l}\left(3-\frac{15}{2}\sin^2 i+\frac{47}{8}\sin^4 i\right)+\left(\frac{3}{2}-5\sin^2 i+\frac{117}{16}\sin^4 i\right)e^2 \\ -\frac{1}{8}\left(1+5\sin^2 i-\frac{101}{8}\sin^4 i\right)e^4 \\ +\frac{1}{24}\sin^2 i\left[\left(70-123\sin^2 i\right)e^2+2\left(28-33\sin^2 i\right)e^4\right]\cos 2\omega \\ +\frac{9}{128}e^4\sin^4 i\cos 4\omega\end{array}\right\}
\end{aligned}
$$

7.4h

7.6 ELLIPTICAL VS CIRCULAR ORBITS

The perturbing effect of atmospheric drag on an elliptical LEO satellite orbit results in the gradual degradation of an elliptical orbit into a circular one. Atmospheric density is greatest at perigee, causing the satellite to slow at perigee passage. This, in turn, results in the decrease of apogee height, whilst perigee height remains almost constant. The apogee rate of change is subsequently larger than that of

perigee. Altitude decrease causes the orbit to contract and become more circular in shape. This transition occurs at some stage in the decay process when the apogee height has decreased to a point closely approaching that of perigee. At that point, $r_p \approx r_a \approx a$ and the orbit eccentricity approaches zero, i.e. $e \approx 0$ [King-Hele 1987, Pp 8]

The numerical analysis employed in this theory is subsequently employed in two parts, *viz.*, the *elliptical* and the *circular* phases of the satellite's lifetime. For the elliptic case, the variables $\dot{r}_a, \dot{r}_p, \dot{\Omega}$, $\dot{\omega}$ are integrated and for the circular case, $\dot{\Omega}$ and $\dot{a}$. The transformation from osculating to mean orbital elements (and back) remains valid for elliptical and circular cases.

7.6.1 Elliptical Case

7.6.1.1 Equations of Motion

The combined effects of Earth oblateness and drag render the following equations of motion for the mean elements $\dot{r}_a$, $\dot{r}_p$, $\dot{\Omega}$ and $\dot{\omega}$ to be integrated for the elliptical case

$$\dot{r}_a = (\dot{r}_a)_D + a\dot{e} \qquad \textbf{7.5a}$$

$$\dot{r}_p = (\dot{r}_p)_D - a\dot{e} \qquad \textbf{7.5b}$$

With the rates of change of apogee and perigee due to drag respectively given by

$$(\dot{r}_a)_D = \left[\frac{(1-e^2)^3}{4M\pi n(1-e)^2}\right]\int_{-\pi}^{\pi}\frac{1000C_D A\rho}{(1+e\cos\nu)^3}\cdot\left[\frac{n}{\sqrt{1-e^2}}\cdot\sqrt{1+2e\cos\nu+e^2} - \frac{p\omega_a\cos i}{\sqrt{1+2e\cos\nu+e^2}}\right]\cdot$$
$$\left[\frac{2n(1+\cos\nu)}{\sqrt{1-e^2}} + \frac{p\omega_a\cos i}{(1-e\cos\nu)}\cdot(e\sin^2\nu - 2\cos\nu - 2)\right]d\nu \qquad \textbf{7.5c}$$

and

$$\left(\dot{r}_p\right)_D = \left[\frac{\left(1-e^2\right)^3}{4M\pi n\left(1-e\right)^2}\right]\int_{-\pi}^{\pi}\frac{1000C_D A\rho}{\left(1+e\cos\nu\right)^3}\cdot\left[\frac{n}{\sqrt{1-e^2}}\cdot\sqrt{1+2e\cos\nu+e^2}-\frac{p\omega_a\cos i}{\sqrt{1+2e\cos\nu+e^2}}\right]\cdot$$

$$\left[\frac{2n\left(1-\cos\nu\right)}{\sqrt{1-e^2}}-\frac{p\omega_a\cos i}{\left(1-e\cos\nu\right)}\cdot\left(e\sin^2\nu-2\cos\nu+2\right)\right]d\nu \qquad \textbf{7.5d}$$

The integrals in Equations **7.5 (c-d)** are solved by Gauss-Legendre quadrature.

The rates of change of eccentricity ($\dot{e}$), longitude of ascending node ($\dot{\Omega}$) and argument of perigee ($\dot{\omega}$), are respectively given by

$$\dot{e} = \left(\dot{e}_m\right)_{OB} + \left(\dot{e}_m\right)_D \qquad \textbf{7.5e}$$

where

$$\left(\dot{e}_m\right)_{OB} = -\frac{3}{2}nJ_2^2\left(\frac{R}{p}\right)^4\sin^2 i\cdot\left(14-15\sin^2 i\right)\cdot e\cdot\left(1-e^2\right)\cdot\sin 2\omega$$

$$-\frac{3}{8}nJ_3\left(\frac{R}{p}\right)^3\sin i\cdot\left(4-5\sin^2 i\right)\cdot\left(1-e^2\right)\cdot\cos\omega$$

$$-\frac{15}{32}nJ_4\left(\frac{R}{p}\right)^4\sin^2 i\cdot\left(6-7\sin^2 i\right)\cdot e\cdot\left(1-e^2\right)\cdot\sin 2\omega$$

and $\left(\dot{e}_m\right)_D$ given by **Equation 7.4f**

$$\dot{\Omega} = \left(\dot{\Omega}_m\right)_{OB} = -\frac{3}{2} nJ_2 \left(\frac{R}{p}\right)^2 \cos i$$

$$-\frac{3}{2} nJ_2^2 \left(\frac{R}{p}\right)^4 \cos i \left[\left(\frac{9}{4}+\frac{3}{2}\sqrt{1-e^2}\right)-\sin^2 i\left(\frac{5}{2}+\frac{9}{4}\sqrt{1-e^2}\right)+\frac{1}{4}\left(1+\frac{5}{4}\sin^2 i\right)e^2\right]$$

$$+\frac{15}{16} nJ_4 \left(\frac{R}{p}\right)^4 \left(4-7\sin^2 i\right)\cdot \cos i\left(1+\frac{3}{2}e^2\right)$$

$$-\frac{3}{16} nJ_2^2 \left(\frac{R}{p}\right)^4 \cos i\cdot\left(7-15\sin^2 i\right)e^2 \cos 2\omega$$

$$-\frac{3}{2} nJ_3 \left(\frac{R}{p}\right)^3 \left(\frac{15}{4}\sin^2 i-1\right)e\cot i \sin\omega$$

$$-\frac{15}{16} nJ_4 \left(\frac{R}{p}\right)^4 \cos i\left(3-7\sin^2 i\right)e^2 \cos 2\omega$$

7.5f

$$\dot{\omega} = \left(\dot{\omega}_m\right)_{OB} = \frac{3}{4} nJ_2 \left(\frac{R}{p}\right)^2 \left(4-5\sin^2 i\right)$$

$$+\frac{3}{4} nJ_2^2 \left(\frac{R}{p}\right)^4 \cdot$$

$$\left[12-\frac{103}{4}\sin^2 i+\frac{215}{16}\sin^4 i+\left(\frac{7}{4}-\frac{9}{8}\sin^2 i-\frac{45}{32}\sin^4 i\right)e^2+\frac{3}{2}\left(1-\frac{3}{2}\sin^2 i\right)\left(4-5\sin^2 i\right)\sqrt{1-e^2}\right]$$

$$-\frac{15}{32} nJ_4 \left(\frac{R}{p}\right)^4\left[\left(16-62\sin^2 i+49\sin^4 i\right)+\frac{3}{4}\left(24-84\sin^2 i+63\sin^4 i\right)e^2\right]$$

$$+\frac{3}{64} nJ_2^2 \left(\frac{R}{p}\right)^4 \left[-2\left(14-15\sin^2 i\right)\sin^2 i+\left(28-158\sin^2 i+135\sin^4 i\right)e^2\right]\cos 2\omega$$

$$+\frac{3}{8} nJ_3 \left(\frac{R}{p}\right)^3 \frac{1}{e\sin i}\left[\left(4-5\sin^2 i\right)\left(\sin^2 i-e\cos^2 i\right)+2\sin^2 i\left(13-15\sin^2 i\right)e^2\right]\sin\omega$$

$$-\frac{5}{32} nJ_4 \left(\frac{R}{p}\right)^4\left[3\sin^2 i\left(6-7\sin^2 i\right)+\frac{1}{2}\left(-36+210\sin^2 i-189\sin^4 i\right)e^2\right]\cos\omega$$

7.5g

For orbits with eccentricities greater than 0.0001 and perigee heights between 90-300km, the integrals in **Equations 7.5 (c-d)** are separated into two quadratures whose ranges cover the interval [-π, π] and depend on r_p and e. One quadrature is centred on perigee, with the other covering the remainder of the orbit as indicated in **Figure 7.2**

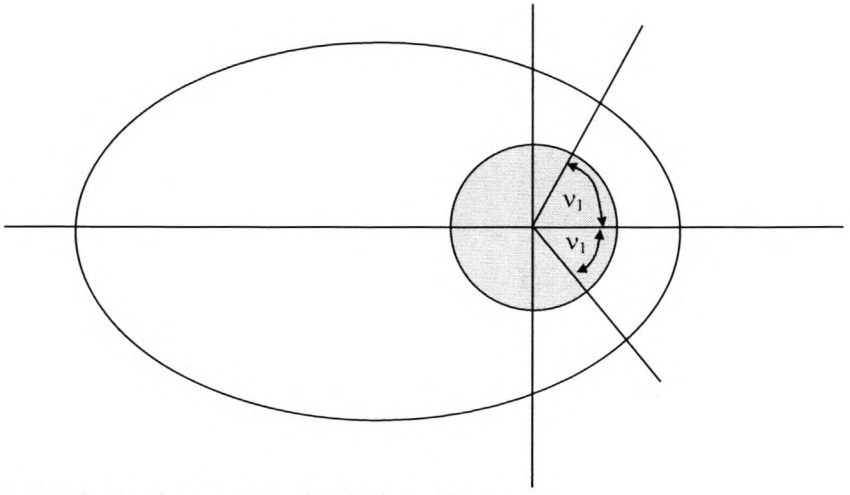

Figure 7.2. Quadrature separation for low altitudes

The value of ν_1 is calculated as a function of r_p and e using the equation

$$\nu_1 = \cos^{-1}\left[\frac{r_p e - \Delta H}{e(r_p + \Delta H)}\right] \qquad \textbf{7.6}$$

Where ΔH is the change in altitude required to decrease the air density to $1/10^{th}$ of its value at perigee. Above equation is derived from the polar equation for two-body motion,

$$r = \frac{r_p(1+e)}{1+e\cos\nu}$$

By letting r = r_p + ΔH and solving for ν. ΔH is calculated from the cubic equation

$$\Delta H = A_0 + A_1 r_p + A_2 r_p^2 + A_3 r_p^3 \qquad \textbf{7.7}$$

With coefficients A_i given in **Table 7.1**

Table 7.1. Polynomial coefficients for altitude interpolation.

Coefficients	90-130km	130-300km
A_0	-107.0217	-383.3304
A_1	4.909437	5.699749
A_2	-0.06363481	-0.02248835
A_3	0.2664102×10^{-3}	0.3111053×10^{-4}

For perigee altitudes above 300km, the integration is performed over [-π, π]. The quadrature is not divided for the circular option.

7.6.1.2 Atmospheric Density Calculation

The atmospheric density used in numerical integration is calculated from the satellite's altitude given by

$$H = r - R\left[1 - \frac{\sin^2 i}{f}\sin^2(\omega + \nu)\right] \qquad \textbf{7.8}$$

Where r is the satellite radius with short periodic terms included

$$r = \frac{p}{(1+e\cos\nu)} - \frac{J_2}{2}\left(\frac{R^2}{p}\right)^2\left(1-\frac{3}{2}\sin^2 i\right)\left[1+\frac{1-\sqrt{1-e^2}}{e}\right]\cos\nu + \frac{2\sqrt{1-e^2}}{(1+e\cos\nu)} + \frac{J_2}{4}\left(\frac{R^2}{p}\right)^2 \sin^2 i\cos(2\omega+2\nu) \qquad \textbf{7.9}$$

The unit vector components of satellite position, $\boldsymbol{r}$, required by the Jacchia atmosphere model, is given by

$$\begin{aligned} \hat{r}_x &= \cos(\omega+\nu)\cos\Omega - \sin(\omega+\nu)\sin\Omega\cos i \\ \hat{r}_y &= \cos(\omega+\nu)\sin\Omega + \sin(\omega+\nu)\cos\Omega\cos i \\ \hat{r}_z &= \sin(\omega+\nu)\sin i \end{aligned} \qquad \textbf{7.10}$$

7.6.2 Circular Case

7.6.2.1 Equations of Motion

The variational equations of motion for an elliptical orbit do not hold for a perfect circular orbit since M and ω are undefined for circular orbits ($e = 0$). The sum of M and ω, though, does exist at e = 0. Since e, under the influence of oblateness is very small and drag tends to keep e at zero, the time rate of change for eccentricity $(\dot{e}_m)$, is zero for the circular phase.

The differential equations for the circular orbit option comprise the rates of change of the semi-major axis and longitude of ascending node. Equations **7.5(e-f)** reduce to the following expression for the mean element, a:

$$\dot{a} = -\left[\frac{1000\sqrt{a\mu}\cdot\left(1-\frac{\omega_a \cos i}{n}\right)^2}{2\pi M}\right]\int_{-\pi}^{\pi} C_D A\rho \cdot dv \qquad \textbf{7.11}$$

$$\dot{\Omega} = \left\{-\frac{3}{2}J_2 + \left[J_4\left(3.75 - 6.5625\sin^2 i\right) + J_2^2\left(5.625 - 7.125\sin^2 i\right)\right]\left(\frac{R}{2}\right)^2\right\} n\left(\frac{R}{a}\right)^2 \cos i \qquad \textbf{7.12}$$

7.6.2.2 Atmospheric Density Calculation

Atmospheric density is based on the altitude calculated from

$$H = a - \frac{3}{2}J_2\left(\frac{R^2}{a}\right)\left[1-\frac{3}{2}\sin^2 i\right] + \frac{1}{4}J_2\left(\frac{R^2}{a}\right)\cos 2v \sin^2 i - R_{eq}\left[1-\frac{\sin^2 i}{f}\sin^2 v\right] \qquad \textbf{7.13}$$

And the satellite unit vector calculated as

$$\begin{aligned}\hat{r}_x &= \cos(\nu)\cos\Omega - \sin(\nu)\sin\Omega\cos i \\ \hat{r}_y &= \cos(\nu)\sin\Omega + \sin(\nu)\cos\Omega\cos i \\ \hat{r}_z &= \sin(\nu)\sin i\end{aligned} \qquad \textbf{7.14}$$

7.7 ATMOSPHERIC DENSITY MODEL

The atmospheric density is calculated from the simplified Jacchia model [Jacchia 1970]. This model provides for density variations due to solar activity and semi-annual variation and estimates the accurate exospheric temperature at a given time at the satellite's altitude in consideration. It takes into account the eleven-year Solar cycle (**Figure 7.3**). Atmospheric density is then interpolated from a lookup table as a function of altitude and temperature. The complete Jacchia model is presented in Appendix C.

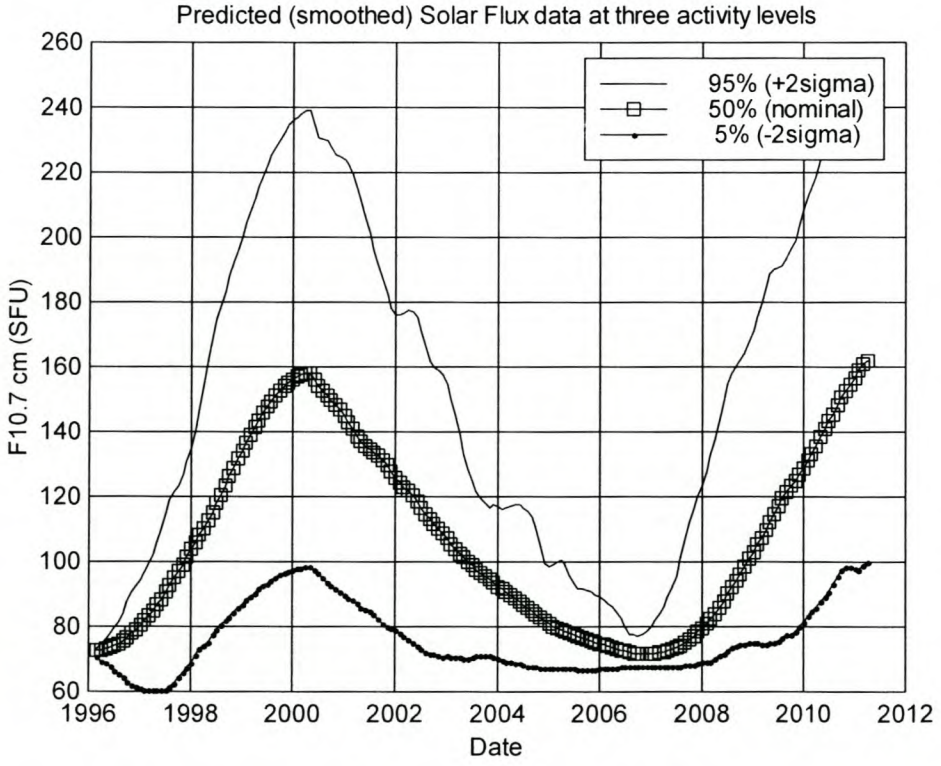

Figure 7.3. Predicted Solar flux values required for calculating atmospheric density.

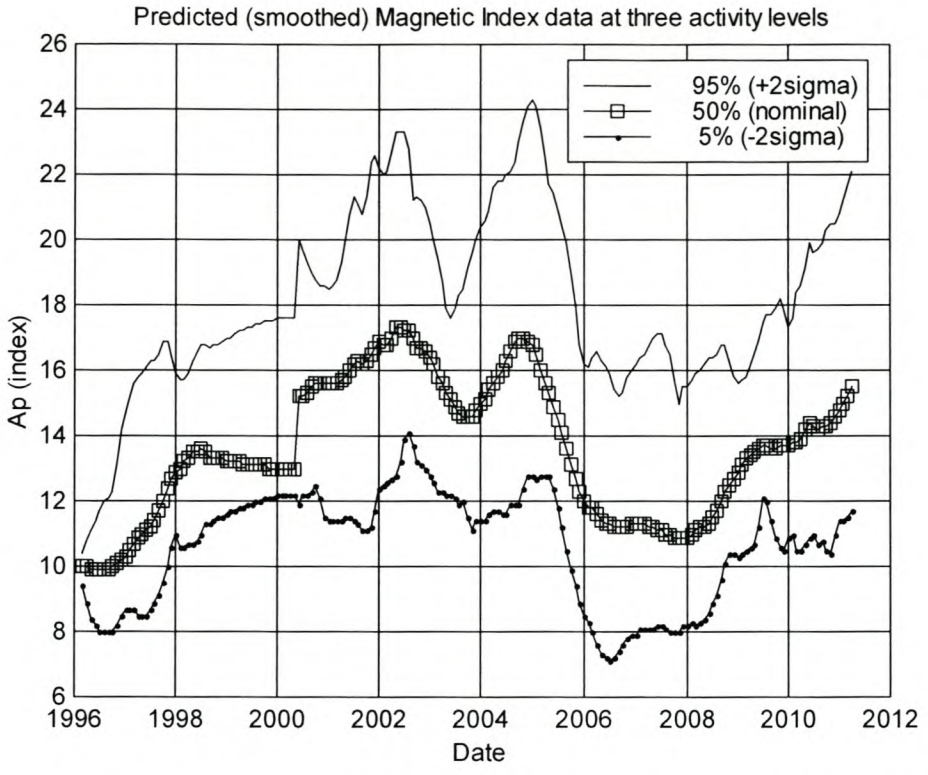

Figure 7.4. Predicted magnetic index values required for calculating atmospheric density.

7.8 NUMERICAL INTEGRATION

7.8.1 Runge-Kutta Integration

For the purpose of numerical integration, a pair of fourth-order Runge-Kutta integrators with adaptive step size through error control, has been employed [Butcher 1987, Pp 178-181]. The Runge-Kutta 4-4 is used as the self-starting method to take the first step before employing the Runge-Kutta 4-3 method. The RK 4-4 and RK 4-3 formulas are respectively given by

$$
\begin{aligned}
f_{0i} &= f(t_i, x_i) \\
f_{1i} &= f\left(t_i + \frac{h}{2}, x_i + h\frac{f_{0i}}{2}\right) \\
f_{2i} &= f\left(t_i + \frac{h}{2}, x_i + h\frac{f_{1i}}{2}\right) \\
f_{3i} &= f(t_i + h, x_i + hf_{2i}) \\
x_{i+1} &= x_i + \frac{h}{6}[f_{0i} + 2f_{1i} + 2f_{2i} + f_{3i}]
\end{aligned}
\qquad \textbf{7.15}
$$

And

$$
\begin{aligned}
f_{0i} &= f(t_i, x_i) \\
f_{1i} &= f[t_i - h, x_i(t_i - h)] \\
f_{2i} &= f\left(t_i + \frac{h}{2}, x_i + + \frac{h}{8}(5f_{0i} - f_{1i})\right) \\
f_{3i} &= f\left(t_i + h, x_i + \frac{h}{2}(-3f_{0i} + f_{1i} + 4f_{2i})\right) \\
x_{i+1} &= x_i + \frac{h}{6}[f_{0i} + 4f_{1i} + f_{3i}]
\end{aligned}
\qquad \textbf{7.16}
$$

Where h denotes the step size.

Error control is accomplished by estimating the truncation error of a single R-K 4-3 step by the calculation

$$\varepsilon = \frac{h}{6}|6f_{0i} - f_{1i} - 8f_{2i} + 3f_{3i}| \qquad \textbf{7.17}$$

and dividing by r_p for the elliptic case and a for the circular case. The result is compared to a specified tolerance, T and, if required, step size is adjusted to keep the error below T.

7.8.2 Gauss-Legendre Quadrature

Gauss quadrature is a powerful method of integration, which employs unequally spaced base points. The Gauss-Legendre method uses Lagrange polynomials to approximate the function and then applies orthogonal polynomials to locate the loci

of the base points. The function $f(x)$ is replaced by the Lagrange polynomial and its remainder [Constantinides 1987, Pp, 315, 351]

$$f(x) = P_n(x) + R_n(x)$$

$$= \sum_{i=0}^{n} L_i(x) f(x_i) + \prod_{i=0}^{n} (x - x_i) \frac{f^{(n+1)}(v)}{(n+1)!}, \quad a < v < b \qquad \textbf{7.18}$$

Where

$$L_i(x) = \prod_{\substack{j=0 \\ j \neq i}}^{n} \frac{x - x_j}{x_i - x_j} \qquad \textbf{7.19}$$

The integral $\int_a^b f(x)dx$ is evaluated by

$$\int_a^b f(x)dx = \int_a^b P_n(x)dx + \int_a^b R_n(x)dx \qquad \textbf{7.20}$$

The interval $[a, b]$ is transformed to $[-1, 1]$. An element $x \in [a, b]$ is transformed to an element $z \in [-1, 1]$ by the transformation

$$z = \frac{2x - (a+b)}{(b-a)} \qquad \textbf{7.21}$$

Using **Equations 7.18**, **7.19** and **7.21** in **Equation 7.20**, the transformed integral is given by

$$\int_{-1}^{1} F(z)dz = \sum_{i=0}^{n} w_i F(z_i) + \int_{-1}^{1} R_n(z)dz \qquad \textbf{7.22}$$

Where the weights w_i are given by

$$w_i = \int_{-1}^{1} L_i(z)dz = \int_{-1}^{1} \prod_{\substack{j=0 \\ j \neq i}}^{n} \frac{z - z_j}{z_i - z_j} dz \qquad \textbf{7.23}$$

And the error term is given by

$$\int_{-1}^{1} R_n(z)dz = \int_{-1}^{1} \prod_{i=0}^{n} (z - z_i) q_n(z)dz \qquad \textbf{7.24}$$

where $q_n(z)$ and $\prod(z\text{-}z_i)$ are polynomials of degree n and n+1, respectively.

In order to eliminate the error term in **Equation 7.24**, the two polynomials in the error term are expanded in terms of *Legendre orthogonal* polynomials. The values of z_i are chosen as the roots of the $(n+1)^{st}$-degree Legendre polynomial. The choice of roots combined with the orthogonality of the Legendre polynomials causes the errors to vanish. Therefore **Equation 7.22** becomes

$$\int_{-1}^{1} F(z)dz = \sum_{i=0}^{n} w_i F(z_i) \qquad \textbf{7.25}$$

Equation 7.25 yields the integral of the function $F(z)$ exactly when $F(z)$ is a polynomial of degree (2n+1) or less.

7.9 Model Implementation and Application

The semi-analytical Liu Theory was implemented in a FORTRAN programme, *Satdecay*. This is an adaptation of the *Lifetime* programme developed as part of the SALT [Liu and Alford 1974]. A listing of the source code is attached in Appendix H. The SALT was first evaluated against the actual orbit decay histories of two LEO satellites, *Iridium-85* and *Starshine-2*, prior to applying the solution to the

SUNSAT orbit. The results of the orbit decay prediction are respectively presented and discussed in Chapters 8 and 9.

7.9.1 Data Preparation

The critical parameters required by the decay software are: satellite *state* (***r***, ***v***) at some epoch, satellite geometry (*mass* and *cross-sectional area)* and *drag coefficient* (C_D). Satellite geometry was assumed to be constant during the satellite's lifetime. General geometry information for these satellites was obtained from [Astronautix] and is given in **Table 7.2**. For satellite state information, J2000-ECI state vectors and osculating Kepler elements were extracted from the first available TLE files after time of launch. TLE's were obtained from the [Celestrak] archive and parsed through *Satellite Toolkit* [Analytical Graphics] to obtain the desired states. These TLE's and derived state vectors are presented in **Tables 7.3**. and **7.4** respectively.

Table 7.2 Geometry of decayed satellites used in evaluating SALT

Satellite	International designator	Mass (kg)	Area (m^2)	Launch Date	Decay Date
Iridium-85 (cube with panels)	25529	689	5.12	06 Nov. 1998	30 Dec 2000
Starshine-2 (sphere)	25769	39	0.18	27 May 1999	18 Feb 2000

Table 7.3. Satellite Two-Line Elements at time closest after launch.

Iridium 85

1 25529U 98066C 98310.67459616 .00000038 00000-0 00000+0 0 11
2 25529 86.0152 311.9254 0013613 223.7877 136.0772 15.14192003 04

Starshine-2

1 25769U 99030B 99156.34105187 .02711664 00000-0 29127-1 0 12
2 25769 51.5915 257.3806 0012795 323.4372 36.5573 15.59813944 1386

Table 7.4 . TLE-derived state vectors and osculating (Kepler) elements of dates closest to launch.

	Iridium-85 6 Nov. 1998 16:11:25.11 UTC	**Starshine-2** 5 June 1999 08:11:6.88UTC	**SUNSAT** 9 March 1999 05:32:38.12 UTC
X (km)	4615.72658	-1470.88476	6798.25947
Y	-5140.06454	-6597.40002	2455.08495
Z	-3.25021	7.57515	14.89957
Vx (km.s^{-1})	0.39972	4.65907	0.32093
Vy	0.34453	-1.0378	-0.76881
Vz	7.57386	6.02051	7.32982
a (km)	6901.57000	6766.33242	7134.02304
e	0.00136	0.00128	0.01519
i (°)	86.0152	51.5915	96.4768
Ω (°)	311.9254	257.3806	19.8698
ω (°)	223.7877	323.4372	209.5613
M (°)	136.0772	36.5573	149.6933
r_p	514.04	379.541	647.523
r_a	532.82	396.856	864.255

7.9.2 Drag Coefficient Calculation

Drag coefficients strongly depend on satellite geometry and attitude. Such coefficients are difficult to model and are usually the solution of a non-linear estimation process using least squares or Kalman Filtering [Vallado 1997, Pp 683, 707].

For the purpose of this exercise, drag coefficients were estimated by precision orbit analysis using the precision propagator, *Orblitz*, developed in Chapter 5. For *Iridium-85* and *Starshine-2*, two TLE's five days apart, were used to derive an analysis epoch state, ($\boldsymbol{r}_0$, $\boldsymbol{v}_0$) at an epoch t_0 and a final reference state, ($\boldsymbol{r}_f$, $\boldsymbol{v}_f$), at time $t_f = t_0 + 5\text{days}$. Using constant geometry (**Table 7.2**) and an initial C_D-estimate, each satellite's initial state, ($\boldsymbol{r}_0$, $\boldsymbol{v}_0$), was propagated from t_0 to t_f. Their respective propagated states at t_f, ($\boldsymbol{r}_{fp}$ $\boldsymbol{v}_{fp}$), were compared to the reference state, ($\boldsymbol{r}_f$, $\boldsymbol{v}_f$) and the error $\left\|\left(\mathbf{r}_f, \mathbf{v}_f\right) - \left(\mathbf{r}_{fp}, \mathbf{v}_{fp}\right)\right\|$ was calculated. The C_D-value was adapted and the process repeated until a sufficiently small error was obtained (<5 km for Starshine-2 and Iridium-85 and 63 m for SUNSAT).

Relevant state information for SUNSAT was taken from the SLR reference data set and is listed in **Table 7.5a.**

Table 7.5a. Relevant states used in SUNSAT drag analysis

t_0	**SUNSAT** 6 Feb 2000 0.0 UTC					
($\boldsymbol{r}_0$, $\boldsymbol{v}_0$)	X (km)	Y	Z	Vx (km.s^{-1})	Vy	Vz
	-611.35969	6818.31296	1885.99917	0.70590	1.95650	-7.21813
t_f	11 Feb 2000 0UTC					
($\boldsymbol{r}_f$, $\boldsymbol{v}_f$)	X (km)	Y	Z	Vx (km.s^{-1})	Vy	Vz
	-1011.12013	6865.80536	1337.51520	0.661407	1.45079	-7.37681

As the propagation reference frame of *Orblitz* requires (J2000-ECI) *mean-equinox, mean-equator of date* (*memod*) co-ordinates, it was necessary to adjust the TLE-derived states for *Iridium-85* and *Starshine-2* prior to use in the analysis. This was accomplished with a reverse nutation rotation (**Equation 4.9)** which reduced the mean *equinox, true-equator of date* (*metod*) co-ordinates to the required *memod* co-ordinates (m-file *revprecnut.m* in Appendix I). The relevant TLE's, with corresponding *memod* ECI co-ordinates of Iridium-85 and Starshine-2, are presented in **Table 7.5b.** The results of the drag analysis are given in Chapter 8 along with the orbit decay results. Relevant data files used in the drag analysis are listed in Appendix I.

Table 7.5b. TLE's and derived *memod* states as implemented in drag analysis.

t_0	**Iridium-85** 9 Feb 2000 02:22:00.0 UTC
TLE t_0	1 25529U 98066C 00040.09813231 .00024176 00000-0 91389-3 0 3619 2 25529 85.9994 69.2640 0009969 47.5068 312.7124 15.26807116 69720
$(\boldsymbol{r}_0, \boldsymbol{v}_0)$	X(km) Y Z Vx (km.s^{-1}) Vy Vz 2405.91474 6418.03709 316.24762 -0.62654 -0.15451 7.59919
t_f	14 Feb 2000 01:54:00.0 UTC
TLE t_f	1 25529U 98066C 00050.05820934 .00028719 00000-0 10655-2 0 3730 2 25529 86.0014 63.9212 0007743 17.4262 342.7179 15.27434411 71249
$(\boldsymbol{r}_f, \boldsymbol{v}_f)$	X(km) Y Z Vx (km.s^{-1}) Vy Vz 2701.71766 6297.47063 321.84253 -0.63543 -0.12849 7.59990
t_0	**Starshine-2** 20 Jan 2000 20:31:00.00
TLE t_0	1 25769U 99030B 00020.85429062 .00262727 38879-4 59291-3 0 2197 2 25769 51.5823 161.2574 0002186 161.8698 198.2421 15.97144359 37484
$(\boldsymbol{r}_0, \boldsymbol{v}_0)$	X(km) Y Z Vx (km.s^{-1}) Vy Vz -6374.85041 1912.45491 298.842140 -1.11478 -4.68863 6.05368
t_f	25 Jan 2000 05:33:00.00
TLE t_f	1 25769U 99030B 00025.23069419 .00308618 51002-4 60250-3 0 2325 2 25769 51.5839 137.9365 0000769 5.4735 354.5892 15.99696117 38182
$(\boldsymbol{r}_f, \boldsymbol{v}_f)$	X(km) Y Z Vx (km.s^{-1}) Vy Vz -5084.87301 4281.09565 287.74158 -2.89480 -3.85659 6.05947

7.9.3 Orbit decay prediction

Input files were created for the *Iriudium-85* and *Starshine-2* satellites using epoch states (**Table 7.4**), geometry (**Table 7.2**), and calculated drag coefficients. Input files are listed in Appendix I. The predicted decay date for each of these satellites was compared to their actual decay dates (**Table 7.2**) and graphs were generated of the change in their respective perigee and apogee radii. After evaluation of these results, an orbit decay prediction was done for SUNSAT using epoch state in **Table 7.5a**. Relevant graphs were created. Results are respectively presented and discussed in Chapters 8 and 9.

Chapter 8

Results: Drag Analysis and Orbit Decay

8.1 RESULTS FROM DRAG ANALYSIS

Optimum drag coefficients with associated ballistic coefficients, as calculated in the drag analysis section in paragraph 7.9.2, are presented in **Table 8.1**. These drag coefficients were used in the subsequent implementation of the orbit decay prediction. Position errors resulting from all drag coefficients evaluated during the analysis process are presented in **Figures 8.1** to **8.3**. The observed C_D and error values are tabled in Appendix I.

Table 8.1. Optimum satellite drag coefficients with corresponding errors in position and velocity.

Satellite	C_D	BC ($m/(C_D*A)$)	***r***-error (km)	***v***-error ($km.s^{-1}$)
Iridium-85	5.0	26.9	4.4	0.004
Starshine-2	2.1375	100.8	3.6	0.004
SUNSAT	3.10	50.8	0.063	1.254e-4

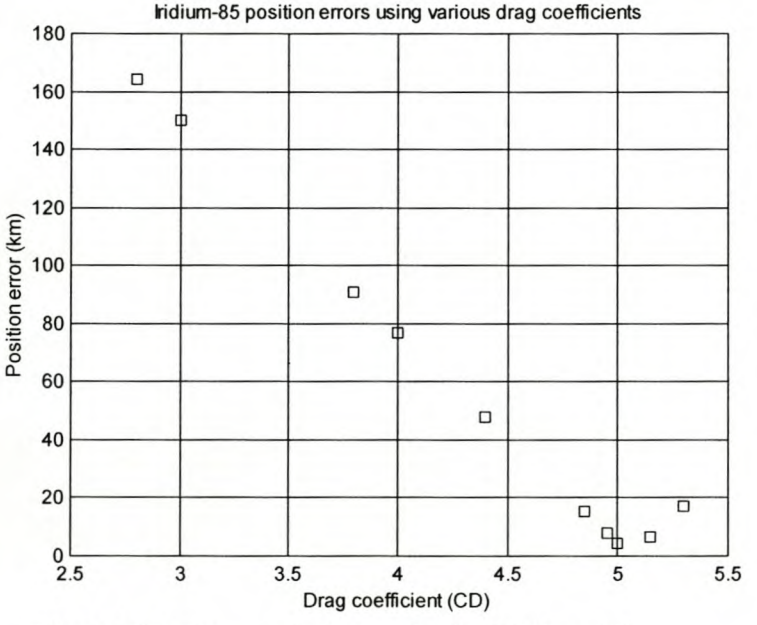

Figure 8.1 Drag analysis results for Iridium-85

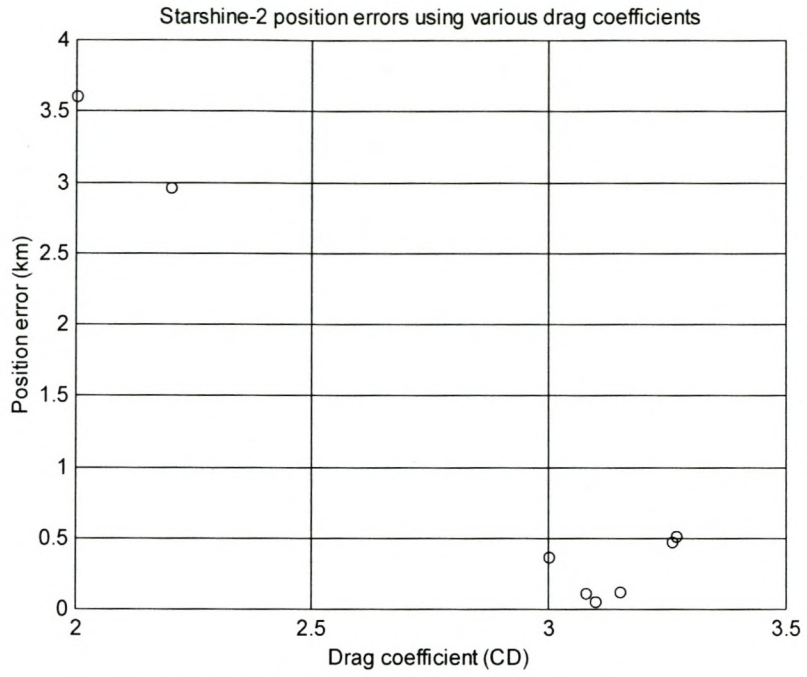

Figure 8.2 Drag analysis results for Starshine-2.

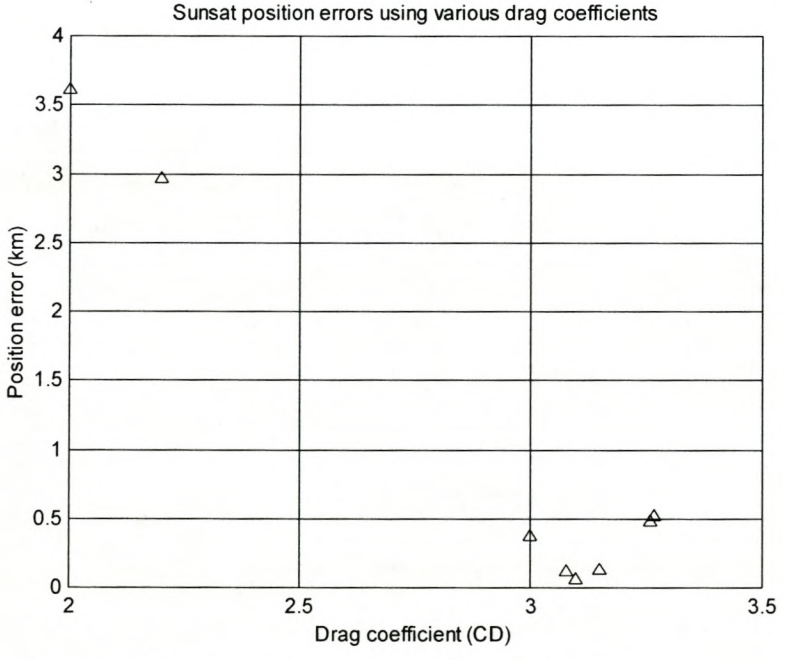

Figure 8.3 Drag analysis results for SUNSAT

8.2 ORBIT DECAY PREDICTION RESULTS

The *observed* and *predicted* decay dates obtained for the test case satellites *Iridium-85* and *Starshine-2,* are presented in **Table 8.2.** Time histories of their predicted perigee and apogee heights and semi-major axes are presented in **Figures 8.4** and **8.5**. The predicted decay dates for SUNSAT, using two possible solar activity levels, are presented in **Table 8.3.** Time histories of SUNSAT's predicted perigee and apogee heights at these two solar activity levels are presented in **Figure 8.6**. A short discussion of the presented results is given with final conclusions presented in Chapter 9.

Table 8.2. Observed and predicted decay dates for the test case satellites

Satellite	Observed decay date	Predicted decay date
Iridium-85	30 Dec 2000	3 Jan 2001
Starshine-2	18 Feb 2000	29 Feb 2000

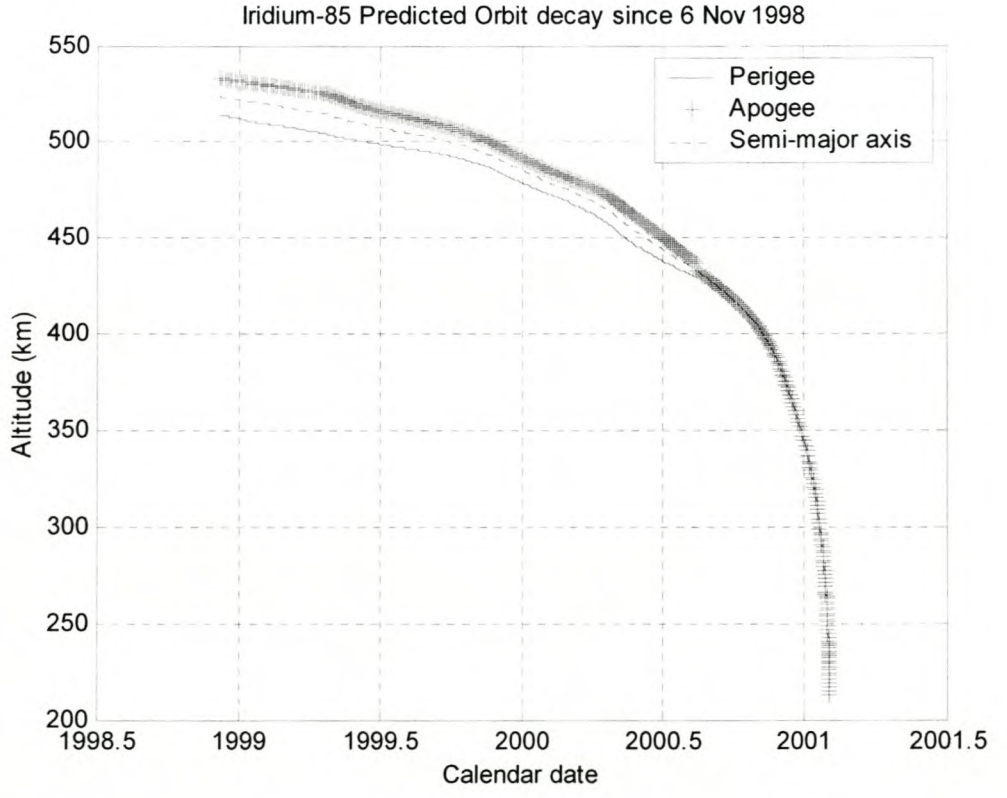

Figure 8.4. Predicted orbit decay for Iridium-85 .

Table 8.3. SUNSAT's predicted decay dates using two solar activity levels

Solar activity level	Predicted decay date
50% (Nominal)	9 Dec 2073
95%(+2 σ)	30 July 2024

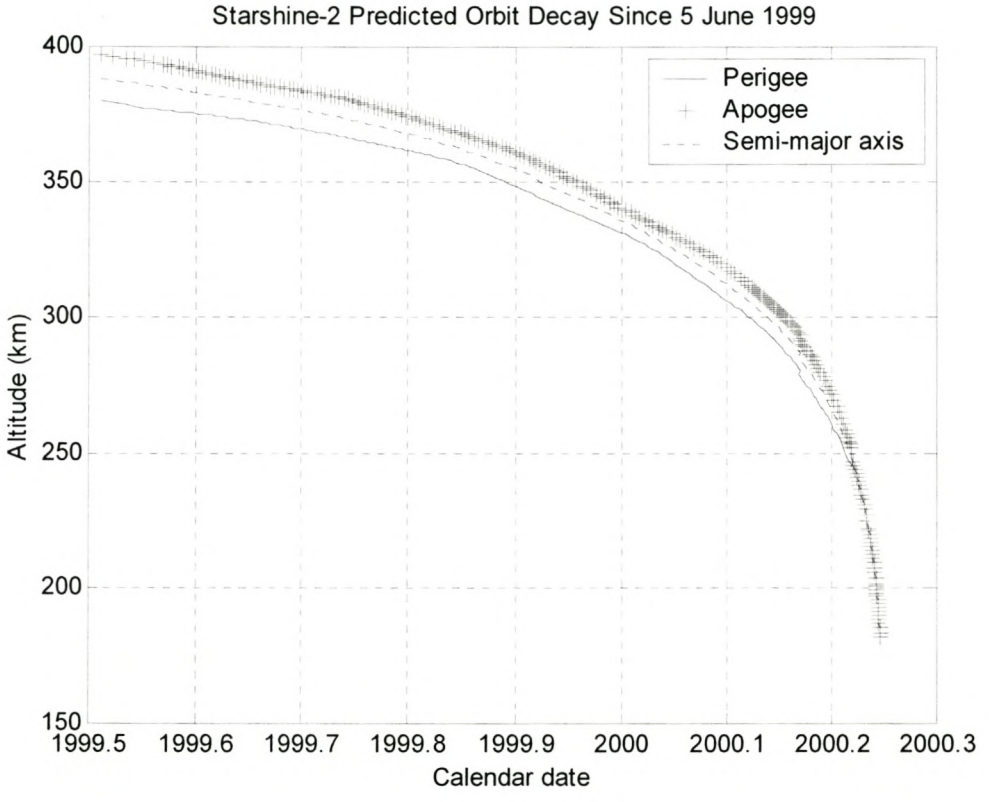

Figure 8.5. Predicted orbit decay for Starshine-2 .

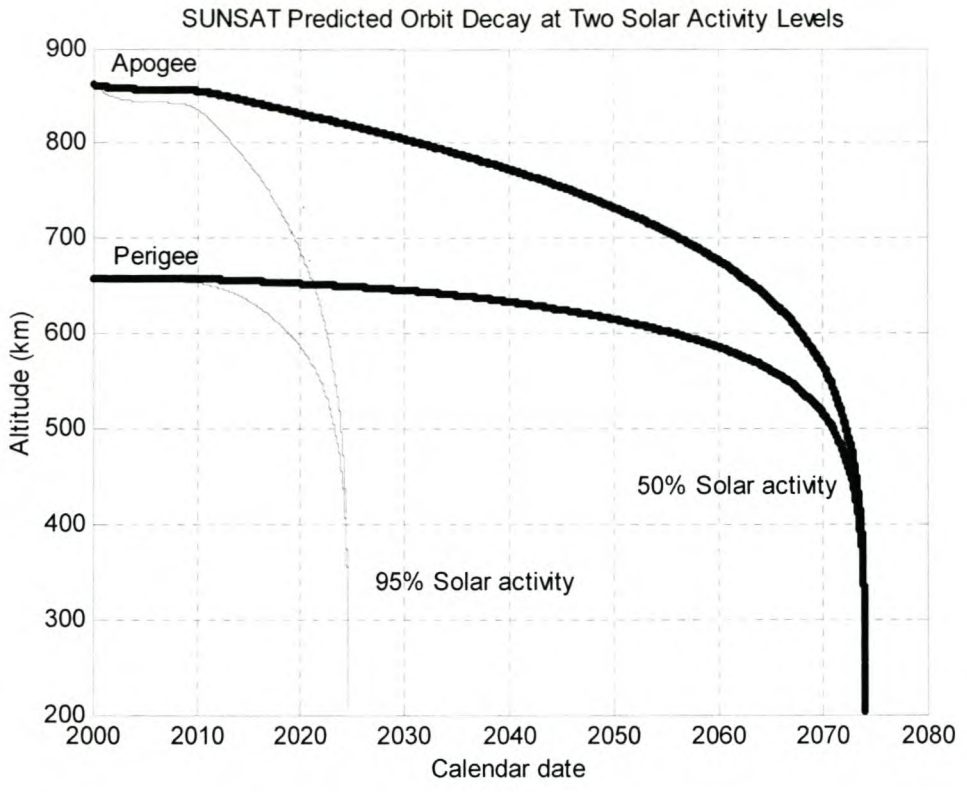

Figure 8.6. Predicted orbit decay for SUNSAT.

8.3 DISCUSSION

The effect of non-optimum drag coefficients on propagation errors is evident from the relative large position errors obtained using non-optimum drag coefficient values in the drag analysis (**Figures 8.1**, **8.2** and **8.3**). Results from the drag analysis subsequently underwrite the importance of accurate drag coefficients for minimising propagation errors during long term propagation in the presence of atmospheric drag.

The predicted time histories of perigee and apogee radii in **Figures 8.4**, **8.5** and **8.6** illustrate the ultimate contraction of an elliptical orbit into a circular one under the influence of (mostly) atmospheric drag. Orbit decay prediction for *Iridium-85* and *Starshine-2* was conducted at nominal (50%) solar activity (**Figures 7.3** and **7.4**), using optimised drag coefficients and rendered predicted decay dates differing by respectively four and eleven days from observed decay dates (**Table 8.2**). Given the uncertainty in estimated drag coefficients and atmospheric density calculations, the relative small errors in decay prediction date for the test cases suggests that SALT was successful in predicting satellite lifetime for the test cases.

Chapter 9

Conclusions and Future Work

9.1 CONCLUSIONS

Two methods for orbit propagation were presented: Cowell's method of special perturbations for short-term precision orbit propagation and Liu's semi-analytical theory for satellite lifetime prediction. Cowell's method incorporated the perturbative effects of an aspherical Earth, atmospheric drag, solar-lunar attractions, and solar radiation pressure and resulted in a computer programme, *Orblitz*. Liu's theory utilized the variational equations of orbit mean elements due to the Earth's oblateness and atmospheric drag only and resulted in a computer programme, *Satdecay*.

For the short period precision test case, results indicate that *Orblitz* outperformed a commercial product and a public domain product. *Orblitz*'s improved performance to the public domain SGP4 propagator may largely be contributed to the better theory employed by *Orblitz* and the inherent epoch errors in the TLE files used by SGP4. The comparable theories employed in *Orblitz* and *WinHpop*, in turn, only differ in choice of atmospheric model to quantify drag perturbation. Both programmes used the same drag coefficient and mean cross-sectional area values in the ballistic coefficient, but *Orblitz* used the superior MSISe-90 density model compared to the simpler Harris-Priester model employed by *WinHpop*. Though mathematically simple to express, atmospheric drag is difficult to quantify due to uncertainties in ballistic coefficient (**Equation 3.17**) and atmospheric density.

From **Figure 6.2** it is evident that drag is responsible for 60% of the error in position, making it an important force to quantify. As these errors are unbiased, it is possible to correct for them and set them close to zero. To this end, the drag coefficient, C_D, was employed as a "free" parameter to absorb uncertainties in the drag perturbation model, as well as the effects of other, smaller unmodelled perturbations. This approach is similar to that followed in the "B-star" parameter in TLE files. The feasibility of "tuning" drag coefficients by means of drag analysis was demonstrated.

In this regard, compare the 4.2km position error for a C_D textbook value of 2.2 (**Figure 6.1**), to the 63m errors using a "tuned" C_D value of 3.1 (**Figure 8.3**), using a five-day propagation period for SUNSAT SLR data. Further refinement of C_D is possible by employing a parameter estimation method such as Monte Carlo simulation, non-linear least squares estimation or extended Kalman filtering. The difficulty of estimating appropriate, optimum drag coefficients is emphasized in the literature [Vallado, Wertz, King-Hele].

According to [Alford, Liu 1974], *a priori* uncertainties in solar heating parameters and satellite ballistic coefficients are of greater significance on the prediction accuracy of satellite orbital lifetime than any shortcomings in Liu's prediction model. In the strictest sense, the ballistic coefficient varies with change in satellite attitude during a mission. In the absence of such accurate attitude information, estimates of the satellite parameters were used to obtain a mean value for the ballistic coefficient. Uncertainties in ballistic coefficients of the two test case LEO satellites, *Starshine-2* and *Iridium*-85, were further reduced by calculating optimum drag coefficients by means of drag analysis using five day period TLE-derived states (**Figures 8.1** and **8.2**). The effects of uncertainties in the predicted solar heating parameters are accommodated in the choice of solar and magnetic index parameters at three different solar activity levels, but remain difficult to quantify.

Given uncertainties in ballistic and future solar and geomagnetic parameters, the relative small differences between predicted and observed decay dates for the two test case satellites illustrate the success of Liu's semi-analytical theory in predicting satellite lifetime for the test cases. The observed and predicted orbital lifetimes for these test cases also compare well with predicted satellite lifetimes tabulated by [Wertz and Larson 1997, Pp 210]. The expected lifetime for SUNSAT, according to Liu's theory, is between 25 and 74 years, depending on solar activity levels. This result remains to be verified.

The development of the two software programmes resulted in a number of modular routines, which can be utilised in a variety of orbit analysis applications. In addition, the resulting computer source code liberates from dependence on expensive and restrictive black box COTS. The accuracy of predicted results attained by *Orblitz*

gives an indication on how far a set of initial conditions may be propagated into the future and stay within pre-defined limits of accuracy (**Table 6.1**). This might find use in applications such as error budget analysis.

9.2 FUTURE WORK

The propagator could be made more complete by expanding the force model to include other perturbation effects such as planetary attractions, geodynamic effects (Earth crust and tidal effects) and Earth radiation pressure. Provision can also be made to accommodate satellite attitude dynamics for improved ballistic coefficient estimation and other requirements. The execution speed of the program could be improved by investigating the use of other integrators, such as Adams-Bashforth, Adams-Moulton predictor-corrector, or Bulirsch-Stoer methods. In general, the programme could be adapted to become a useful analysis tool. Numerous applications are possible with the availability of historical ephemeris data (e.g. NORAD TLE's and SLR data) and well-described dynamic models. A dedicated drag analysis utility can be developed, employing the six equations of motion in a non-linear parameter estimation regime using extended Kalman filtering. It could also be useful to conduct drag analyses using long-term TLE-derived states and observed solar and geomagnetic parameters. To this end, it would be useful to develop a utility for handling and processing large sets of historic TLE's. It would also be informative to compare *Orblitz* results obtained using *predicted* solar flux and magnetic index values, with results obtained using *observed* solar and geomagnetic parameters.

The numerical integration algorithm of Liu's model could be replaced with a higher order embedded integrator and the Jacchia-70 model, replaced with the MSISe-90 model. The performance of Liu's semi-analytical theory should be evaluated for a variety of orbit classes and lifetimes.

References

(References are listed alphabetically under **Publications**, **Software** and **URL's**)

Publications

Bate R., Mueller D.D., White J.E., 1971. *Fundamentals of Astrodynamics*. First Edition. Dover Publications, Inc., New York. ISBN 73-157430.

Battin R.H., 1987. *An Introduction to the Mathematics and Methods of Astrodynamics*. AIAA Education series. ISBN 0-930403-25-8.

Bergamini, D. Ed., 1965. *Life Science Library: Mathematics*. Time-Life International (Nederland) N.V.

Butcher J.C. 1987. *The Numerical Analysis of Ordinary Differential Equations* – Runge Kutta and General Linear Methods. John Wiley and Sons. ISBN 0-471-91046.

Bursa M., Pec K., 1988. *Gravity Field and Dynamics of the Earth*. Springer Verlag. ISBN 3-540-56817-4.

Chabrillat, S. 1995. *Optimization and Use of Hedin's Atmospheric Model MSIS*. Aeronomica Acta B (Technical Reports of the Belgium Institute for Space Aeronomy) - Number 55, 1995.

Chao C.C., 1979. *An Analytical Integration of the Averaged Equations of Variation due to Sun-Moon Perturbations and its Applications*. The Aerospace Corp., Technical Report SD-TR-80-12, Oct. 1979

Chao C. C., Gunning G.R., Moe K , Settecerri T. J., 1996. *An Evaluation of Jacchia 71 and MSIS90 Atmospheric Models with NASA ODERACS Decay Data*. AIAA/AAS Space Flight Mechanics Meeting, Austin, Texas. Feb 1996. Technical Sessions. AAS 96-127.

Chobotov, V.A. Ed., 1996. *Orbital Mechanics*. Second Edition. AIAA Education Series. Reston, Virginia. ISBN 1-56347-179-5.

Constantinides, A., 1987. *Applied Numerical Methods With Personal Computers.* McGraw-Hill International Editions, Chemical Engineering Series. ISBN 0-07-100168-9.

Du Toit, D.N.J., 1997. *Low Earth Orbit Satellite Constellation Control Using Atmospheric Drag*. PhD Dissertation, University of Stellenbosch, South Africa.

EGM96, 1996. University of Texas, Austin and Godard Space Flight Center.

Escobal, P.R., 1985. *Methods of Orbit Determination.* Second Edition. Krieger Publishing Company, Malabar, Florida. ISBN 0-88275-319-3.

Fehlberg E., 1969. *Klassische Runge-Kutta-Formeln fünfter und siebenter Ordnung mit Schrittweiten-Kontrolle*. Computing Vol. 4, pp 93-106. Korrektion. Vol 5, pp 184.

Golub G.H., Van Loan C.F., 1996. *Matrix Computations*. Third Edition. The John Hopkins University Press, Baltimore and London. ISBN 0-8018-5414-8.

Hairer E., Norsett S.P., Wanner G., 1987. *Solving Ordinary Differential Equations I – Nonstiff Problems*. Springer-Verlag Berlin Heidelberg New York. ISBN 3-540-17145-2.

Hedin, A. E., 1991. *Extension of the MSIS Thermospheric Model into the Middle and Lower Atmosphere.* Journal of Geophysical Research. Vol. 96, pp 1159. 1991.

Heiskanen, Moritz , 1967. *Physical Geodesy.* W.H. Freeman and Co., San Francisco.

Hoots F.R., Roehrich, R. L., Kelso T.S. 1988. *Models for Propagation of NORAD lement Sets*. Spacetrack report no. 3. Defense Documentation Center Cameron Station Alexandria VA 22314. 31 December 1988.

Jacchia, L.G. 1970. *New Static Models for the Thermosphere with Empirical Temperature Profiles*. SAO Special Report No. 313. Cambridge, MA: Smithsonian Institution Astrophysical Observatory

Jacchia L.G., 1971. *Revised Static Models of the Thermosphere and Exosphere with Empirical Temperature Profiles*. SAO Report No. 332, May 5, 1971

Kaplan G.H., Hughes J.A., Seidelmann P.K., Yallop B.D., 1989. *Mean and Apparent Place Computations in the new IAU System III* - Appparent, Topocentric and astrometric places of planets and stars. The Astronomical Journal, Vol. 97, No. 4, April 1989, pp 1197.

King-Hele, D., 1987. *Satellite Orbits in an Atmosphere*. Blackie, London. ISBN 0-216-92252-6.

Liu J.J.F., 1974. *A Second–order Theory of an Artificial Satellite under the Influence of the Oblateness of The Earth*. AIAA paper 74-166. AIAA 12th Aerospace Sciences meeting, Jan. 30-Feb. 1, 1974.

Liu J.J.F., Alford R.L., 1974. *The Orbit Decay and Lifetime (LIFTIM) Prediction Program.* Northrop Report M-240-21278. May 1974.

Liu J.J.F., 1975. *Satellite Motion about an Oblate Earth with Drag.* Northrop Services Inc. *Huntsville Ala.* Report TN-240-1383 Feb 1975.

Liu J.J.F., Alford R.L., 1980. *Semianalytic Theory for a Close-Earth Artificial Satellite*. AIAA Journal of Guidance and Control. Vol 3, No. 4, July-Agust 1980.

Meeus, J., 1991. *Astronomical Algorithms*. Willman-Bell, Inc. Richmond Virginia, 23235, ISBN 0-943396-35-2.

Minkler G., Minkler J. 1990. *Aerospace Coordinate Systems and Transformations.* Magellan Book Company. ISBN 0-9621618-0-2.

Montenbruck O., Gill E. 2000. *Satellite Orbits: Models, Methods, Applications.* Springer. ISBN 3-540-67280-x

National Imaging and Mapping Agency (NIMA) Technical Report TR8350.2 Third Edition, July 1997. Department of Defense World Geodetic System 1984.

Prince P.J., Dormand J.R.. 1981. *High Order Embedded Runge-Kutta Formulae.* Journal of Computational and Applied Mathematics, Vol. 7, No. 1, 1981, pp 67-75.

Sears F.W., Zemansky M.W., Young H.D., 1982. *University Physics*, Sixth Edition. Addison-Wesly Publishing Company, Inc. ISBN 0-201-07199-1.

Seidelmann, P. (Ed.), 1992. *Explanatory Supplement to the Astronomical Almanac.* University Science Books, Sausalito, California. ISBN 0-935702-68-7.

Vallado, D. A., 1997. *Fundamentals of Astrodynamics and Applications.* McGraw-Hill. ISBN 0-07-066834-5.

Wertz, J.R., Larson W.J Ed., 1995. *Space Mission Analysis and Design.* Second Edition. Microcosm Inc. and Kluwer Academic Publishers, Torrance California. ISBN 0-7923-1998-2.

Software

[Analytical Graphics] *Satellite Toolkit v. 4.3.0a.* Analytical Graphics, Inc. 35 Technology Drive, Malvern, PA 19355, USA. http:///www.stk.com

[Microcosm]. *Advanced High Precision Orbit Propagator, version 3.0* Microcosm, Inc. 401 Coral Circle, El Segundo, CA 90245 (310) 726-4100, USA. http://www.smad.com

URL's

[Astronautix]. Encyclopedia Astronautica
http://www.astronautix.com

[Celestrak]. Two Line Element Files from Celestrak.
http://www.celestrak.com

[IERS] International Earth Rotation Service
http://hpiers.obspm.fr

[GSFC]. Goddard Space Flight Centre
Code 130, Office of Public Affairs
Greenbelt, MD 20771
http://www.gsfc.nasa.gov/

[HTSI] Honeywell-Technical Services Inc.
Honeywell
101 Columbia Road
Morristown, NJ 07962
http://www.honeywell-tsi.com/

[LAGEOS.] Laser Geodynamic Satellite Experiment
http://ilrs.gsfc.nasa.gov/lageos.html

[NGDC] National Geophysical Data Centre
National Geophysical Data Center
E/GC 325 Broadway
Boulder, Colorado USA 80305-3328 http://www.ngdc.noaa.gov/ngdc.html
ftp://ftp.ngdc.noaa.gov/STP/GEOMAGNETIC_DATA/INDICES/KP_AP/
ftp://ftp.ngdc.noaa.gov/STP/SOLAR_DATA/SOLAR_RADIO/FLUX/

[NIMA]. National Imaging and Mapping Agency.
Office of Corporate Relations
Public Affairs Division, MS D-54
4600 Sangamore Road
Bethesda, MD 20816-5003
http://www.nima.mil/

Appendix A

Development of Equations of Motion

1. THE N-BODY PROBLEM

(Following is a synthesis of [Bate *et al.* 1971, Pp 5-33; Vallado 1997; Pp 103-114; Chobotov 1996, Escobal 1985])

Assume a system of N bodies (m_1, m_2, m_3, ...m_N), one of which, the ith body m_i, is the body whose motion is to be studied. The vector sum of all *gravitational* and *other* external forces acting on m_i determines its equation of motion. To determine the gravitational forces, Newton's law of universal gravitation is applied. Other external forces may be attributed to thrust (if the ith body is a rocket expelling mass); atmospheric drag; solar radiation pressure; gravitational effects due to the shape of the attracting bodies, etc. All of these effects must be considered in the general equation of motion.

Assume a suitable inertial (un-accelerated, non-rotating) co-ordinate system (X, Y, Z) in which the positions of the N masses are known $\mathbf{r}_1$, $\mathbf{r}_2$, ...$\mathbf{r}_N$. This system is illustrated in **Figure A.1**.

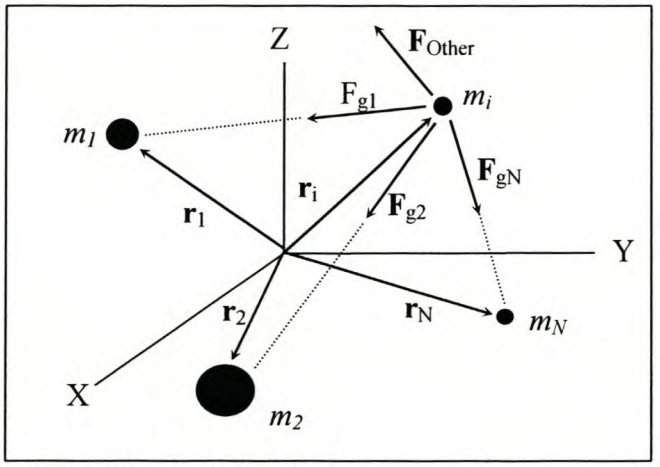

Figure A.1. The N-Body Problem

Applying Newton's law of universal gravitation, the force $\mathbf{F}_{gN}$ exerted on m_i by m_N is

$$\mathbf{F}_{gN} = -\frac{Gm_i m_N}{r_{Ni}^3}\mathbf{r}_{Ni}$$

Where

$$\mathbf{r}_{Ni} = \mathbf{r}_i - \mathbf{r}_N$$

The vector sum $\mathbf{F}_{gN}$, of all such gravitational forces acting on the ith body can be written as

$$\mathbf{F}_g = -\frac{Gm_i m_1}{r_{i1}^3}\mathbf{r}_{i1} - \frac{Gm_i m_2}{r_{2i}^3}\mathbf{r}_{2i} - \cdots - \frac{Gm_i m_N}{r_{Ni}^3}\mathbf{r}_{Ni}.$$

Simplify this equation

$$\mathbf{F}_g = -Gm_i \sum_{\substack{J=1 \\ j\neq i}}^{N} \frac{m_j}{r_{ji}^3}\mathbf{r}_{ji}. \qquad \textbf{A-1}$$

The other external force, $\mathbf{F}_{\text{Other}}$, is composed of drag, thrust, solar radiation pressure, non-spherical gravitational perturbations, etc. The total force on the ith body, $\mathbf{F}_{\text{Total}}$, is

$$\mathbf{F}_{\text{Total}} = \mathbf{F}_{\text{g}} + \mathbf{F}_{\text{Other}} \qquad \textbf{A-2}$$

Apply Newton's second law of motion.

$$\frac{d}{dt}(m\mathbf{v}_i) = \mathbf{F}_{\text{Total}}$$

This expands to

$$m_i \frac{d}{dt}\mathbf{v}_i + \mathbf{v}_i \frac{d}{dt}m_i = \mathbf{F}_{\text{Total}}.$$

Dividing by m_i renders the most general equation for the ith body

$$\ddot{\mathbf{r}}_i = \frac{\mathbf{F}_{Total}}{m_i} - \dot{\mathbf{r}}_i \frac{\dot{m}_i}{m_i} \qquad \textbf{A-3}$$

Where

$\ddot{\mathbf{r}}_i$: Acceleration vector of the ith body relative to the X, Y, Z co-ordinate system.

$\dot{\mathbf{r}}_i$: Velocity vector of the ith body relative to the X, Y, Z co-ordinate system.

m_i : Mass of the ith body.

$\dot{m}_i$: Time rate of change of the mass of the ith body (due to expelling mass or relativistic effects)

Combining **Equations A-1** to **A-3** renders

$$\ddot{\mathbf{r}}_i = -G\sum_{\substack{j=1\\ j\neq i}}^{N}\frac{m_j}{r_{ji}^3}\mathbf{r}_{ji} + \frac{1}{m_i}\left(-\dot{\mathbf{r}}_i\dot{m}_i + \mathbf{F}_{\text{Drag}} + \mathbf{F}_{\text{Thrust}} + \mathbf{F}_{\text{Solar pressure}} + \mathbf{F}_{\text{Perturb}} + \text{etc.}\right) \qquad \textbf{A-4}$$

Equation A-4 is a second order, non-linear, vector differential equation describing the equation of motion of a body influenced by gravitational and other external forces.

2. THE TWO-BODY PROBLEM.

The equation for two-body motion is derived uunder the assumptions stated in paragraph 2.2, Chapter 2. Consider the system of two bodies of masses M and m as illustrated in **Figure.2.1**. Their position vectors with respect to the inertial frame are $\mathbf{r}_M$ and $\mathbf{r}_m$ respectively.

Define

$$\mathbf{r} = \mathbf{r}_m - \mathbf{r}_M$$

By applying Newton's second law and law of gravitation, it follows that

$$\mathbf{F}_m = m\ddot{\mathbf{r}}\,,\quad \mathbf{F}_m = \frac{-GMm}{r^2}\frac{\mathbf{r}}{r}$$

$$\therefore m\ddot{\mathbf{r}}_m = \frac{-GMm}{r^2}\frac{\mathbf{r}}{r}$$

And similarly

$$M\ddot{\mathbf{r}}_M = \frac{-GMm}{r^2}\frac{\mathbf{r}}{r}\,.$$

Simplification and subtraction yields

$$\ddot{\mathbf{r}} = -\frac{G(M+m)}{r^3}\mathbf{r} \qquad \textbf{A-5}$$

3. SPECIFIC MECHANICAL ENERGY.

The two-body equation of motion is given by **Equation 2.**3 as

$$\ddot{\mathbf{r}} + \frac{\mu}{r^3}\mathbf{r} = \mathbf{0}$$

Dot multiply by $\dot{\mathbf{r}}$

$$\dot{\mathbf{r}} \bullet \ddot{\mathbf{r}} + \dot{\mathbf{r}} \bullet \frac{\mu}{r^3}\mathbf{r} = \mathbf{0}$$

Since in general $\mathbf{a} \bullet \dot{\mathbf{a}} = a\dot{a}$, $\mathbf{v} = \dot{\mathbf{r}}$ and $\dot{\mathbf{v}} = \ddot{\mathbf{r}}$, then

$$\mathbf{v} \bullet \dot{\mathbf{v}} + \frac{\mu}{r^3}\mathbf{r} \bullet \dot{\mathbf{r}} = 0$$

$$v\dot{v} + \frac{\mu}{r^3} r\dot{r} = 0$$

Noticing that $\frac{d}{dt}\left(\frac{v^2}{2}\right) = v\dot{v}$ and $\frac{d}{dt}\left(-\frac{\mu}{r}\right) = \frac{\mu}{r^2}\dot{\mathbf{r}}$,

$$\frac{d}{dt}\left(\frac{v^2}{2}\right) + \frac{d}{dt}\left(-\frac{\mu}{r}\right) = 0$$

Or

$$\frac{d}{dt}\left(\frac{v^2}{2} - \frac{\mu}{r}\right) = 0$$

Which, upon integration renders

$$\left(\frac{v^2}{2} - \frac{\mu}{r}\right) + C = \text{Constant}$$

Where C is an integration constant. Setting $C = 0$ is equivalent to choosing the zero reference for potential energy at infinity. The potential energy of the satellite, $-\frac{\mu}{r}$, will thus always be negative. The specific mechanical energy, E, of a satellite is then given by

$$E = \frac{v^2}{2} - \frac{\mu}{r} \qquad \textbf{A-6}$$

4. CONSERVATION OF ANGULAR MOMENTUM

Cross-multiply **Equation 2.3**, Chapter 2 by **r**

$$\mathbf{r}\times\ddot{\mathbf{r}}+\frac{\mu}{r^3}\mathbf{r}\times\mathbf{r}=\mathbf{0}$$

Since, in general, $\mathbf{a}\times\mathbf{a}=0$, the second term vanishes and

$$\mathbf{r}\times\ddot{\mathbf{r}}=\mathbf{0}$$

Noticing that $\frac{d}{dt}(\mathbf{r}\times\dot{\mathbf{r}})=\dot{\mathbf{r}}\times\dot{\mathbf{r}}+\mathbf{r}\times\ddot{\mathbf{r}}$, the equation above becomes

$$\frac{d}{dt}(\mathbf{r}\times\dot{\mathbf{r}})=\mathbf{0}$$

Or

$$\frac{d}{dt}(\mathbf{r}\times\mathbf{v})=\mathbf{0}$$

The expression $\mathbf{r}\times\mathbf{v}$, which must be a constant of the motion, is simply the vector **h**, called the *specific angular momentum.*

$$\mathbf{h}=\mathbf{r}\times\mathbf{v} \qquad \textbf{A-7}$$

5. THE TRAJECTORY EQUATION

Cross-multiply **Equation 2.3** by **h**:

$$\ddot{\mathbf{r}}\times\mathbf{h}=\frac{\mu}{r^r}(\mathbf{h}\times\mathbf{r}) \qquad \textbf{A-8}$$

The left side is equal to $\frac{d}{dt}(\dot{\mathbf{r}}\times\mathbf{h})$. To express the right side of above equation as a time rate of change of some vector quantity, we see that

$$\frac{\mu}{r^3}(\mathbf{h}\times\mathbf{r})=\frac{\mu}{r^3}(\mathbf{r}\times\mathbf{v})\times\mathbf{r}=\frac{\mu}{r^3}[\mathbf{v}(\mathbf{r}\bullet\mathbf{r})-\mathbf{r}(\mathbf{r}\bullet\mathbf{v})]$$

$$=\frac{\mu}{r^3}\mathbf{v}-\frac{\mu\dot{r}}{r^2}\mathbf{r}$$

Because

$$\mu\frac{d}{dt}\left(\frac{\mathbf{r}}{r}\right)=\frac{\mu}{r^3}\mathbf{v}-\frac{\mu\dot{r}}{r^2}\mathbf{r}$$

Rewrite **Equation A-8** as

$$\frac{d}{dt}(\mathbf{r}\times\mathbf{h}) = \mu\frac{d}{dt}\left(\frac{\mathbf{r}}{r}\right)$$

Integrating both sides

$$\mathbf{r}\bullet\dot{\mathbf{r}}\times\mathbf{h} = \mathbf{r}\bullet\mu\frac{\mathbf{r}}{r} + \mathbf{r}\bullet\mathbf{B} \qquad \textbf{A-9}$$

Since, in general, $\mathbf{a}\bullet\mathbf{b}\times\mathbf{c} = \mathbf{a}\times\mathbf{b}\bullet\mathbf{c}$ and $\mathbf{a}\bullet\mathbf{a} = a^2$

$$h^2 = \mu r + rB\cos\nu$$

Where ν (nu) is the angle between the constant vector **B** and the radius vector, **r**. Solving for r, we obtain

$$r = \frac{h^2/\mu}{1+(B/\mu)\cos\nu} \qquad \textbf{A-10}$$

Substituting $p = h^2/\mu$ and $e = B/\mu$ renders

$$r = \frac{p}{1+e\cos\nu} \qquad \textbf{A-11}$$

6. Direction Cosine Matrices

If three vectors forming a co-ordinate system are unit vectors and mutually orthogonal to (form right angles with) each other, then the co-ordinate system is called orthonormal. Let [**i**, **j**, **k**] be an orthonormal frame and **V** be a three-dimensional vector placed at the origin of the orthonormal frame. **V** can subsequently be represented as a linear combination of **i**, **j** and **k** [Minkler and Minkler 1990, Pp 9-16], i.e. there exists three scalars a, b and c satisfying

$$\mathbf{V} = a\mathbf{i} + b\mathbf{j} + c\mathbf{k} \qquad \textbf{A-12}$$

Taking the dot product of **V** with **i** on both sides of the equation renders

$$\mathbf{V}\bullet\mathbf{i} = a(\mathbf{i}\bullet\mathbf{i}) + b(\mathbf{j}\bullet\mathbf{i}) + c(\mathbf{k}\bullet\mathbf{i})$$

Since $(\mathbf{j}\bullet\mathbf{i}) = 0$, $(\mathbf{k}\bullet\mathbf{i}) = 0$, $(\mathbf{i}\bullet\mathbf{i}) = 1$

$$a = \mathbf{V}\bullet\mathbf{i} = |\mathbf{V}|.|\mathbf{i}|.\cos(\,ang(\mathbf{V}, \mathbf{i})) = |\mathbf{V}|\cos(\,ang(\mathbf{V}, \mathbf{i}))$$

where $ang(\ ,\ )$ represents the angle spanning the two vectors.

Similarly,

$$b = \mathbf{V}\bullet\mathbf{j} = |\mathbf{V}|\cos(\,ang(\mathbf{V}, \mathbf{j}))$$

$$c = \mathbf{V}\bullet\mathbf{k} = |\mathbf{V}|\cos(\,ang(\mathbf{V}, \mathbf{k}))$$

The scalars a, b, c are thus the projections of **V** onto **i**, **j** and **k** respectively. Equation 1 can subsequently be written as

$$\mathbf{V} = (\mathbf{V}\bullet\mathbf{i})\mathbf{i} + (\mathbf{V}\bullet\mathbf{j})\mathbf{j} + (\mathbf{V}\bullet\mathbf{k})\mathbf{k} \qquad \textbf{A-13}$$

$$= |\mathbf{V}|\cos(\,ang(\mathbf{V}, \mathbf{i}))\mathbf{i} + |\mathbf{V}|\cos(\,ang(\mathbf{V}, \mathbf{j}))\mathbf{j} + |\mathbf{V}|\cos(\,ang(\mathbf{V}, \mathbf{k}))\mathbf{k} \qquad \textbf{A-14}$$

A vector **V** presented in the orthonormal co-ordinate system $\mathbf{A} = [\mathbf{i}_A, \mathbf{j}_A, \mathbf{k}_A]$ as

$$\mathbf{V} = a\mathbf{i}_A + b\mathbf{j}_A + c\mathbf{k}_A$$

can be written in matrix notation as

$$\mathbf{V} = a\mathbf{i}_A + b\mathbf{j}_A + c\mathbf{k}_A = = [\mathbf{i}_A, \mathbf{j}_A, \mathbf{k}_A].[a, b, c]^T$$

$[a, b, c]^T$ is called the representation of **V** in **A** and is denoted by. $\mathbf{V}^A$

$$\mathbf{V}^A = \begin{bmatrix} a \\ b \\ b \end{bmatrix} = \begin{bmatrix} \mathbf{V}\bullet\mathbf{i}_A \\ \mathbf{V}\bullet\mathbf{j}_A \\ \mathbf{V}\bullet\mathbf{k}_A \end{bmatrix} = |\mathbf{V}| \begin{bmatrix} \cos(ang(\mathbf{V},\mathbf{i}_A)) \\ \cos(ang(\mathbf{V},\mathbf{j}_A)) \\ \cos(ang(\mathbf{V},\mathbf{k}_A)) \end{bmatrix}$$

Direction cosine matrices (Transformation matrices)

Let $\mathbf{A} = [\mathbf{i}_A\ \mathbf{j}_A\ \mathbf{k}_A]$ and $\mathbf{B} = [\mathbf{i}_B\ \mathbf{j}_B\ \mathbf{k}_B]$ be two right-handed orthonormal coordinate systems (with coinciding origins). Similar to vector **V** in **Equation A-13**, $\mathbf{i}_B$, $\mathbf{j}_B$ and $\mathbf{k}_B$ can be represented in **A**

$$\mathbf{i}_B = (\mathbf{i}_B\bullet\mathbf{i}_A)\mathbf{i}_A + (\mathbf{i}_B\bullet\mathbf{j}_A)\mathbf{j}_A + (\mathbf{i}_B\bullet\mathbf{k}_A)\mathbf{k}_A$$

$$\mathbf{j}_B = (\mathbf{j}_B\bullet\mathbf{i}_A)\mathbf{i}_A + (\mathbf{j}_B\bullet\mathbf{j}_A)\mathbf{j}_A + (\mathbf{j}_B\bullet\mathbf{k}_A)\mathbf{k}_A$$

$$\mathbf{k_B} = (\mathbf{k_B} \bullet \mathbf{i_A})\mathbf{i_A} + (\mathbf{k_B} \bullet \mathbf{j_A})\mathbf{j_A} + (\mathbf{k_B} \bullet \mathbf{k_A})\mathbf{k_A}$$

which can be written as

$$\begin{bmatrix}\mathbf{i_B} & \mathbf{j_B} & \mathbf{k_B}\end{bmatrix} = \begin{bmatrix}\mathbf{i_A} & \mathbf{j_A} & \mathbf{k_A}\end{bmatrix} \begin{bmatrix} \mathbf{i_B} \bullet \mathbf{i_A} & \mathbf{j_B} \bullet \mathbf{i_A} & \mathbf{k_B} \bullet \mathbf{i_A} \\ \mathbf{i_B} \bullet \mathbf{j_A} & \mathbf{j_B} \bullet \mathbf{j_A} & \mathbf{k_B} \bullet \mathbf{j_A} \\ \mathbf{i_B} \bullet \mathbf{k_A} & \mathbf{j_B} \bullet \mathbf{k_A} & \mathbf{k_B} \bullet \mathbf{k_A} \end{bmatrix} \qquad \textbf{A-15}$$

Let

$$\mathbf{C} = \begin{bmatrix} \mathbf{i_B} \bullet \mathbf{i_A} & \mathbf{j_B} \bullet \mathbf{i_A} & \mathbf{k_B} \bullet \mathbf{i_A} \\ \mathbf{i_B} \bullet \mathbf{j_A} & \mathbf{j_B} \bullet \mathbf{j_A} & \mathbf{k_B} \bullet \mathbf{j_A} \\ \mathbf{i_B} \bullet \mathbf{k_A} & \mathbf{j_B} \bullet \mathbf{k_A} & \mathbf{k_B} \bullet \mathbf{k_A} \end{bmatrix}$$

Then, from **Equation A-14**

$$\mathbf{C} = \begin{bmatrix} \cos(ang(\mathbf{i_B}, \mathbf{i_A})) & \cos(ang(\mathbf{j_B}, \mathbf{i_A})) & \cos(ang(\mathbf{k_B}, \mathbf{i_A})) \\ \cos(ang(\mathbf{i_B}, \mathbf{j_A})) & \cos(ang(\mathbf{j_B}, \mathbf{j_A})) & \cos(ang(\mathbf{k_B}, \mathbf{j_A})) \\ \cos(ang(\mathbf{i_B}, \mathbf{k_A})) & \cos(ang(\mathbf{j_B}, \mathbf{k_A})) & \cos(ang(\mathbf{k_B}, \mathbf{k_A})) \end{bmatrix} \qquad \textbf{A-16}$$

and **Equation A-15** can be written

$$[\mathbf{i_B}\ \mathbf{j_B}\ \mathbf{k_B}] = [\mathbf{i_A}\ \mathbf{j_A}\ \mathbf{k_A}]\ \mathbf{C} \qquad \textbf{A-17}$$

Suppose **V** is a vector and **C** a matrix defined by **Equation A-16**. Let $\mathbf{V^A}$ and $\mathbf{V^B}$ be the representation of **V** in frames **A** and **B** respectively. Then

$$\mathbf{V} = [\mathbf{i_A}\ \mathbf{j_A}\ \mathbf{k_A}]\mathbf{V^A}$$

$$\mathbf{V} = [\mathbf{i_B}\ \mathbf{j_B}\ \mathbf{k_B}]\ \mathbf{V^B}$$

From **Equation 6**

$$\mathbf{V} = [\mathbf{i_A}\ \mathbf{j_A}\ \mathbf{k_A}]\mathbf{V^A}$$

$$= [\mathbf{i_B}\ \mathbf{j_B}\ \mathbf{k_B}]\ \mathbf{V^B}$$

$$= [\mathbf{i_A}\ \mathbf{j_A}\ \mathbf{k_A}]\mathbf{CV^B}$$

Therefore

$$[\mathbf{i_A}\ \mathbf{j_A}\ \mathbf{k_A}](\mathbf{V^A} - \mathbf{CV^B}) = \mathbf{0}$$

Since $\mathbf{i_A}$, $\mathbf{j_A}$, $\mathbf{k_A}$ are linearly independent, then by definition, $(\mathbf{V^A} - \mathbf{CV^B}) = \mathbf{0}$ so that

$$\mathbf{V^A} = \mathbf{CV^B} \qquad \textbf{A-18}$$

Equation A-18 provides a relationship between the representations of a vector in two co-ordinate systems and is called a *vector transformation* from frame **B** to frame **A**. The matrix **C** is called the *transformation matrix* or *direction cosine matrix* from frame **B** to frame **A** and is denoted by $\mathbf{C}_{\mathbf{B}}^{\mathbf{A}}$. Direction cosine matrices can be shown to have the following properties

$$\mathbf{C}_{\mathbf{A}}^{\mathbf{A}} = \mathbf{I}_3$$

$$\left(\mathbf{C}_{\mathbf{B}}^{\mathbf{A}}\right)^{-1} = \left(\mathbf{C}_{\mathbf{B}}^{\mathbf{A}}\right)^{\mathrm{T}} = \mathbf{C}_{\mathbf{A}}^{\mathbf{B}}$$

$$\mathbf{C}_{\mathbf{B}}^{\mathbf{A}} = \mathbf{C}_{\mathbf{C}}^{\mathbf{A}}\mathbf{C}_{\mathbf{B}}^{\mathbf{C}}$$

The matrix **C** will be *orthonormal*, i.e. its row vectors will be mutually orthogonal and have norm of 1. An orthogonal transformation does not alter the original size or orientation of a vector, only its representation in different frames.

For two orthonormal basis frames with coinciding origins, a direction cosine matrix may be constructed from a composition of rotations about three axes. Each rotation about an axis can be represented by a 3x3 matrix operating on a vector. For arbitrary rotation angles θ, ϕ, λ axes rotation matrices about X, Y and Z-axes are defined as

$$\mathbf{R}_z(\theta) = \begin{bmatrix} \cos\theta & \sin\theta & 0 \\ -\sin\theta & \cos\theta & 0 \\ 0 & 0 & 1 \end{bmatrix}$$ Rotation about the Z-axis through an angle θ:

$$\mathbf{R}_y(\phi) = \begin{bmatrix} \cos\phi & 0 & -\sin\phi \\ 0 & 1 & 0 \\ \sin\phi & 0 & \cos\phi \end{bmatrix}$$ Rotation about the Y-axis through an angle ϕ:

$$\mathbf{R}_x(\lambda) = \begin{bmatrix} 1 & 0 & 0 \\ 0 & \cos\lambda & \sin\lambda \\ 0 & -\sin\lambda & \cos\lambda \end{bmatrix}$$ Rotation about the X-axis through an angle λ:

Rotation matrices are subsequently employed to construct the required direction cosine matrix for expressing the orthogonal set of unit vectors **P**, **Q**, **W** (perifocal

system) in the orthogonal set of unit vectors **I**, **J**, **K** (RAD or ECI system). [Escobal 1985, Pp 77-79].

Consider **Figure 4.9**, Chapter 4. By aligning both fundamental sets so that **P**, **Q**, **W** are coincident with **I**, **J**, **K** the following sequence of rotations is implemented
Rotate through the angle Ω about the Z-axis, rotate the result through an angle i about the Y-axis and rotate the result through an angle ω about the Z-axis:

$$\begin{bmatrix} \mathbf{P} \\ \mathbf{Q} \\ \mathbf{W} \end{bmatrix} = \mathbf{R}_z(\omega)\mathbf{R}_y(i)\mathbf{R}_z(\Omega)\begin{bmatrix} \mathbf{I} \\ \mathbf{J} \\ \mathbf{K} \end{bmatrix}$$

which, upon multiplying, yields

$$\begin{bmatrix} \mathbf{P} \\ \mathbf{Q} \\ \mathbf{W} \end{bmatrix} = \begin{bmatrix} (\cos\omega\cos\Omega - \sin\omega\cos i\sin\Omega) & (\cos\omega\sin\Omega + \sin\omega\cos i\cos\Omega) & \sin\omega\sin i \\ (-\sin\omega\cos\Omega - \cos\omega\cos i\sin\Omega) & (-\sin\omega\sin\Omega + \cos\Omega\cos\omega\cos i) & \cos\omega\sin i \\ \sin\Omega\sin i & -\sin i\cos\Omega & \cos i \end{bmatrix}\begin{bmatrix} \mathbf{I} \\ \mathbf{J} \\ \mathbf{K} \end{bmatrix}$$

It follows from matrix multiplication of the right side of the equation that

$$\mathbf{P} = a_{11}\mathbf{I} + a_{12}\mathbf{J} + a_{13}\mathbf{K}$$
$$\mathbf{Q} = a_{21}\mathbf{I} + a_{22}\mathbf{J} + a_{23}\mathbf{K}$$
$$\mathbf{W} = a_{31}\mathbf{1} + a_{32}\mathbf{J} + a_{33}\mathbf{K}$$

with the coefficients being associated with each element of the transformation matrix a_{ij}.

Upon dotting each of these equations with **I**, **J** and **K,**

$$\mathbf{P}\bullet\mathbf{I} = a_{11}, \quad \mathbf{Q}\bullet\mathbf{I} = a_{21}, \quad \mathbf{W}\bullet\mathbf{I} = a_{31}$$
$$\mathbf{P}\bullet\mathbf{J} = a_{12}, \quad \mathbf{Q}\bullet\mathbf{J} = a_{22}, \quad \mathbf{W}\bullet\mathbf{J} = a_{32}$$
$$\mathbf{P}\bullet\mathbf{K} = a_{13}, \quad \mathbf{Q}\bullet\mathbf{K} = a_{32}, \quad \mathbf{W}\bullet\mathbf{K} = a_{33}$$

Since $\mathbf{P}\bullet\mathbf{I}$ = (1).(1).cos(*ang*(**P**, **I**)) etc. it follows that the components of **P**, **Q**, **W,** expressed in **I**, **J**, **K**, are the direction cosines of the **P**, **Q**, **W** axes:

$$\mathbf{P} = [P_x\ P_y\ P_z] = [a_{11}\ a_{12}\ a_{13}]$$

$$\mathbf{Q} = [Q_x\ Q_y\ Q_z] = [a_{21}\ a_{22}\ a_{23}]$$

$$\mathbf{W} = [W_x\ W_y\ W_z] = [a_{31}\ a_{32}\ a_{33}]$$

Appendix B

Kepler's Equation

1 RELATING TIME AND ANGULAR DISPLACEMENT

The following development of equations is a synthesis of the work of [Vallado 1997, Pp 210-215; Escobal 1985; Bate *et al.* 1971, Pp 185]

The formula for the area of an ellipse is πab, with a and b the semi-major and semi-minor axii respectively. Assume the satellite starts at perigee and progresses through its orbit as indicated in **Figure B-1**.

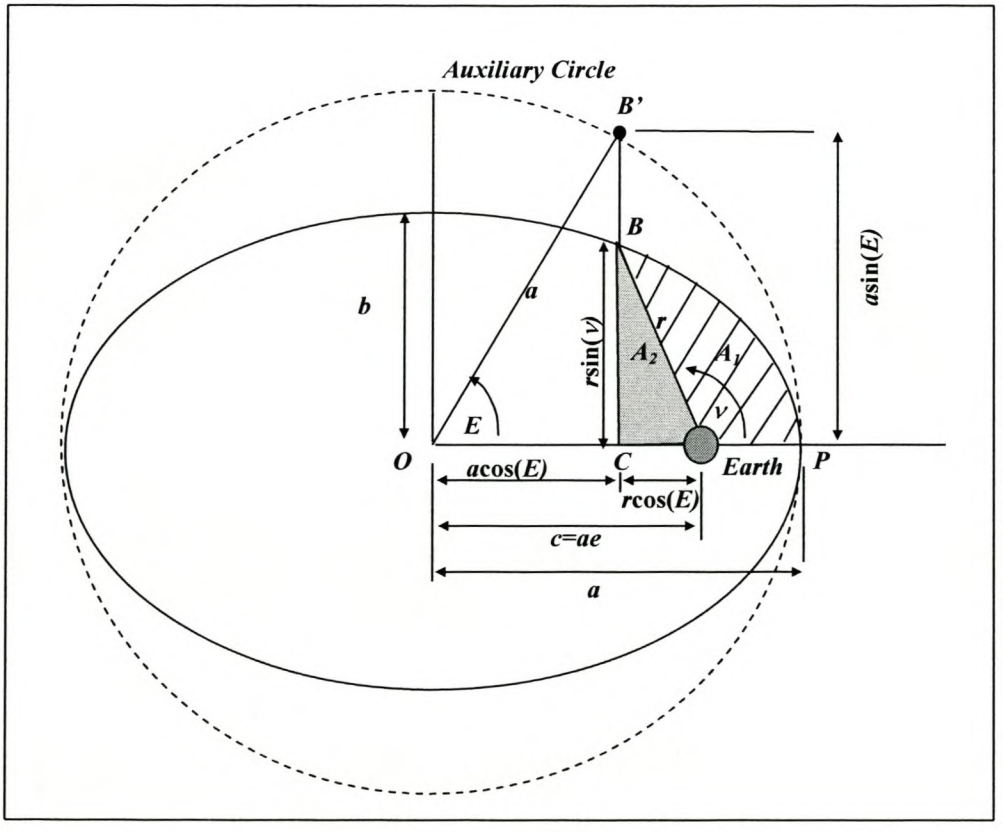

Figure B-1. Geometry of Kepler's Equation

Kepler's second law states that equal areas are swept out in equal times, or

$$\frac{t-T}{A_1} = \frac{P}{\pi ab} \qquad \textbf{B-1}$$

where $(t-T)$ represents the time change and P is the orbital period.

From **Table 1.1** (Chapter 1) define the scaling factor between a and b as

$$\frac{a}{b} = \sqrt{\left(1-e^2\right)} \qquad \textbf{B-2}$$

The area of the area A_1 is determined as

$$\boldsymbol{A_1} = \text{Area } \boldsymbol{PCB} - \text{Triangle } \boldsymbol{A_2} \qquad \textbf{B-3}$$

The area of A_2 is calculated as

$$A_2 = \frac{1}{2}\left(ae - a\cos E\right)\left(\frac{b}{a}a\sin E\right) = \frac{ab}{2}\left(e\sin E - \cos E\sin E\right) \qquad \textbf{B-4}$$

The area of the ellipse segment, PCB, is found by subtracting the area $OB'C$ from POB' and scaling the result:

$$\text{Area } PCB = \frac{abE}{2} - \frac{a^2}{2}\cos E\sin E\frac{b}{a}$$

$$= \frac{ab}{2}\left(E - \cos E\sin E\right) \qquad \textbf{B-5}$$

Substituting **Equation B-5** in **Equation B-3** renders the area for A_1

$$A_1 = \frac{ab}{2}\left(E - \sin E\right) \qquad \textbf{B-6}$$

Substitute into **Equation B-1** and solve for the period, P

$$P = \frac{2\pi\left(t-T\right)}{E - e\sin E} \qquad \textbf{B-7}$$

By using an alternate definition for P (**Table 2.1, Chapter 2**), it follows that

$$\sqrt{\frac{a^3}{\mu}} = \frac{(t-T)}{E - e\sin E} \qquad \textbf{B-8}$$

This equation is known as Kepler's equation. Kepler introduced the notation for the *mean anomaly*, M

$$M = E - e\sin E = \sqrt{\frac{\mu}{a^3}}(t-T) \qquad \textbf{B-9}$$

as wel as the *mean motion, n* (angular velocity). From Kepler's third law, relating orbital period to semi-major axis, it follows that n is a function of a

$$n \equiv \sqrt{\frac{\mu}{a^3}} \qquad \textbf{B-10}$$

Kepler's equation is generally written as

$$M = n(t-T) = E - e\sin E \qquad \textbf{B-11}$$

2 CONVERSIONS BETWEEN *E* AND *ν*.

From **Figure B-1** it can be seen that

$$\sin E = \frac{r\sin\nu}{a\sqrt{(1-e^2)}}, \quad \cos E = \frac{ae + r\cos\nu}{a} \qquad \textbf{B-12}$$

Substituting the trajectory equation (**Equation. 2.6, Chapter 2**) in **Equation B-12** renders

$$\sin E = \frac{a(1-e^2)\sin\nu}{a(1+e\cos\nu)\sqrt{1-e^2}}$$

$$\cos E = \frac{e(1+e\cos\nu)+(1-e^2)\cos\nu}{(1+e\cos\nu)}$$

Simplification reduces to

$$\sin E = \frac{\sqrt{1-e^2}\sin\nu}{1+e\cos\nu}, \quad \cos E = \frac{e+\cos\nu}{1+e\cos\nu} \qquad \textbf{B-13}$$

Solving for $\cos\nu$ from **Equation B-13**

$$\cos\nu = \frac{\cos E - e}{1-e\cos E} \qquad \textbf{B-14}$$

The trajectory equation can be expressed in terms of a and E by solving for r in **Equation B-12** and substituting $\cos\nu$ from **Equation B-13**:

$$r = \frac{(a\cos E - ae)(1-e\cos E)}{\cos E - e} = a(1-e\cos E) \qquad \textbf{B-15}$$

By solving for $\sin\nu$ in **Equation B-12** and substituting r from **Equation B-15**, it follows that

$$\sin\nu = \frac{\sqrt{1-e^2}\sin E}{1-e\cos E} \qquad \textbf{B-16}$$

Dividing **Equations B-14** and **B-16** and using the tangent half-angle formula obtain a single equation relating true and eccentric anomalies

$$\tan\left(\frac{\nu}{2}\right) = \frac{\dfrac{\sqrt{1-e^2}\sin E}{1-e\cos E}}{\dfrac{\cos E - e}{1-e\cos E}+1}$$

Simplification renders

$$\tan\left(\frac{\nu}{2}\right) = \frac{\sqrt{1-e^2}\sin E}{\cos E - e + 1 - e\cos E}$$

The denominator is the product of $(1 - e)(\cos E + 1)$, thus,

$$\tan\left(\frac{\nu}{2}\right) = \frac{\sqrt{1-e^2}\sin E}{(1-e)(\cos E + 1)}$$

Reduction of the terms containing e with a half-angle tangent formula renders

$$\tan\left(\frac{\nu}{2}\right) = \frac{\sqrt{1+e}}{\sqrt{1-e}}\tan\left(\frac{E}{2}\right) \qquad \textbf{B-16}$$

Inversely

$$\tan\left(\frac{E}{2}\right) = \frac{\sqrt{1-e}}{\sqrt{1+e}}\tan\left(\frac{\nu}{2}\right) \qquad \textbf{B-17}$$

Appendix C

Jacchia-Roberts Atmosphere

(Quoted from [Vallado 1997, Pp 843-852])

1 INTRODUCTION

The atmospheric density is determined using a modified analytical expression of the Jacchia-Roberts theory. The overall approach is to model the atmospheric temperature and add corrections for molecular composition and solar activity to the basic temperature formula. The atmospheric density is subsequently obtained for various regions of the atmosphere.

2 EVALUATING TEMPERATURE.

The exospheric temperature is firstly approximated using the *night time global exospheric* temperature, T_c (K), excluding all effects of electromagnetic and solar activity:

$$T_c = 379 + 3.24\overline{F}_{10.7} + 1.3\left[F_{10.7} - \overline{F}_{10.7}\right]$$

With

$F_{10.7}$ = Average daily solar flux at 10.7cm wavelength for the day of interest.

$\overline{F}_{10.7}$ = 81-Day running average of $F_{10.7}$ values, centred on the day of interest.

Because the effect of solar flux on atmospheric density lags one day behind the observed values, T_c calculations can use values which are one day old. These values are calculated on each day of a simulation before running the program.

The resulting value of T_c is used to determine the uncorrected exospheric temperature, T_{unc}.

$$T_{unc} = T_c\left\{1+0.3\left[Sin^{2.2}\theta+\left(Cos^{2.2}\eta-Sin^{2.2}\theta\right)Cos^3\left(\frac{\tau}{2}\right)\right]\right\}$$

Determine the following:

δ_S: The Sun's declination.

LHA_S: The Sun's local hour angle from the upper culmination.
ϕ_{gd}: Geodetic latitude of the satellite.

$\tau \in (-180°, 180°)$

$$\eta = \frac{\left|\phi_{gd}-\delta_S\right|}{2},\ \theta = \frac{\left|\phi_{gd}+\delta_S\right|}{2},$$

$$\tau = LHA_S - 37.0^\circ + 6.0^\circ Sin\left(LHA_S + 43.0^\circ\right),$$

$$LHA_S = \frac{180^\circ}{\pi}\left\{\frac{r_x r_J - r_y r_I}{\left|r_x r_J - r_y r_I\right|}Cos^{-1}\left(\frac{r_x r_I + r_y r_J}{\sqrt{r_x{}^2+r_y{}^2}\sqrt{r_I{}^2+r_J{}^2}}\right)\right\},$$

$$\phi_{gd} = Tan^{-1}\left\{\frac{1}{(1-f)^2}\left[\frac{r_K}{\sqrt{r_I{}^2+r_J{}^2}}\right]\right\} \qquad \textbf{C-1}$$

The satellite vector, $\mathbf{r}$ (r_I, r_J, r_K) and the Sun's unit vector, $\hat{\mathbf{r}}_\mathrm{S}$ (r_x, r_y, r_z), are in true-of-date (ECI_{tod}) coordinates. LHA_S is actually calculated from the dot product of the two vectors for the Sun and the satellite.

The next step involves the correction of the temperature for geomagnetic activity. The *correction factor for exospheric temperature*, ΔT_{corr}, depends on the geomagnetic index, k_p, and is calculated for altitudes of at least 200km. The actual value for k_p is set for a three-hour lag, during which the molecular interactions build up and the change in density is noticed.

$$\Delta T_{corr} = 28.0^{\circ} k_p + 0.03 e^{k_p}$$

For altitudes below 200km,

$$\Delta T_{corr} = 14.0^{\circ} k_p + 0.02 e^{k_p}$$

The corrected exospheric temperature, T_{corr}, is

$$T_{corr} = T_{unc} + \Delta T_{corr}$$

and the inflection temperature, T_x, is

$$T_x = 371.6678° + 0.0518806 T_{corr} - 294.3505\, e^{(-002\,162\,22 T_{corr})} \qquad \textbf{C-2}$$

Using the base value temperature, $T_0 = 183°$ K, Jacchia defines the empirical temperature function for altitudes below 125 km as

$$T(h_{ellp})_{0-125} = T_x + \frac{T_x - T_0}{35^4} \sum_{n=0}^{4} C_n h_{ellp}{}^n \qquad \textbf{C-3}$$

C_0 = -89 284 375.0, C_1 = 3 542 400.0, C_2 = -52 687.5

C_3 = 340.5, C_4 = -0.8

Where the coefficients C_i have units of 1/km^i, i =0,…4.

Jacchia defines the region above 125 km in altitude with an empirical, asymptotic function for temperature (h_{ellp} is in km).

$$T(h_{ellp})_{125+} = T_x + \frac{2}{\pi}(T_{corr} - T_x).$$
$$\times Tan^{-1}\left\{0.95\pi\left(\frac{T_x - T_0}{T_{corr} - T_x}\right)\left(\frac{h_{ellp} - 125}{35}\right)\left(1 + 4.5\times10^{-6}(h_{ellp} - 125)^{2.5}\right)\right\}$$

C-4

3 ROBERT'S CORRECTION FOR TEMPERATURE

Roberts replaced Jacchia's temperature expression with

$$T(h_{ellp})_{125+} = T_{corr} + (T_{corr} - T_x).e^{\left\{-\left(\frac{T_x - T_0}{T_{corr} - T_x}\right)\left(\frac{h_{ellp} - 125}{35}\right)\left(\frac{l}{R_{pole} + h_{ellp}}\right)\right\}} \quad \textbf{C-5}$$

With

h_{ellp}: the spacecraft's altitude (km),

R_{pole}: the Earth's polar radius (km) and

l = 12 315.3554 km (by Jacchia)

Draper laboratory uses a least squares fit for the best value of l:

$$l = \sum_{j=0}^{4} l_j T_{corr}^{j}$$

With coefficients:

l_0 = 0.103 144 5 x 10^5

l_1 = 0.234 123 0 x 10

l_2 = 0.157 920 2 x 10^{-2}

l_3 = -0.125 248 7 x 10^{-5}

l_4 = 0.246 270 8 x 10^{-9}

4 JACCHIA'S CORRECTIONS FOR DENSITY

For altitudes below 200 km the *geomagnetic effect* on density is included:

$$(\Delta \log_{10} \rho)_G = 0.012k_p + 1.2\times10^{-5} e^{k_p} \quad \textbf{C-6}$$

With k_p the geomagnetic planetary index.

Determine the number of years from 1958 using the Julian date of 1958 (2436204). JD_{1958} is the number of days from January 1, 1958:

$$T_{1958} = \frac{JD_{1958}}{365.2422}$$

Calculate the correction for *seasonal latitudinal variation* in the lower thermosphere.

$$\begin{aligned}\left(\Delta \log_{10} \rho\right)_{LT} &= 0.014\left(h_{ellp} - 90\right) \cdot Sin\left(2\pi T_{1958} + 1.72\right) \cdot Sin\left(\phi_{gd}\right) \\ &\times \left|Sin\left(\phi_{gd}\right)\right| \cdot e^{\left[-0.0013\left(h_{ellp}-90\right)^2\right]}\end{aligned} \qquad \textbf{C-7}$$

Calculate an intermediate value, $\tau_{SA,}$ for use in the correction for semi-annual variations in density:

$$\tau_{SA} = T_{1958} + 0.09544\left\{\left[\frac{1}{2} + \frac{1}{2} Sin\left(2\pi T_{1958} + 6.035\right)\right]^{1.65} - \frac{1}{2}\right\}$$

The correction is

$$\begin{aligned}\left(\Delta \log_{10} \rho\right)_{SA} &= \left(5.876 \times 10^{-7} h_{ellp}^{2.331} + 0.06328\right) \cdot e^{-0.002868 h_{ellp}} \\ &\times \left\{0.02835 + \left[0.3817 + 0.17829 \cdot Sin\left(2\pi\tau_{SA} + 4.137\right)\right] \cdot Sin\left(4\pi\tau_{SA} + 4.259\right)\right\}\end{aligned} \qquad \textbf{C-8}$$

(The trigonometric terms use radians)

The correction for density because of *seasonal variations of Helium by latitude* is:

$$\left(\Delta \log_{10} \rho\right)_{He} = 0.65\left|\frac{\delta_S}{\varepsilon}\right| \cdot \left[Sin^3\left(\frac{\pi}{4} - \frac{\phi_{gd}\delta_S}{2\left|\delta_S\right|}\right) - 0.35355\right]$$

With

ε : The obliquity of the ecliptic

δ_S: The declination of the Sun

5 ROBERT'S CORRECTIONS FOR DENSITY

Roberts sections the atmosphere in three altitude bands to account for major variations in density: 90-100 km, 100-125 km and above 125 km.

90-100 km

For these altitudes, Roberts uses the Jacchia temperature profile (**Equation C-3**) and integrates with partial fractions to obtain a standard density.

$$\rho_{std_{90-100}}(h_{ellp}) = \frac{\rho_{90} T_{90}}{M_{90}} \cdot \frac{M(h_{ellp})}{T(h_{ellp})_{125+}} F_1^k \cdot e^{kF_2} \qquad \textbf{C-9}$$

This equation assumes atmospheric mixing is predominant. The constants used for h_{ellp} = 90 km are:

M_{90} = 28.826 78 g.mol^{-1}. Mean molecular mass.
ρ_{90} = 3.46 x 10^{-6} kg.m^{-3}. Assumed density.

The constant k is

$$k = \frac{-35^4 \, g_{SL} R_{pole}^2}{R(T_x - T_0)C_4}$$

With

g_{SL} = 9.80665m.s^{-2}. Gravity acceleration at sea level.

R_{pole} = 6356.766 km. Earth polar radius.

R = 8.314 32 Joules.K^{-1}.mol^{-1}. Universal gas constant.

C_4 = -0.8. **Equation C-3**.

Determine the mean molecular mass

$$M(h_{ellp}) = \sum_{n=0}^{6} A_n h_{ellp}^n$$

With coefficients given in **Table C-1**

Table C-1. Coefficients of mean Molecular Mass. Units are the reciprocal of the index in km. E.g., for $n = 2$, units are km^{-2}.

Index$_n$	**A$_n$**	**Index$_n$**	**A$_n$**
0	-435 093.363 387	**4**	-0.089 587 909 95
1	28 275.564 6391	**5**	0.000 387 375 86
2	-765.334 661 08	**6**	-0.000 000 607 444
3	11.043 387 545		

Solve for F_1 and F_2 in **Equation C-9** using quadratic expressions:

$$F_1 = \left(\frac{h_{ellp} + R_{pole}}{90 + R_{pole}}\right)^{P_1} \left(\frac{h_{ellp} - x_{r1}}{90 - x_{r1}}\right)^{P_2} \left(\frac{h_{ellp} - x_{r2}}{90 - x_{r2}}\right)^{P_3} \left(\frac{h_{ellp}^2 - 2x_{r3}h_{ellp} + x_{r3}^2 + x_{i3}^2}{8100 - 180x_{r3} + x_{r3}^2 + x_{i3}^2}\right)^{P_4}$$

$$F_2 = \left(h_{ellp} - 90\right) \cdot \left[A_6 + \frac{P_5}{\left(h_{ellp} + R_{pole}\right) \cdot \left(90 + R_{pole}\right)}\right] + \frac{P_6}{x_{i3}} \cdot Tan^{-1}\left[\frac{x_{i3}\left(h_{ellp} - 90\right)}{x_{i3}^2 + \left(h_{ellp} - x_{r3}\right)\left(90 - x_{r3}\right)}\right]$$

There are two real roots (x_{r1}, x_{r2}) and two complex conjugate roots (x_{r3}, $\pm x_{i3}$). Calculate the roots from the following polynomial function with coefficients and only use the positive imaginary component.

$$f\left(h_{ellp}\right) = \sum C_n^* h_{ellp}^n, \qquad C_0^* = \frac{35^4 T_x}{C_4\left(T_x - T_0\right)} + \frac{C_0}{C_4}, \qquad C_n^* = \frac{C_n}{C_4}, (1 \le n \le 4)$$

With values of C_n given by **Equation C-3**.

Calculate the following relations:

$$X^* = -2x_{r1}x_{r2}R_{pole}\left(R_{pole}^2 + 2x_{r3}R_{pole} + x_{r3}^2 + x_{i3}^2\right)$$

$$V = \left(R_{pole} + x_{r1}\right)\left(R_{pole} + x_{r2}\right)\left(R_{pole}^2 + 2x_{r3}R_{pole} + x_{r3}^2 + x_{i3}^2\right)$$

$$U\left(r_i\right) = \left(r_i + R_{pole}\right)^2\left(x_{ri}^2 - 2x_{r3}r_i + x_{r3}^2 + x_{i3}^2\right)\left(x_{r1} - x_{r2}\right)$$

$$W(r_i) = x_{r1}x_{r2}R_{pole}\left(R_{pole} + r_i\right)\left(R_{pole} + \frac{x_{r3}^2 + x_{i3}^2}{r_i}\right)$$

Using coefficients in **Table C-2**, the coefficients B_n and the function $S(h_{ellp})$ are given by

$$B_n = \alpha_n + \beta_n \frac{T_x}{T_x - T_0}, \qquad S(h_{ellp}) = \sum_{n=0}^{5} B_n h_{ellp}^n$$

The parameters P_i for the functions F_i are

$$P_2 = \frac{S(x_{r1})}{U(x_{r1})}, \quad P_3 = \frac{-S(x_{r2})}{U(x_{r2})}, \quad P_5 = \frac{S(-R_{pole})}{V}$$

$$P_4 = \frac{1}{X^*}\left\{\begin{array}{l} B_0 - x_{r1}x_{r2}R_{pole}^2\left[B_4 + B_5\left(2x_{r3} + x_{r1} + x_{r2} - R_{pole}\right)\right] \\ + W(x_{r1})P_2 - x_{r1}x_{r2}B_5R_{pole}(x_{r3}^2 + x_{i3}^2) + W(x_{r2})P_3 \\ + x_{r1}x_{r2}\left(R_{pole}^2 - x_{r3}^2 - x_{i3}^2\right)P_5 \end{array}\right\}$$

$$P_6 = B_4 + B_5\left(2x_{r3} + x_{r1} + x_{r2} - R_{pole}\right) - P_5 - 2\left(x_{r3} + R_{pole}\right)P_4 - \left(x_{r2} + R_{pole}\right)P_3 - (x_{r1} + R_{pole})P_2$$

$$P_1 = B_5 - 2P_4 - P_3 - P_2$$

Table C-2. Coefficients. These coefficients help determine the functions that lead to the density between 90 and 125 km.

n	α_i	β_i
0	3 144 902 516.672 729	-52 864 482.179 109 69
1	-123 774 885.483 291 7	-16 632.508 473 368 28
2	1 816 141.096 520 398	-1.308 252 378 125
3	-11 403.310 794 892 67	0.0
4	24.364 986 121 055 95	0.0
5	0.008 957 502 869 707 995	0.0

100 to 125 km

Roberts assumes diffusive equilibrium above altitudes of 100km and integrates **Equation C-3** by partial fractions for each atmospheric constituent to obtain the standard density between 100 km and 125 km.

$$\rho_{std_{100-125}}(h_{ellp}) = \sum_{i=1}^{5} \rho(100) \frac{M_i}{M_s} \mu_i \left[\frac{T(100)}{T(h_{ellp})} \right]^{1+\alpha_i} F_3^{M_i k} \cdot e^{M_i k F_4} \qquad \textbf{C-10}$$

With

M_s = 28.96 g.mol^{-1}. Mean molecular mass at sea level.

μ_i, α_i, and Mi listed in **Table C-3**.

k and C_n the same as in the 90-100 km case

Long proposes the following polynomial fit to evaluate the density at 100 km [$\rho(100)$] as an alternate method to using the intensive **Equation C-9**.

$$\rho_{std_{100-125}}(100) = M_s \sum_{n=0}^{6} \xi_n T_{corr}^n$$

ξ_0 = 0.198 554 9 x 10^{-10}, ξ_1 = -0.183 349 x 10^{-14}, ξ_2 = 0.1711735 x 10^{-17},

ξ_3 = -0.102 147 4 x 10^{-20}, ξ_4 = 0.372 789 4 x 10^{-24}, ξ_5 = -0.773 411 0 x10^{-28},

ξ_6 = 0.702 694 2 x 10^{-32}

Using **Equation C-3**, the temperature at 100 km, $T(100)$, is calculated as

$$T(100) = -0.945\ 855\ 89(T_x - T_0)$$

The parameters k and C_n in **Equation C-10** are the same as in the 90-100km case. The functions F_3 and F_4 are given by

$$F_3 = \left(\frac{h_{ellp} + R_{pole}}{R_{pole} + 100} \right)^{q_1} \left(\frac{h_{ellp} - x_{r1}}{100 - x_{r1}} \right)^{q_2} \left(\frac{h_{ellp} - x_{r2}}{100 - x_{r2}} \right)^{q_3} \times \left(\frac{h_{ellp}^2 - 2x_{r3}h_{ellp} + x_{r3}^2 + x_{i3}^2}{1000 - 200x_{r3} + x_{r3}^2 + x_{i3}^2} \right)^{q_4}$$

$$F_4 = \left[\frac{q_5(h_{ellp}-100)}{(h_{ellp}+R_{pole})(R_{pole}+100)}\right] + \frac{q_6}{x_{i3}} Tan^{-1}\left[\frac{x_{i3}(h_{ellp}-100)}{x_{i3}^2+(h_{ellp}-x_{r3})(100-x_{r3})}\right]$$

The parameters q_i are defined similar to the p_i parameters with the F_1 and F_2 functions.

$$q_2 = \frac{1}{U(x_{r1})}, \quad q_3 = \frac{-1}{U(x_{r2})}, \quad q_5 = \frac{1}{V}$$

$$q_4 = \frac{1}{X^*}\left[1 + x_{r1}x_{r2}(R_{pole}^2 - x_{r3}^2 - x_{i3}^2)q_5 + W(x_{r1})q_2 + W(x_{r2})q_3\right]$$

$$q_6 = -q_5 - 2(x_{r3}+R_{pole})q_4 - (x_{r2}+R_{pole})q_3 - (x_{r1}+R_{pole})q_2$$
$$q_1 = -2q_4 - q_3 - q_2$$

The roots (x_{r1}, x_{r2}, x_{r3}, x_{i3}), X^*, U and W are the same as in the 90-100 km case.

Above 125 km

To obtain the total standard atmospheric density at altitudes h_{ellp} above 125km, the diffusion differential equation must be integrated using the temperature profile (**Equation C-5)**, to achieve the individual effect of the five basic atmospheric constituents (**Table C-3**) on the standard density.

$$\rho_{std_{125+}}(h_{ellp}) = \sum_{i=1}^{5} \rho_i(125)\left(\frac{T_x}{T(h_{ellp})}\right)^{1+a_i+\gamma_i} \cdot \left(\frac{T_{corr}-T_x}{T_{corr}-T_0}\right)^{\gamma_i} \qquad \textbf{C-11}$$

$$\gamma_i = \frac{M_i g_0 R_{pole}^2}{RlT_{corr}}\left(\frac{T_{corr}-T_x}{T_x-T_0}\right)\left(\frac{35}{6481.766}\right)$$

With

g_0 : Mean surface gravitation acceleration

R_{pole}: Polar radius

R : Universal gas constant

ρ_i : Constituent *mass density*

M_i : Constituent molecular mass (g.mole^{-1})

a_i : Constituent thermal diffusion coefficient (see **Table C-3**)

Table C-3. Atmospheric Constituents and Related Constants. The constituent number density is multiplied by $M_S/\rho(100)$ and divided by Avagadro's number.

Index i	Constituent	Molecular Mass (M_i) g.mol^{-1}	Thermal diffusion Coefficient (a_i)	Constituent density (μ_i)
1	N_2	28.0134	0	0.781 10
2	Ar	39.948	0	0.009 343 2
3	He	4.0026	-0.38	0.614 71 x 10^{-5}
4	O_2	31.9988	0	0.161 778
5	O	15.9994	0	0.095 544
6	H	1.00797	0	

Although we can explicitly determine the constituent mass density, d_i (125 km) from **Equation C-10**, Draper Laboratory uses a polynomial curve fit approximation in the Goddard Trajectory Determination System (Long et al., 1989,pp4-49):

$$\log_{10}[d_i(125)] = \sum_j^6 \delta_{ij} T_{corr}^j \qquad d_i = \frac{P_i}{M_i}$$

Here, δ_{ij} are curve-fit coefficients in **Table C-4**. The final correction for Helium is

$$\left[\rho_{He}(h_{ellp})\right]_{corr} = \rho_{He}(h_{ellp}) 10^{(\Delta \log_{10} \rho_{He})}$$

Table C-4. Curve-fitting Coefficients δ_{ij}. The degree of the polynomial (j) and the index (i) helps determine the constants used to define the constituent mass density.

j	*(i=1)*N_2	*(i=2)*Ar	*(i=3)*He	*(i=4)*O_2	*(i=5)*O
0	0.1093155e2	0.8049405e1	0.7646886e1	0.9924237e1	0.109708e2
1	0.1186783e-2	0.2382822e-2	-0.4383486e-3	0.1600311e-2	0.6118742e-4
2	-0.1677341e-5	-0.3391366e-5	0.4694319e-6	-0.2274761e-5	-0.1165003e-6
3	0.1420228e-8	0.2909714e-8	-0.2894886e-9	0.1938454e-8	0.9239354e-10
4	-0.7139785e-12	-0.1481702e-11	0.9451989e-13	-0.9782183e-12	-0.3490739e-13
5	0.1969715e-15	0.4127600e-15	-0.1270838e-16	0.2698450e-15	0.5116298e-17
6	-0.2296182e-19	-0.4837461e-19	0.0	-0.3131808e-19	0.0

We must also account for the concentration of Hydrogen whenever altitudes exceed 500 km.

$$\rho_H(h_{ellp}) = \rho_H(500)\left[\frac{T_{500}}{T(h_{ellp})}\right]^{(1+a_H+\gamma_H)} \cdot \left[\frac{T_{corr} - T(h_{ellp})}{T_{corr} - T_{500}}\right]^{\gamma_H}$$

The Hydrogen density at 500 km, $\rho_H(500)$, is calculated using

$$\rho_H(500) = \frac{M_H}{A} 10^{[73.13-(39.4-5.5\log_{10}(T_{500}))(\log_{10}(T_{500}))]}$$

With

γ_H calculated from **Equation C-11**

A = 6.022 57 x10^{23} : Avogadro's number

T_{500} is the temperature at 500 km calculated from **Equation C-5**

M_H, a_H : The molecular mass and thermal diffusion coefficient for Hydrogen, from **Table C-3**.

Finally, the correction terms of **Equations C-6**, **C-7** and **C-8** are applied to the standard density:

$$(\Delta \log_{10} \rho)_{corr} = (\Delta \log_{10} \rho)_G + (\Delta \log_{10} \rho)_{SA} + (\Delta \log_{10} \rho)_{LT}$$

giving the final corrected density as

$$\rho(h_{ellp}) = \rho_{std}(h_{ellp}) 10^{(\Delta \log_{10} \rho)_{corr}} \qquad \textbf{C-12}$$

References

Jacchia, L.G. 1970. *New Static Models for the Thermosphere with Empirical Temperature Profiles*. SAO Special Report No. 313. Cambridge, MA: Smithsonian Institution Astrophysical Observatory.

Jacchia, L.G. 1971. *Revised Static Models for the Thermosphere with Empirical Temperature Profiles*. SAO Special Report No. 332. Cambridge, MA: Smithsonian Institution Astrophysical Observatory.

Long, A.C.et al, 1989. *Goddard Trajectory Determination System (GTDS) Mathematical Theory (Rev. 1).* FDD/552-89/6001. Goddard Space Flight Center: NASA.

Roberts, C.E. Jr, 1971. An Analytic Model for Upper Atmosphere Densities based upon Jacchia's 1970 Models. *Celestial Mechanics*. 4(314):368-377.

Vallado, D. A., 1997. *Fundamentals of Astrodynamics and Applications*. McGraw-Hill. ISBN 0-07-066834-5.

Appendix D

Position of the Sun and Moon

1. SUN, MOON, PLANETARY EPHEMEREDES

Accurate positions for of the Sun, Moon and planets are obtained from their ephemerides, which are regularly published in the Astronomical Almanac.

2. POSITION OF THE SUN

The position of the Sun may be calculated accurately to within 0.01° using the following formula [Meeus 1991, Pp 151].

$$\mathbf{r}_{Sun} = r_{Sun}\begin{bmatrix}\cos(\lambda_{Sun})\\ \cos(\varepsilon)\sin(\lambda_{Sun})\\ \sin(\varepsilon)\sin(\lambda_{Sun})\end{bmatrix} AU$$

Where the following definitions apply:

Mean obliquity of the ecliptic

$$\varepsilon = 23^{\circ}.4392911 - 0^{\circ}.0130041 \cdot T - 1.64\times10^{-7}\cdot T^2 + 5.04\times10^{-7}\cdot T^3$$

True geometric longitude

$$\lambda_{Sun} = L_{Sun} + C$$

Mean geometric longitude

$$L_{Sun} = 280^{o}.46645 + 36000^{o}.76983 \cdot T + 0^{o}.0003032 \cdot T^2$$

Mean anomaly

$$M_{Sun} = 357^{o}.52910 + 35999^{o}.05030 \cdot T - 0^{o}.0001559 \cdot T^2 - 0^{o}.00000048 \cdot T^3$$

Equation of centre

$$C = +(1^o.914600 - 0^o.004817 \cdot T - 0^o.000014 \cdot T^2)\sin M + (0^o.019993 - 0^o.000101 \cdot T)\sin 2M + 0^o.000290 \sin 3M$$

Eccentricity of Earth's orbit

$$e = 0.016708617 - 0.000042037 \cdot T - 0.0000001236 \cdot T^2$$

Sun's true anomaly

$$\nu = M_{Sun} + C$$

Radial distance from Earth to the Sun (Astronomical Units)

$$r_{Sun} = \frac{1.000001018\left(1 - e^2\right)}{1 + e\cos\nu}$$

Julian centuries from epoch J2000

$$T = \frac{JD - 2451545.0}{36525}$$

JD = Julian day of observation

3. POSITION OF THE MOON

The motion of the Moon is complex motion and accurate calculation thereof is computer intensive. The following algorithm from the Astronomical Almanac renders sufficient positional accuracy (10") for calculating gravitational attraction of the Moon as third body.

$$\mathbf{r}_{Moon} = r_{Moon}\begin{bmatrix} \cos(\phi_{ecliptic}) \cdot \cos(\lambda_{ecliptic}) \\ \cos(\varepsilon) \cdot \cos(\phi_{ecliptic}) \cdot \sin(\lambda_{ecliptic}) - \sin(\varepsilon) \cdot \sin(\phi_{ecliptic}) \\ \sin(\varepsilon) \cdot \cos(\phi_{ecliptic}) \cdot \sin(\lambda_{ecliptic}) + \cos(\varepsilon) \cdot \sin(\phi_{ecliptic}) \end{bmatrix}$$

Where the following definitions apply:

Ecliptic longitude

$$\lambda_{ecliptic} = \lambda_{Moon} + 6.29 \cdot \sin(M_{Moon}) - 1.27 \cdot \sin(M_{Moon} - 2D_{Sun}) + 0.66 \cdot \sin(2D_{Sun}) + 0.21 \cdot \sin(2M_{Moon}) - 0.19 \cdot \sin(M_{Sun}) - 0.11 \cdot \sin(2u_{M_{Moon}})$$

Moon's longitude

$$\lambda_{Moon} = 218^{\circ}.3165 + 481267^{\circ}.8813 \cdot T$$

Ecliptic latitude

$$\phi_{ecliptic} = 5.13 \cdot \sin(u_{M_{Moon}}) + 0.28 \cdot \sin(M_{Moon} + u_{M_{Moon}}) - 0.28 \cdot \sin(u_{M_{Moon}} - M_{Moon}) - 0.17 \cdot \sin(u_{M_{Moon}} - 2D_{Sun})$$

Moon's mean anomaly ($k = 360°$)

$$M_{Moon} = 134^{\circ}.9729814 + (1325k + 198^{\circ}.867398) \cdot T + 0.0086972 \cdot T^2 + 1.778 \times 10^{-5} \cdot T^3$$

Moon's mean argument of latitude

$$u_{M_{Moon}} = 93^{\circ}.2719103 + (1342k + 82^{\circ}.0175381) \cdot T - 0.0036825 \cdot T^2 + 3.06 \times 10^{-6} \cdot T^3$$

Mean elongation of the Sun

$$D_{Sun} = 297^{\circ}.8503631 + (1236k + 307^{\circ}.111480) \cdot T - 0^{\circ}.00191417 \cdot T^2 + 5.28 \times 10^{-6} \cdot T^3$$

Radial distance from the Earth to the Moon (In Earth radii units)

$$r_{Moon} = \frac{1}{\sin(\wp)}$$

Parallax

$$\wp = 0^{\circ}.9508 + 0.0518\cos(M_{Moon}) + 0.0095\cos(M_{Moon} - 2D_{Sun}) + 0.0078\cos(2D_{Sun}) + 0.0028\cos(2M_{Moon})$$

Appendix E

Program Listing for ORBLITZ

(Supplied on CD-ROM because of large file size)

Appendix F

Data

Table F.1 Format of a Two Line Element (TLE) file

Line 1

Column	*Description*
01	Line Number of Element Data
03-07	Satellite Number
08	Classification
10-11	International Designator (Last two digits of launch year)
12-14	International Designator (Launch number of the year)
15-17	International Designator (Piece of the launch)
19-20	Epoch Year (Last two digits of year)
21-32	Epoch (Day of the year and fractional portion of the day)
34-43	First Time Derivative of the Mean Motion
45-52	Second Time Derivative of Mean Motion (decimal point assumed)
54-61	BSTAR drag term (decimal point assumed)
63	Ephemeris type
65-68	Element number
69	Checksum (Modulo 10) (Letters, blanks, periods, plus signs = 0; minus signs = 1)

Line 2

Column	*Description*
01	Line Number of Element Data
03-07	Satellite Number
09-16	Inclination [Degrees]
18-25	Right Ascension of the Ascending Node [Degrees]
27-33	Eccentricity (decimal point assumed)
35-42	Argument of Perigee [Degrees]
44-51	Mean Anomaly [Degrees]
53-63	Mean Motion [Revs per day]
64-68	Revolution number at epoch [Revs]
69	Checksum (Modulo 10)

Table F.2. Format of the *parameters.dat* file used by ORBLITZ.

Line no.	*Parameter*	Description	Units/values
1	*IYEAR*	Epoch Year	2000
	IMONTH	Month	02
	IDAY	Day	06
	IHOUR	Hour	0
	IMIN	Minute	0
	FSEC	Second	0.0
2	*ICOORD*	Co-ordinate type 0 : Osculating Kepler 1: ECI mean-of-J2000	
3 (*ICOORD*=0)	*a*	Semi-major axis	km
	e	Eccentricity	dimensionless
	i	Inclination	degrees
	Ω	Longitude of asc. node	degrees
	ω	Argument of perigee	degrees
	ν	True anomly	degrees
3 (*ICOORD*=1)	*x, y, z, vx, vy ,vz*	Epoch position , velocity	km, km.s^{-1}
4	*L*	Harmonics degree	$0 \leq L \leq 360$
	M	Harmonics order	$0 \leq M \leq 360$
	NSTP	Number of integration steps	14400
5	*ISUN*	Sun third body	0/1 (N/Y)
	IMOON	Moon third body	0/1 (N/Y)
	IDRAG	Drag perturbation	0/1 (N/Y)
	IDENS	Density model	1/2/3
	ISRP	Solar radiation pressure	0/1
6	*RELERR*	(Integration) Relative error	1.0e-8
	ABSERROR	(Integration) Absolute error	1.0e-8
7	*CDRAG*	Coefficient of drag	2.0
	AREAD	Drag surface area	0.35e-6 km^2
	AREAS	SRP surface area	0.35e-6 km^2
	SATMASS	Satellite mass	62 kg
	CSRP	SRP value	4.56e-3
	CR	Solar reflectivity constant	2.0
8	*GS*	Sun gravitational parameter	0.13271244e12 km^3.s^{-2}
	GE	Earth gravitational parameter	3.9860045e5 km^3.s^{-2}
	GM	Moon gravitational parameter	0.490279e4 km^3.s^{-2}
	RE	Earth equatorial radius	6378.140 km
	RATE	Earth rotation rate	4.178074216e-3 deg.s^{-1}
	ELLIP	Earth ellipticity	0.8182e-1

Table F.3. Example of an input file for ORBLITZ. Epoch 6 April 2000, 00.00UTC. Values in the same line are separated by blank spaces; lines are separated by carriage returns.

Line no	*Parameters*
1	2000 2 6 0 0 0
2	2
3	-611.3596933947160D0 6818.3129602830699D0 1885.99916780365D0
4	0.7058965616152D0 1.9564987352054D0 -7.2181300644107D0
5	70 70 0 14401
6	0 1 1 1 1 2 1 0 0 0
7	1.0D-10 1.0D-10
8	2.0 0.35D-6 0.35D-6 62.0D0 4.56D-3 2.0 0.13271244D12 3.9860045D5 0.490279D4 6378.14D0 4.178074216D-3 0.8182D-1

Table F.4. Format of the *Solar.dat* file

Column no	*Description*
1	Day of year
2	Julian day
3	F10.7 Solar flux (Solar Flux Units)
4	F10.7A. 81-day mean Solar flux value centred on day of interest
5-12	Ap magnetic index for each 3-hour period
13	Mean Ap value for 8x3h intervals

		Daily Solar Flux (F10.7cm) and Magnetic Index (Ap) values for 2000.										
DayofYR	Julian Day	F10.7	F10.7 81Mn	Ap3	Ap6	Ap9	Ap12	Ap15	Ap18	Ap21	Ap24	Ap Mn
1	2451545	125.6	160.611	56	39	27	18	32	15	32	22	30.13
2	2451546	128.5	160.268	15	18	18	18	12	18	18	15	16.50
3	2451547	128.7	159.963	18	15	12	12	9	9	15	6	12.00
4	2451548	130.3	159.632	9	9	9	15	18	12	9	22	12.88
5	2451549	132.0	159.305	27	18	18	18	9	15	22	27	19.25
6	2451550	140.0	159.166	12	18	7	18	32	32	15	18	19.00
7	2451551	144.8	159.165	18	15	5	7	7	9	12	7	10.00
8	2451552	149.6	158.771	7	3	5	6	6	9	3	0	4.88
9	2451553	155.3	158.551	5	5	0	0	2	2	2	6	2.75
10	2451554	157.8	158.449	5	7	3	3	4	6	7	15	6.25
11	2451555	171.8	158.306	15	9	6	9	22	22	56	56	24.38
12	2451556	189.3	158.400	22	15	12	7	4	7	9	7	10.38
13	2451557	195.4	158.811	7	9	9	15	9	12	4	6	8.88
14	2451558	194.7	159.360	15	9	4	3	6	9	9	6	7.63
15	2451559	203.9	160.184	7	7	5	3	7	5	5	6	5.63
16	2451560	201.0	161.062	5	4	5	5	6	6	6	7	5.50
17	2451561	190.1	161.966	5	2	4	2	3	2	3	0	2.63
18	2451562	188.4	162.809	2	2	3	3	4	5	3	3	3.13
19	2451563	172.9	163.584	3	2	3	2	3	5	7	15	5.00
20	2451564	165.3	164.428	9	6	9	7	15	9	22	6	10.38
21	2451565	154.3	165.102	3	0	0	2	3	2	0	2	1.50
22	2451566	145.8	165.663	5	9	9	15	18	18	56	48	22.25
23	2451567	136.1	166.102	94	67	7	22	22	12	4	4	29.00
24	2451568	136.3	166.757	6	12	27	18	9	9	9	15	13.13
25	2451569	133.1	167.318	7	12	7	5	4	5	9	6	6.88
26	2451570	136.4	167.691	7	15	7	5	4	4	5	15	7.75
27	2451571	128.4	167.904	18	9	6	7	15	15	32	32	16.75
28	2451572	122.2	167.954	48	48	32	22	32	22	18	32	31.75
29	2451573	123.9	167.959	32	27	32	27	32	39	32	22	30.38
30	2451574	128.7	167.937	12	12	18	7	18	15	22	15	14.88
31	2451575	134.5	167.823	18	9	12	9	9	12	7	7	10.38
32	2451576	134.1	167.712	9	5	7	3	15	7	9	12	8.38
33	2451577	140.2	167.574	9	5	3	6	12	18	7	7	8.38
34	2451578	149.7	167.567	4	4	9	5	15	12	12	22	10.38
35	2451579	162.7	167.689	7	5	7	3	4	4	3	7	5.00
36	2451580	163.1	167.926	4	2	2	4	4	15	32	32	11.88
37	2451581	172.8	168.372	39	48	22	32	27	18	39	48	34.13
38	2451582	177.0	169.117	56	22	22	27	39	27	27	27	30.88
39	2451583	169.0	169.967	22	18	6	12	15	15	22	12	15.25
40	2451584	170.8	171.159	6	15	12	5	15	22	7	6	11.00
41	2451585	171.1	172.456	12	9	15	6	7	9	7	18	10.38
42	2451586	165.8	173.640	15	32	12	12	9	15	12	32	17.38
43	2451587	159.1	174.728	80	80	80	11	67	32	18	15	47.88
44	2451588	155.9	175.648	18	7	12	22	18	18	9	12	14.50
45	2451589	154.7	176.624	22	32	27	32	56	39	27	27	32.75
46	2451590	152.2	177.504	27	27	9	6	9	7	22	32	17.38
47	2451591	156.3	178.239	12	9	4	3	7	9	7	5	7.00
48	2451592	164.4	179.013	3	3	4	12	9	6	6	3	5.75
49	2451593	137.8	179.690	0	2	2	2	2	0	2	0	1.25
50	2451594	141.5	180.541	0	0	5	7	3	3	3	3	3.00
51	2451595	149.9	181.333	2	3	6	4	2	0	4	22	5.38
52	2451596	148.7	181.912	22	39	15	12	22	39	12	7	21.00
53	2451597	168.6	182.232	7	9	3	3	7	6	4	6	5.63
54	2451598	181.2	182.372	7	3	6	15	27	18	4	6	10.75
55	2451599	188.3	182.372	15	39	22	39	27	27	32	39	30.00
56	2451600	206.2	182.057	22	32	27	18	22	18	9	15	20.38
57	2451601	210.6	181.745	15	12	15	18	7	15	27	18	15.88
58	2451602	222.9	181.652	22	7	9	15	18	15	9	9	13.00
59	2451603	214.7	181.512	15	27	15	15	27	12	7	9	15.88
60	2451604	215.1	181.582	3	5	9	15	9	5	4	5	6.88

DayofYR	Julian Day	F10.7	F10.7 81Mn	Ap3	Ap6	Ap9	Ap12	Ap15	Ap18	Ap21	Ap24	Ap Mn
61	2451605	228.7	181.790	9	22	32	22	18	18	15	32	21.00
62	2451606	209.6	182.029	39	18	6	4	7	4	3	7	11.00
63	2451607	200.4	182.263	4	2	2	4	7	5	9	6	4.88
64	2451608	197.0	182.632	0	0	2	3	6	7	3	3	3.00
65	2451609	216.8	182.980	2	7	3	4	5	6	7	15	6.13
66	2451610	219.1	183.311	6	9	15	15	12	15	9	15	12.00
67	2451611	218.5	183.589	15	22	18	15	15	15	12	18	16.25
68	2451612	211.8	183.996	9	12	6	15	15	27	22	7	14.13
69	2451613	203.0	184.570	9	3	2	3	6	3	4	4	4.25
70	2451614	200.7	185.283	4	3	5	7	9	9	7	27	8.88
71	2451615	200.6	186.021	22	18	12	6	22	7	5	9	12.63
72	2451616	200.8	186.870	12	22	27	32	27	15	7	9	18.88
73	2451617	186.0	187.776	12	5	2	0	0	0	6	6	3.88
74	2451618	180.6	188.604	7	6	4	6	4	5	6	6	5.50
75	2451619	175.9	189.279	3	0	2	2	2	3	2	0	1.75
76	2451620	182.5	189.641	0	0	0	2	2	3	3	4	1.75
77	2451621	190.6	189.921	7	5	6	6	6	2	2	0	4.25
78	2451622	193.0	190.082	0	2	2	6	6	7	15	6	5.50
79	2451623	206.5	190.088	7	15	7	6	7	6	6	4	7.25
80	2451624	208.7	190.124	4	2	5	15	12	3	2	3	5.75
81	2451625	228.9	189.994	2	2	5	3	6	6	5	0	3.63
82	2451626	232.2	189.801	6	9	12	7	15	18	18	12	12.13
83	2451627	222.7	189.482	15	18	12	15	22	18	5	5	13.75
84	2451628	217.7	189.210	9	9	5	15	22	18	5	6	11.13
85	2451629	204.1	188.920	7	9	9	6	5	15	12	2	8.13
86	2451630	210.4	188.607	2	0	3	3	3	6	5	5	3.38
87	2451631	204.1	188.378	4	5	4	3	5	3	3	4	3.88
88	2451632	200.3	188.174	6	6	5	5	3	3	2	0	3.75
89	2451633	208.3	188.029	2	2	3	4	4	4	27	32	9.75
90	2451634	205.1	188.578	15	9	7	4	9	9	32	15	12.50
91	2451635	225.1	189.063	18	39	22	22	32	12	18	22	23.13
92	2451636	222.7	189.606	12	9	6	7	7	18	27	18	13.00
93	2451637	219.3	190.500	27	22	18	12	15	5	7	15	15.13
94	2451638	215.5	191.341	12	12	6	6	7	9	5	15	9.00
95	2451639	206.9	192.179	48	22	9	5	22	15	39	15	21.88
96	2451640	194.7	193.109	27	32	6	3	3	6	5	4	10.75
97	2451641	178.1	193.863	6	32	12	9	18	11	36	36	20.00
98	2451642	175.4	194.451	0	80	80	27	27	32	22	22	36.25
99	2451643	182.5	194.909	9	9	15	15	7	6	9	12	10.25
100	2451644	176.9	195.359	9	15	9	6	18	15	22	22	14.50
101	2451645	178.6	195.638	22	27	22	18	15	15	12	18	18.63
102	2451646	182.4	195.535	6	15	18	6	7	6	9	5	9.00
103	2451647	173.9	195.534	9	12	9	2	4	6	5	6	6.63
104	2451648	165.0	195.460	9	22	7	4	3	2	0	0	5.88
105	2451649	166.3	195.221	0	2	2	3	2	3	5	2	2.38
106	2451650	164.9	194.679	2	4	4	6	5	6	9	12	6.00
107	2451651	160.2	194.034	18	32	32	32	32	12	9	7	21.75
108	2451652	159.2	193.323	15	15	27	12	4	7	5	7	11.50
109	2451653	161.8	192.607	5	9	4	2	3	3	12	6	5.50
110	2451654	169.2	191.967	15	27	6	6	15	15	6	6	12.00
111	2451655	182.4	191.455	15	18	18	7	15	15	9	6	12.88
112	2451656	189.2	190.866	12	5	3	22	12	12	6	5	9.63
113	2451657	204.1	190.767	4	6	7	7	6	3	4	4	5.13
114	2451658	208.4	190.580	4	3	9	7	5	7	5	7	5.88
115	2451659	208.1	190.509	6	18	27	27	56	15	7	9	20.63
116	2451660	205.1	190.511	6	2	3	9	6	6	7	4	5.38
117	2451661	192.4	190.627	0	0	4	3	3	0	3	3	2.00
118	2451662	186.0	190.568	15	6	7	12	9	15	12	27	12.88
119	2451663	186.0	190.409	39	18	15	9	7	7	9	9	14.13
120	2451664	177.5	190.013	12	12	6	9	15	12	12	22	12.50
121	2451665	172.0	189.726	15	32	5	4	7	9	15	6	11.63
122	2451666	160.1	189.283	6	22	12	15	15	18	18	15	15.13

DayofYR	Julian Day	F10.7	F10.7 81Mn	Ap3	Ap6	Ap9	Ap12	Ap15	Ap18	Ap21	Ap24	Ap Mn
123	2451667	155.3	188.874	18	7	7	32	39	22	18	22	20.63
124	2451668	139.6	188.665	9	9	12	5	7	27	48	22	17.38
125	2451669	136.8	188.533	5	5	6	9	6	6	7	7	6.38
126	2451670	132.1	188.591	7	7	18	7	12	5	7	15	9.75
127	2451671	129.1	188.511	18	18	6	6	9	7	6	15	10.63
128	2451672	133.4	188.454	7	7	6	4	4	2	6	4	5.00
129	2451673	139.6	188.373	3	0	3	3	4	4	6	7	3.75
130	2451674	152.5	188.079	5	9	4	6	6	12	12	9	7.88
131	2451675	182.8	187.891	12	9	4	3	5	4	4	5	5.75
132	2451676	181.3	187.515	5	5	5	2	5	2	3	7	4.25
133	2451677	194.4	187.062	7	18	27	15	7	4	12	27	14.63
134	2451678	222.0	186.595	27	7	7	9	18	22	15	7	14.00
135	2451679	237.6	186.088	22	9	5	5	6	5	12	6	8.75
136	2451680	249.9	185.771	32	12	9	12	7	9	6	9	12.00
137	2451681	264.5	185.633	12	32	15	15	12	12	15	15	16.00
138	2451682	268.1	185.712	80	80	18	9	6	4	12	15	28.00
139	2451683	258.8	185.783	18	9	6	6	4	3	3	5	6.75
140	2451684	260.4	185.616	7	7	7	9	9	6	5	5	6.88
141	2451685	251.6	185.471	4	3	4	3	4	4	9	5	4.50
142	2451686	238.0	185.356	6	7	6	4	4	5	4	7	5.38
143	2451687	220.3	185.179	5	9	7	12	7	5	9	7	7.63
144	2451688	209.5	185.028	6	9	9	6	7	18	11	67	16.63
145	2451689	194.3	185.012	7	79	80	67	48	48	80	32	55.13
146	2451690	177.4	185.111	39	39	27	27	15	22	27	27	27.88
147	2451691	172.4	185.296	15	18	18	18	9	22	18	2	15.00
148	2451692	166.2	185.702	7	6	5	6	9	12	9	12	8.25
149	2451693	160.2	186.409	5	6	7	9	9	12	12	12	9.00
150	2451694	153.1	187.099	7	15	9	9	22	39	48	39	23.50
151	2451695	150.5	188.117	32	12	32	18	22	22	15	22	21.88
152	2451696	158.7	188.938	12	27	9	4	4	4	6	12	9.75
153	2451697	152.3	190.595	15	15	12	3	6	4	3	9	8.38
154	2451698	192.7	191.028	6	7	9	4	4	4	7	7	6.00
155	2451699	170.7	191.055	12	7	9	18	15	6	15	7	11.13
156	2451700	174.7	191.201	4	6	12	2	3	15	32	22	12.00
157	2451701	176.1	191.457	27	15	27	18	39	15	27	27	24.38
158	2451702	192.0	191.987	15	9	9	12	18	48	6	5	15.25
159	2451703	185.8	193.017	6	5	9	12	12	12	12	22	11.25
160	2451704	179.9	193.895	12	22	32	94	32	94	80	48	51.75
161	2451705	174.1	194.915	3	5	5	9	5	4	2	9	5.25
162	2451706	185.1	195.976	22	22	22	32	27	18	15	12	21.25
163	2451707	192.6	197.182	7	15	12	39	32	48	39	6	24.75
164	2451708	198.7	198.023	12	12	18	5	22	22	15	15	15.13
165	2451709	205.5	199.150	6	9	9	12	18	7	6	12	9.88
166	2451710	206.9	200.021	22	7	27	9	32	39	56	39	28.88
167	2451711	208.9	200.606	67	12	12	12	22	22	32	7	23.25
168	2451712	203.8	201.073	9	4	4	4	4	3	3	6	4.63
169	2451713	199.4	201.430	5	3	4	4	7	9	6	7	5.63
170	2451714	193.7	201.654	5	2	3	6	7	18	27	15	10.38
171	2451715	184.2	201.678	12	15	2	3	2	7	6	5	6.50
172	2451716	189.7	201.307	9	6	7	7	9	4	4	4	6.25
173	2451717	194.2	200.973	4	3	3	4	5	6	6	18	6.13
174	2451718	185.6	200.494	22	7	7	15	9	6	18	5	11.13
175	2451719	181.0	199.723	9	22	7	6	56	32	56	27	26.88
176	2451720	173.9	198.761	39	27	27	9	5	4	4	7	15.25
177	2451721	180.9	197.704	5	3	3	3	3	3	6	18	5.50
178	2451722	183.4	196.561	12	18	32	48	56	32	80	39	39.63
179	2451723	184.6	195.384	32	12	15	9	22	15	15	22	17.75
180	2451724	181.2	194.370	15	15	5	5	7	7	7	15	9.50
181	2451725	168.8	193.477	18	9	12	4	6	5	3	5	7.75
182	2451726	165.0	192.676	2	2	2	5	4	5	9	6	4.38
183	2451727	169.2	192.118	9	4	9	5	4	3	12	9	6.88
184	2451728	167.9	191.801	4	6	4	3	4	5	4	4	4.25

DayofYR	Julian Day	F10.7	F10.7 81Mn	Ap3	Ap6	Ap9	Ap12	Ap15	Ap18	Ap21	Ap24	Ap Mn
185	2451729	161.5	191.574	7	6	5	7	12	6	7	12	7.75
186	2451730	163.7	191.574	9	7	3	7	18	7	7	6	8.00
187	2451731	174.4	191.837	5	6	9	12	18	15	6	3	9.25
188	2451732	180.1	192.055	3	5	5	4	7	6	7	5	5.25
189	2451733	193.5	192.241	7	5	4	5	4	4	6	6	5.13
190	2451734	217.1	192.405	6	7	3	6	9	9	6	2	6.00
191	2451735	218.4	192.499	3	4	6	6	6	5	6	9	5.63
192	2451736	252.7	192.566	6	9	27	18	22	22	39	15	19.75
193	2451737	249.7	192.520	18	32	18	32	56	32	32	48	33.50
194	2451738	325.1	192.461	22	12	5	9	3	6	6	6	8.63
195	2451739	239.6	191.817	4	7	9	67	32	94	12	15	30.00
196	2451740	210.6	191.363	15	15	18	27	27	54	11	39	25.75
197	2451741	220.1	190.891	15	22	39	32	7	0	0	0	14.38
198	2451742	226.1	190.450	79	80	32	39	39	15	7	6	37.13
199	2451743	235.8	189.977	15	12	9	9	9	5	4	5	8.50
200	2451744	270.5	189.701	6	9	9	5	15	15	15	18	11.50
201	2451745	258.0	189.538	9	4	3	4	7	32	22	32	14.13
202	2451746	261.1	189.462	39	80	56	48	27	9	18	15	36.50
203	2451747	259.0	189.228	12	7	4	5	9	5	5	6	6.63
204	2451748	259.0	188.837	6	9	9	18	9	22	15	7	11.88
205	2451749	224.3	188.324	7	9	5	6	22	39	80	18	23.25
206	2451750	232.0	187.729	9	9	5	2	3	2	2	6	4.75
207	2451751	208.2	187.323	5	5	3	4	6	7	5	7	5.25
208	2451752	180.1	187.009	7	9	18	12	22	12	32	39	18.88
209	2451753	167.4	186.737	22	7	3	2	3	4	6	9	7.00
210	2451754	162.7	186.449	12	15	39	32	67	67	18	6	32.00
211	2451755	157.9	186.107	27	22	22	67	39	18	9	12	27.00
212	2451756	154.5	185.727	12	15	4	5	9	6	7	7	8.13
213	2451757	152.4	185.151	5	7	18	7	12	15	56	48	21.00
214	2451758	153.9	184.450	9	7	6	9	7	22	15	18	11.63
215	2451759	155.1	183.823	18	15	7	6	5	9	15	9	10.50
216	2451760	158.8	183.260	9	9	7	9	7	12	12	7	9.00
217	2451761	158.7	182.999	18	15	18	18	15	22	18	12	17.00
218	2451762	163.2	182.757	9	15	48	39	18	27	15	27	24.75
219	2451763	170.8	182.672	27	32	9	9	15	12	9	18	16.38
220	2451764	171.6	182.655	5	4	6	12	12	5	7	7	7.25
221	2451765	175.6	182.954	6	5	7	5	9	6	7	7	6.50
222	2451766	187.2	183.441	6	6	4	4	4	4	4	9	5.13
223	2451767	185.9	184.028	4	12	39	27	32	15	18	56	25.38
224	2451768	192.3	184.729	67	67	48	32	32	12	48	67	46.63
225	2451769	194.3	185.533	48	54	79	79	54	54	94	22	60.50
226	2451770	190.9	186.328	32	67	15	6	9	6	6	12	19.13
227	2451771	194.3	187.085	3	4	3	4	9	18	22	32	11.88
228	2451772	198.9	187.724	15	22	4	6	5	5	6	5	8.50
229	2451773	190.3	188.268	7	7	9	5	7	5	6	7	6.63
230	2451774	181.5	188.415	7	12	6	7	6	4	5	5	6.50
231	2451775	173.6	188.243	6	5	2	2	2	3	3	3	3.25
232	2451776	160.8	187.928	4	2	2	3	4	9	5	4	4.13
233	2451777	156.0	187.212	0	2	0	6	3	9	7	4	3.88
234	2451778	154.9	186.629	7	18	6	12	6	6	7	22	10.50
235	2451779	147.5	185.139	5	5	3	0	2	2	0	3	2.50
236	2451780	139.9	184.560	2	0	3	7	9	18	9	5	6.63
237	2451781	133.5	184.237	9	15	12	7	6	5	4	3	7.63
238	2451782	136.0	183.671	0	4	2	2	3	3	6	4	3.00
239	2451783	139.9	182.839	4	5	6	5	6	5	3	3	4.63
240	2451784	153.2	181.857	7	4	3	4	12	7	7	9	6.63
241	2451785	163.2	180.371	9	5	7	18	27	48	56	48	27.25
242	2451786	166.5	178.937	67	39	48	27	15	32	39	15	35.25
243	2451787	167.9	177.449	22	15	7	12	9	9	7	18	12.38
244	2451788	165.9	176.129	18	12	9	18	15	12	7	18	13.63
245	2451789	160.5	174.945	18	12	22	18	12	12	22	12	16.00
246	2451790	156.7	174.249	27	22	32	32	27	27	9	9	23.13

DayofYR	Julian Day	F10.7	F10.7 81Mn	Ap3	Ap6	Ap9	Ap12	Ap15	Ap18	Ap21	Ap24	Ap Mn
247	2451791	156.7	173.399	3	7	3	3	5	6	15	12	6.75
248	2451792	173.6	172.812	5	4	6	6	12	15	67	27	17.75
249	2451793	183.1	172.565	5	6	5	4	5	9	15	9	7.25
250	2451794	181.5	172.389	5	3	5	2	9	27	22	27	12.50
251	2451795	175.8	172.233	15	12	15	12	12	18	18	18	15.00
252	2451796	165.7	172.216	15	7	12	22	22	22	15	22	17.13
253	2451797	153.0	172.274	9	7	6	5	7	4	2	0	5.00
254	2451798	142.5	172.324	0	2	3	6	4	5	6	5	3.88
255	2451799	136.7	172.382	0	0	2	4	5	9	5	6	3.88
256	2451800	134.2	172.500	7	18	12	27	32	15	32	27	21.25
257	2451801	134.8	172.484	27	22	6	3	5	5	4	6	9.75
258	2451802	152.5	172.524	4	7	6	3	3	4	4	4	4.38
259	2451803	161.1	172.594	2	12	3	4	4	6	18	48	12.13
260	2451804	176.4	172.629	22	15	12	18	15	22	32	94	28.75
261	2451805	183.2	172.728	39	27	9	15	27	39	56	36	31.00
262	2451806	205.7	172.837	79	67	48	80	80	80	15	15	58.00
263	2451807	208.8	172.883	15	15	15	48	80	27	15	22	29.63
264	2451808	213.1	172.939	22	22	4	12	18	7	6	6	12.13
265	2451809	226.7	173.048	7	12	7	15	12	6	7	6	9.00
266	2451810	233.8	173.034	12	9	6	5	6	5	6	3	6.50
267	2451811	226.7	173.090	7	15	6	4	6	6	5	4	6.63
268	2451812	225.8	173.055	2	5	3	4	5	15	48	18	12.50
269	2451813	226.8	172.862	12	12	15	18	18	27	22	27	18.88
270	2451814	224.7	172.674	39	27	22	22	32	15	15	18	23.75
271	2451815	205.5	172.615	12	12	18	12	9	9	7	12	11.38
272	2451816	203.0	172.565	9	22	6	18	18	12	4	3	11.50
273	2451817	192.6	172.591	7	9	3	9	7	6	6	6	6.63
274	2451818	194.0	172.523	18	27	56	48	67	48	48	94	50.75
275	2451819	201.9	172.422	27	22	18	7	6	12	6	4	12.75
276	2451820	202.9	172.374	2	4	5	6	9	32	9	12	9.88
277	2451821	192.1	172.383	32	39	48	27	56	27	5	7	30.13
278	2451822	184.1	172.528	7	18	48	48	94	67	54	67	50.38
279	2451823	173.7	172.616	56	11	79	54	79	11	94	48	54.00
280	2451824	157.9	172.748	12	3	3	2	4	2	4	3	4.13
281	2451825	155.3	172.826	0	4	5	4	9	6	6	0	4.25
282	2451826	148.6	172.944	0	2	2	2	2	2	3	7	2.50
283	2451827	140.4	172.995	3	2	2	2	4	4	6	7	3.75
284	2451828	139.1	173.016	7	9	15	9	6	7	4	7	8.00
285	2451829	150.8	173.199	27	39	9	6	12	5	18	4	15.00
286	2451830	161.9	173.560	9	4	4	5	6	4	4	15	6.38
287	2451831	167.2	174.089	80	11	15	9	27	27	15	6	23.75
288	2451832	162.3	174.521	22	39	67	48	48	56	32	48	45.00
289	2451833	160.1	174.806	7	15	6	6	7	6	7	7	7.63
290	2451834	159.8	174.976	32	7	5	5	6	12	7	7	10.13
291	2451835	153.0	175.038	15	15	7	7	7	7	15	12	10.63
292	2451836	149.9	175.215	15	9	6	7	12	6	6	12	9.13
293	2451837	156.5	175.428	12	12	9	7	15	5	5	7	9.00
294	2451838	159.3	175.843	3	4	2	3	2	3	4	2	2.88
295	2451839	156.5	176.291	2	0	2	3	6	5	4	2	3.00
296	2451840	158.6	176.604	3	3	7	15	18	39	32	12	16.13
297	2451841	164.8	176.905	27	18	22	22	9	6	7	9	15.00
298	2451842	157.5	177.061	9	6	9	18	12	5	6	6	8.88
299	2451843	162.0	176.941	2	3	7	7	12	4	6	7	6.00
300	2451844	168.9	176.646	12	9	7	7	7	4	6	9	7.63
301	2451845	173.7	176.201	9	2	5	5	4	4	3	4	4.50
302	2451846	179.7	175.602	3	3	9	39	27	9	15	56	20.13
303	2451847	184.5	174.688	80	80	22	27	15	18	18	12	34.00
304	2451848	191.0	173.874	48	22	12	18	6	7	6	4	15.38
305	2451849	190.5	172.973	12	12	6	9	7	27	12	18	12.88
306	2451850	201.2	171.979	18	9	7	2	4	4	5	9	7.25
307	2451851	193.2	171.073	12	3	2	2	4	3	3	3	4.00
308	2451852	195.5	170.461	0	0	2	2	4	4	7	7	3.25

DayofYR	Julian Day	F10.7	F10.7 81Mn	Ap3	Ap6	Ap9	Ap12	Ap15	Ap18	Ap21	Ap24	Ap Mn
309	2451853	191.4	169.926	15	48	27	27	22	27	22	22	26.25
310	2451854	183.1	169.409	22	15	7	3	15	18	18	18	14.50
311	2451855	174.9	168.990	18	22	27	48	56	67	32	67	42.13
312	2451856	176.6	168.821	80	11	56	56	22	12	27	7	33.88
313	2451857	169.5	168.689	7	22	39	32	18	12	6	9	18.13
314	2451858	163.0	168.716	12	7	6	4	15	18	15	27	13.00
315	2451859	150.4	168.645	27	27	80	94	56	18	15	15	41.50
316	2451860	146.6	168.424	9	18	6	9	18	27	27	15	16.13
317	2451861	143.6	168.202	15	27	27	22	18	27	9	12	19.63
318	2451862	140.6	168.137	6	15	5	12	7	7	9	9	8.75
319	2451863	145.4	168.098	7	12	3	3	3	3	5	6	5.25
320	2451864	143.2	168.206	4	4	4	3	4	2	7	4	4.00
321	2451865	150.7	168.493	3	0	3	0	2	0	4	9	2.63
322	2451866	159.6	168.785	5	2	3	3	3	3	2	0	2.63
323	2451867	172.9	169.113	0	0	0	2	5	5	12	15	4.88
324	2451868	170.7	169.549	6	9	7	7	5	6	4	7	6.38
325	2451869	169.6	169.851	5	6	12	7	6	15	9	4	8.00
326	2451870	180.9	0.000	15	7	7	6	9	9	12	9	9.25
327	2451871	190.1	0.000	9	6	5	9	12	12	6	6	8.13
328	2451872	200.1	0.000	7	12	3	6	6	6	6	0	5.75
329	2451873	192.1	0.000	2	9	6	12	6	15	18	22	11.25
330	2451874	197.0	0.000	15	12	3	3	2	3	9	5	6.50
331	2451875	197.0	0.000	5	6	22	12	27	22	67	67	28.50
332	2451876	186.6	0.000	94	80	67	39	27	12	27	12	44.75
333	2451877	190.3	0.000	15	32	48	32	39	22	32	27	30.88
334	2451878	183.2	0.000	94	11	11	39	48	18	9	15	30.63
335	2451879	187.0	0.000	6	7	6	6	5	6	4	7	5.88
336	2451880	179.3	0.000	7	9	3	6	7	9	3	2	5.75
337	2451881	162.3	0.000	0	0	3	3	5	6	4	4	3.13
338	2451882	158.9	0.000	4	7	15	7	15	15	15	5	10.38
339	2451883	147.6	0.000	12	15	12	7	6	4	5	12	9.13
340	2451884	142.7	0.000	5	7	4	6	7	4	2	2	4.63
341	2451885	136.9	0.000	2	4	6	6	5	15	9	12	7.38
342	2451886	139.9	0.000	15	15	18	12	18	7	9	27	15.13
343	2451887	134.1	0.000	22	18	15	15	27	18	15	18	18.50
344	2451888	130.7	0.000	15	22	18	12	9	18	18	32	18.00
345	2451889	142.1	0.000	18	15	9	7	7	7	12	12	10.88
346	2451890	139.2	0.000	15	12	9	6	6	3	5	12	8.50
347	2451891	145.2	0.000	4	5	3	4	6	5	9	5	5.13
348	2451892	159.5	0.000	12	6	3	4	3	2	3	5	4.75
349	2451893	176.5	0.000	2	2	3	3	3	2	2	5	2.75
350	2451894	181.9	0.000	3	0	2	3	3	2	3	2	2.25
351	2451895	184.4	0.000	0	0	2	2	4	5	6	5	3.00
352	2451896	190.4	0.000	7	9	4	5	15	9	18	4	8.88
353	2451897	191.6	0.000	6	12	7	9	6	12	12	7	8.88
354	2451898	192.2	0.000	7	6	3	7	5	5	5	2	5.00
355	2451899	194.8	0.000	0	0	3	5	3	3	5	3	2.75
356	2451900	188.2	0.000	2	0	2	6	6	6	3	5	3.75
357	2451901	183.8	0.000	2	5	4	3	3	4	6	22	6.13
358	2451902	184.7	0.000	32	67	27	9	12	9	7	7	21.25
359	2451903	186.7	0.000	6	15	4	3	3	3	5	5	5.50
360	2451904	180.9	0.000	7	4	3	3	15	9	2	9	6.50
361	2451905	182.6	0.000	6	5	4	4	2	4	7	12	5.50
362	2451906	181.4	0.000	7	5	4	4	9	18	9	6	7.75
363	2451907	179.3	0.000	9	4	5	4	15	5	4	2	6.00
364	2451908	175.5	0.000	4	18	6	4	2	4	5	7	6.25
365	2451909	176.1	0.000	5	3	3	4	4	3	0	4	3.25
366	2451910	163.9	0.000	5	0	2	4	3	0	0	2	2.00

Appendix F. Solar data

Appendix G

Section of Satellite State Vector

(Supplied on CD-ROM because of large file size)

The following pages contain the first twenty-four hour section of the position and velocity calculated for the SUNSAT micro-satellite using *Orblitz*. Co-ordinates are in Earth Centre Inertial (mean equator and equinox of J2000). For reference, the corresponding section of SLR-derived reference orbit is given. The last two columns contain the absolute error between the calculated and reference orbits. Position and velocity components with subscript **orb** denote the output from the calculated orbit (*Orblitz*) and those with subscript **slr** denote the SLR-derived reference orbit components.

Appendix H

Software Listing for SATDECAY

(Supplied on CD-ROM because of large file size)

Appendix I

Various Files Used in Drag and Decay Analysis

Table I-1. Iridium-85 Drag analysis results

CD	Position error	Velocity Error
3.0	150	0.165
2.8	164	0.181
3.8	91	0.101
4.0	76.9	0.085
4.4	47.9	0.050
4.85	15.31	0.016
4.95	8.06	0.008
5.0	**4.4**	**0.004**
5.15	6.45	0.007
5.3	17.34	0.020

Table I-2. Starshine-2 Drag analysis

CD	Pos	Velocity
1.9894	170.0	0.20
2.0822	65.9	0.08
2.0955	51.0	0.06
2.1220	21.1	0.02
2.1300	12.0	0.01
2.1353	6.1	0.01
2.1366	4.7	0.0055
2.1370	4.22	0.0050
2.1375	**3.64**	**0.0043**
2.1485	8.8	0.01
2.1883	53.8	0.06
2.3209	204.0	0.2

Table I-3. Sunsat Drag analysis

CD	Position error	Velocity Error
2.0	3.614	.0038
2.2	2.965	0.003
3.0	0.369	3.834e-4
3.08	0.116	1.52e-4
3.1	**0.063**	**1.254e-4**
3.15	0.129	1.96e-4
3.26	0.4804	5.43e-4
3.27	0.513	5.77e-4

Input file format used in orbit decay calculations

```
&DATA
TITLE =  'Header to be printed in output file'
XJ2 =      J2 harmonic (Earth oblateness  factor, 1.08263D-3).
XJ3 =      J3 harmonic  (-2.54D-6).
XJ4 =      J4 harmonic (-1.58D-6).
REQ =      Earth equatorial radius ( 6378.14D0 km)
FLATN = Earth flattening (298.257D0)
GM =       Earth gravitational parameter (398600.5D0  )
WS =       Earth rotation rate (7.2921151467D-5)
TOL =      Integration error (.0000001D0)
N1 =       Lagrange quadrature degree (10)
N2 =       Lagrange quadrature order (10).
NOCIR = Switch over to circular option (0 =yes, 1 keeps integrating elliptical orbit)
EBND =  Lower eccentricity limit for elliptical orbits ( 0.0005D0)
CUTOFF = Minimum integration stepsize (days) below which program  terminates (1.0D0)
APMIN =  Minimum altitude (km) for decay (6378.0D0)
IOSC =   Type of input orbital elements ( 0 = osculating, 1 = mean)
ICART = Input coordinate type (0 = orbital elements, 1 = cartesian)
EL =  Comma separted orb. elements :  a (km), e , i, RAAN, w, M.   (all angles in degrees)
R = Comma separated initial ECI position ( X,  Y,  Z) km
V = Comma separated initial ECI velocity ( Vx,  Vy, Vz ) km
AREA = Satellite cross-sectional area (m^2)
CD =       Drag coefficient (dimensionless)
YMASS = Satellite mass (kg)
XMDOT1 = mass rate of change # 1. (kg.day^-1).  Not used in simulation (0.0D0)
XMDOT2 = mass rate of change # 2. (kg.day^-1).  Not used in simulation (0.0D0)
XMDOT3 = mass rate of change # 3. (kg.day^-1).  Not used in simulation (0.0D0)
TMS1 = Time to start using XMDOT1 (0.0D0) (days)
TME1 = Time to stop using XMDOT1 (10000.0D0) (days)
TMS2 = Time to start using XMDOT2 (0.0D0) (days)
TME2 = Time to stop using XMDOT2 (10000.0D0) (days)
TMS3 = Time to start using XMDOT3 (0.0D0) (days)
TME3 = Time to stop using XMDOT3 (10000.0D0) (days)
CDATE = Initial calender date ( month, Day, Year) ( e.g. 11, 6,1998)
UT = Initial Universal Time (hh, mm, s) ( e.g. 16, 11, 25)
STTP1 =  Maximum simulation (days) 2000.0D0
DELSAV = Initial integration step size (days)
A1 = User-define altitude of interst # 1 (km)
A3 = User-define altitude of interst # 2 (km)
TLIFEX = Solar activity level ( 'nominal' or '+2sigma' or '-2sigma')
IWRIT = Output indicator file (summary, detail, plot) E.g. (1, 1, 1)
/
```

Iridium-85 input file for decay:

```
&DATA
TITLE = 'IRIDIUM 85 ORBIT DECAY PREDICTION'
XJ2 = 1.08263D-3
XJ3 = -2.54D-6
XJ4 = -1.58D-6
REQ = 6378.14D0
FLATN = 298.257D0
GM = 398600.5D0
WS = 7.2921151467D-5
TOL = .0000001D0
N1 = 10
N2 = 10
NOCIR = 0
EBND = 0.0005D0
CUTOFF = 1.0D0
APMIN = 6378.0D0
IOSC = 1
ICART = 1
EL =  0.0d0, 0.0d0, 0.0d0, 0.0d0,0.0d0
R = 4615.726576913d0,  -5140.0645351089d0,  -3.2502133726271d0
V = 0.39971817161889d0,  0.34452728595463d0,  7.5738578564604d0
AREA = 5.12D0
CD = 5.0D0
YMASS = 689.0D0
XMDOT1 = 0.0D0
XMDOT2 = 0.0D0
XMDOT3 = 0.0D0
TMS1 = 0.0D0
TME1 = 10000.0D0
TMS2 = 0.0D0
TME2 = 10000.0D0
TMS3 = 0.0D0
TME3 = 10000.0D0
CDATE = 11, 6,1998
UT = 16, 11, 25
STTP1 = 2000.0D0
DELSAV = 10.0D0
A1 = 300.0D0
A3 = 200.0D0
TLIFEX = 'nominal'
IWRIT = 1, 1, 1
/
```

Starshine-2 input file for satellite decay prediction

```
&DATA
TITLE = 'STARSHINE2 ORBIT DECAY PREDICTION'
XJ2 = 1.08263D-3
XJ3 = -2.54D-6
XJ4 = -1.58D-6
REQ = 6378.14D0
FLATN = 298.257D0
GM = 398600.5D0
WS = 7.2921151467D-5
TOL = .0000001D0
N1 = 10
N2 = 10
NOCIR = 0
EBND = 0.0005D0
CUTOFF = 1.0D0
APMIN = 6378.0D0
IOSC = 1
ICART = 1
EL =  0.D0, 0.0D0, 0.0D0, 0.D0, 0.0D0
R =  -1470.8847577407d0, -6597.4000198937d0, 7.575148260619d0
V = 4.6590650961199d0,  -1.0378271436944d0,  6.0205117611652d0
AREA = 0.1809D0
CD = 2.1366D0
YMASS = 39.0D0
XMDOT1 = 0.0D0
XMDOT2 = 0.0D0
XMDOT3 = 0.0D0
TMS1 = 0.0D0
TME1 = 10000.0D0
TMS2 = 0.0D0
TME2 = 10000.0D0
TMS3 = 0.0D0
TME3 = 10000.0D0
CDATE = 6, 5,1999
UT = 08, 11, 07
STTP1 = 2000.0D0
DELSAV = 10.0D0
A1 = 200.0D0
A3 = 100.0D0
TLIFEX = 'nominal'
IWRIT = 1, 1, 1
/
```

SUNSAT input file for satellite decay prediction

```
&DATA
TITLE = 'Orbit decay prediction for SUNSAT epoch 6 Feb 2000'
XJ2 = 1.08263D-3
XJ3 = -2.54D-6
XJ4 = -1.58D-6
REQ = 6378.14D0
FLATN = 298.257D0
GM = 398600.5D0
WS = 7.2921151467D-5
TOL = .0000001D0
N1 = 10
N2 = 10
NOCIR = 0
EBND = 0.0005D0
CUTOFF = 1.0D0
APMIN = 6378.0D0
IOSC = 1
ICART = 1
EL = 0.0D0, 0.0D0, 0.0D0, 0.0D0, 0.0D0
R = -611.3596933947160D0,  6818.3129602830699D0,  1885.99916780365D0
V = 0.7058965616152D0,  1.9564987352054D0,  -7.2181300644107D0
AREA = 0.40D0
CD = 3.10D0
YMASS = 63.0
XMDOT1 = 0.0D0
XMDOT2 = 0.0D0
XMDOT3 = 0.0D0
TMS1 = 0.0D0
TME1 = 10000.0D0
TMS2 = 0.0D0
TME2 = 10000.0D0
TMS3 = 0.0D0
TME3 = 10000.0D0
CDATE = 2, 6, 2000
UT = 0, 0, 0
STTP1 = 50000
DELSAV = 10.0D0
A1 = 300.0D0
A3 = 200.0D0
TLIFEX = 'nominal'
IWRIT = 1, 1, 1
/
```

Matlab file revprecnut.m

```
%function [r2000,v2000] = fwdprecnut(jdutc,rtod, vtod, type)
function [r2000,v2000] = revprecnut(jdutc,rtod, vtod, type)

%Purpose
% Transforms ECI Mean Equator and mean Equinox of Date
% Co-ordinates to ECI True Equator and True Equinox of Date and vise-
versa
% Inputs:
%     jdutc: Julian date (UTC) of state vector
%     r2000, v2000:  [3x1], [3x1] position and velocity in mean ECI
[km, km/s]
%     type:
%            -1 reverse precession and nutation
%            -2    "    precession only
%            -3    "    nutation only

% Outputs:
% rtod, vtod: position and velocity in true ECI [km, km/s]

% This is accomplished by calculating precession and nutation at date
and
% rotating the state vector through relevant angles.
% This routine has been tested using the example of Vallado on P87
% Ben Opperman.  Nov 2002.

   seccon = 3600.0*180.0/pi; % conversion factor for arc seconds to
rad
   r2d=180/pi;
   d2r=pi/180;

% Determine direction for transformation. + => forward, - =>
backwards
   direction = sign(type);

% Calculate proper time.  Dynamic Barycentric Time Required
   jd0 = 2451545.000;  % Julian day for 2000.0 (J2000)

   jdtdt = utc2tdt(jdutc);  % Terrestrial dynamic time
   jdtdb = tdt2tdb(jdtdt);  % Barycentric dynamic time julian date

   t=(jdtdb-jd0)/36525.000; % tbd julian centuries elapsed since
J2000
   t2 = t*t;
   t3=t2*t;

   r=rtod;  % Do this to use in either or both of precession
   v=vtod;  % and nutation calculation


%Nutation: Calculate dpsi, deps
if (abs(type) == 1 | abs(type) ==3)
   disp('Calculate Nutation')
   [dpsi, deps] = nutation(jdtdb); %Use 1980 IAU theory (arc seconds)
   dpsi = dpsi/seccon;             % Convert to radians
   deps = deps/seccon;

% Nutation: Mean Obliquity of the ecliptic
```

```
%   Eps0 = (8.80e-09)*t3 -(2.8600e-09)*t2 - 0.0002269660*t +
0.40909280;
   Eps0d = 23.439291 - 0.0130042*t -1.64e-7*t2 + 5.04e-7*t3; %From
Vallado %Check against Seidelman (Expl. Suppl.)
   Eps0 = Eps0d*d2r;
   Eps = Eps0+deps;

% Nutation: Rotate Position and velocity
rotm = R1(-Eps)*R3(-dpsi)*R1(Eps0);
rotm=rotm';         %Inverse transformation
r=rotm*rtod;       % If inverse precession required, these will be
passed on
v=rotm*vtod;
 if (abs(type)==3)  % If only inverse nutation required then
     r2000 = r;     % these are the final values, no precession
applied (exit)
     v2000 = v;
 end

end

%Precession: Calculate precession angles
if (abs(type) == 1 | abs(type) ==2)
   disp('Calculate Precession')
   eta  = 0.6406161*t + 0.0000839*t2 +5.0e-6*t3
   zeta = 0.6406161*t + 0.0003041*t2 +5.1e-6*t3
   theta = 0.5567530*t - 0.0001185*t2 -1.16e-5*t3
   eta   = eta*d2r;
   zeta  = zeta*d2r;
   theta = theta*d2r;

% Precession:
rotm = R3(-zeta)*R2(theta)*R3(-eta);
rotm=rotm';   %Inverse transformation
r2000=rotm*r; %Rotate position
v2000=rotm*v;% Rotate velocity

end
```